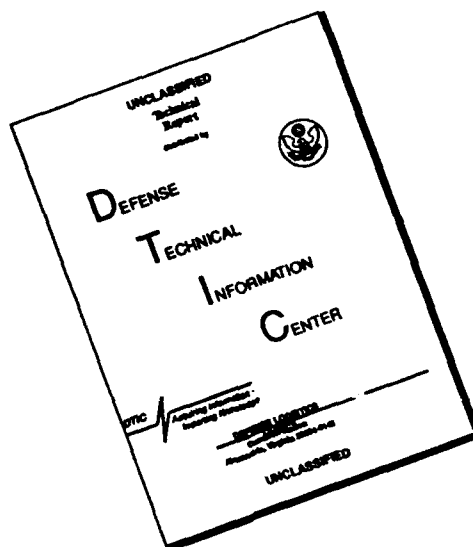AD-A243 376

DTIC
S ELECTE
DEC 7 1991
C D

Lockheed Missiles & Space Company, Inc.
SUNNYVALE, CALIFORNIA

91-17318

91 1209 024

DISCLAIMER NOTICE

THIS DOCUMENT IS BEST QUALITY AVAILABLE. THE COPY FURNISHED TO DTIC CONTAINED A SIGNIFICANT NUMBER OF PAGES WHICH DO NOT REPRODUCE LEGIBLY.

AD-A243 376

DTIC
S ELECTE
DEC 7 1991
C D

⇝☆ *Lockheed Missiles & Space Company, Inc.*
SUNNYVALE, CALIFORNIA

91-17318

91 1209 024

F247083

INVESTIGATION OF MECHANISMS FOR THE SOURCE AND LOSS OF ELECTRONS FROM THE RADIATION BELTS USING DATA FROM SEEP, SCATHA AND P78-1 SATELLITES

Final Report

For Electronics Division
Office of Naval Research

Contract Number

N00014-88-C-0033

W. L. Imhof, D. W. Datlowe, H. D. Voss, J. Mobilia

The Space Sciences Laboratory
Lockheed Palo Alto Research Laboratory
3251 Hanover St., Building 255
Palo Alto, California 94304

19 November 1991

Accession For

NTIS GRA&I	☒
DTIC TAB	☐
Unannounced	☐

Justification

By

Distribution/

Availability Codes

| Dist | Avail and/or Special |
| A-1 | |

REPORT DOCUMENTATION PAGE

Public reporting burden for this collection of information is estimated to average 1 hour per response, including the time for reviewing instructions, searching existing data sources, gathering and maintaining the data needed, and completing and reviewing the collection of information. Send comments regarding this burden estimate or any other aspect of this collection of information, including suggestions for reducing this burden, to Washington Headquarters Services, Directorate for Information Operations and Reports, 1215 Jefferson Davis Highway, Suite 1204, Arlington, VA 22202-4302, and to the Office of Management and Budget, Paperwork Reduction Project (0704-0188), Washington, DC 20503.

1. AGENCY USE ONLY (Leave blank)	2. REPORT DATE	3. REPORT TYPE AND DATES COVERED
	19 Nov. 1991	Final Report (May 1988 to Nov. 1991)

4. TITLE AND SUBTITLE
Investigation of Mechanisms for the Source and Loss of Electrons from the Radiation Belts Using Data from SEEP, SCATHA and P78-1 Satellites

5. FUNDING NUMBERS
Contract Number
N00014-88-C-0033
R & T Number
4149189

6. AUTHOR(S)
W.L. Imhof, D.W. Datlowe, H.D. Voss, and J. Mobilia

7. PERFORMING ORGANIZATION NAME(S) AND ADDRESS(ES)
The Space Sciences Laboratory, O/91-20
Lockheed Palo Alto Research Laboratory
3251 Hanover St., Building 255
Palo Alto, California 94304

8. PERFORMING ORGANIZATION REPORT NUMBER
F247083

9. SPONSORING/MONITORING AGENCY NAME(S) AND ADDRESS(ES)
Office of Naval Research
800 N. Quincy St.
Arlington VA 22217-5000

10. SPONSORING/MONITORING AGENCY REPORT NUMBER
4149189

11. SUPPLEMENTARY NOTES
Distribution Unlimited, available for public release and sale

12a. DISTRIBUTION/AVAILABILITY STATEMENT
Distribution Unlimited, Available for public release and sale

12b. DISTRIBUTION CODE

13. ABSTRACT (Maximum 200 words)

Electron precipitation into the atmosphere entails ionospheric effects that have important consequences for radiowave propagation. Under this contract satellite data as well as ground based measurements have been used to evaluate the source and loss mechanisms for electrons trapped in the radiation belts. With data from the SEEP satellite payload a study was made of short duration (< 0.6 sec) microbursts of electrons from the radiation belts. Several of the electron bursts observed at nighttime were correlated with lightning generated whistlers. A seasonal variation was found for the occurrence in precipitating inner belt electrons with peaks in the energy spectra. The fluxes of relativistic electrons precipitating into the atmosphere were found to be correlated with the fluxes of relativistic electrons at high altitudes. To investigate whether wave - particle interactions are responsible for triggering relativistic electron microbursts an examination was made of wave data recorded at Siple Station at times when the SEEP satellite was near Siple or its conjugate point. The wave data indicate that many of the bursts may not be due to wave-particle interactions.

14. SUBJECT TERMS		15. NUMBER OF PAGES
trapped electrons	electron microbursts	111
electron precipitation	peaked electron spectra	
wave - particle interactions	relativistic electron enhancements	**16. PRICE CODE**

17. SECURITY CLASSIFICATION OF REPORT	18. SECURITY CLASSIFICATION OF THIS PAGE	19. SECURITY CLASSIFICATION OF ABSTRACT	20. LIMITATION OF ABSTRACT
Unclassified	Unclassified	Unclassified	UL

Table of Contents

INVESTIGATION OF MECHANISMS FOR THE SOURCE AND LOSS OF ELECTRONS FROM THE RADIATION BELTS USING DATA FROM SEEP, AND P78-1 SATELLITES

1. SUMMARY

An evaluation of the source and loss mechanisms for electrons trapped in the radiation belts is needed both for a variety of practical applications and for understanding radiation belt dynamics. Electron precipitation into the atmosphere entails ionospheric effects that have important consequences for radiowave propagation. It has been demonstrated that energetic electron precipitation events may cause an enhancement or degradation of ELF signal waves, depending upon where the disturbance is occurring along the path. At VLF frequencies long-lived phase disturbances can be explained by excess D region ionization caused by energetic electron precipitation. Precipitating particles play a significant role in atmospheric chemistry through the production, destruction and transport of reactive nitrogen, oxygen and hydrogen species. The source and loss mechanisms also determine the fluxes of trapped electrons and hence the dose rates that operational satellites will encounter on orbit. For many missions the dose rates determine both the operation lifetime and the spacecraft design in regard to shielding and component selection. Existing data indicate that electrons are precipitated from the radiation belts both by natural mechanisms such as lightning and plasmaspheric hiss, and by man-operated VLF transmitters. The precipitation involves both electrons precipitating directly in the bounce loss cone and electrons which mirror at altitudes above 100 km at most longitudes and which after they have drifted to the vicinity of the South Atlantic Anomaly mirror below 100 km and therefore precipitate into the atmosphere. Under this contract we have used satellite particle and bremsstrahlung x-ray data as well as ground based measurements to evaluate the source and loss mechanisms for electrons trapped in the radiation belts.

2. THE PRECIPITATION OF LOWER ENERGY ELECTRONS IN MICROBURSTS

With data from the SEEP payload on the low altitude polar orbiting S81-1 satellite a study was made of short duration (< 0.6 sec) microbursts of electrons from the radiation belts. These events were studied at mid latitudes ($2 < L < 3$) during nighttime and daytime as well as at higher latitudes ($L > 3$). Comparison of the electron data with simultaneous VLF receiver data from ground stations

chorus emissions. Several of the electron bursts observed at nighttime and at 2< L <3 were correlated with lightning generated whistlers. When daytime bursts at higher latitudes (L> 3) were observed chorus was inevitably detected, but correlation of electron bursts with individual spectral elements was not evident. The results of this investigation are summarized in a reprint in Appendix A.

3.   PRECIPITATING ELECTRONS WITH PEAKED ENERGY SPECTRA

A systematic survey of S81-1 SEEP electron spectra found a large number of spectra with narrow peaks. The peaks occurred at low geomagnetic latitudes near L=1.65, and the energies of the peaks changed with L-value in a characteristic way. Similar peaks were reported by previous satellite experiments and have been attributed to resonant interaction between the electrons and VLF waves from powerful communications transmitters. The SEEP investigation was the first to publish a map of the location on the globe where the peaks are observed. At satellite nighttime the events cluster strongly at the longitudes of either NWC in Australia or NAA/NSS in the eastern United States, confirming that waves from VLF transmitters are the origin of the majority of the peaks. A catalog of the resonant peaks in the SEEP data was searched for characteristic time variations. The data revealed that the occurrence of peaks varies with the 27 day solar rotation period. The SEEP data also suggested a seasonal variation in the occurrence of the peaks, but a mission which lasted 7 months cannot confirm this phenomenon. To make a definitive study of seasonal phenomena 5.5 years of P78-1 data were searched for the occurrence of peaks associated with VLF transmitters. The seasonal variation was found to be statistically significant, with peaks occurring 2.5 times more often in the spring and summer. The data also suggest that there is a variation in the occurrence of peaks with the 11 year solar cycle, but this cannot be confirmed without 11 years of homogeneous data. The results have been submitted for publication in Radio Science and a preprint is included in Appendix B.

4   COMPARISONS BETWEEN RELATIVISTIC ELECTRONS AT LOW AND HIGH ALTITUDES

For the first time a comparison was made between simultaneous measurements of trapped relativistic electron enhancements at synchronous altitude and precipitating electrons in the bounce loss cone at low altitudes. It was found that the precipitating flux levels correlated well with the variations in the flux at high altitude. Within narrow spikes the precipitating directional fluxes

were often within a factor of 10 of the daily averaged trapped fluxes at synchronous altitude. Strong depletions in the synchronous altitude fluxes were found to be associated with low altitude measurements of the equatorward movement of precipitating spikes to lower L shells. In a related study the fluxes of relativistic electrons precipitating into the atmosphere were found to be correlated with the fluxes of relativistic electrons at high altitudes measured from the SCATHA satellite over the L shell range of 5.3 to 8.7. The precipitating fluxes were obtained from P78-1 measurements in both the bounce and drift loss cones. The quasi-trapped electrons in the drift-loss cone were less intermittent and generally more intense, thereby providing a greater sensitivity for detecting precipitation. The results are presented in more detail in Appendix C.

5.   MICROBURSTS OF PRECIPITATING RELATIVISTIC ELECTRONS

Studies have been made under this contract of the mechanisms responsible for the precipitation of relativistic electrons into the atmosphere. Significant fluxes of precipitating relativistic electrons above 1 MeV within the bounce loss cone were much more often observed near midnight than noon, generally in narrow spikes < 100 km in width, and typically at L values between 4 and 6 near the radiation belt boundary. This preferred location of the broader bursts as well as narrow microbursts with durations of less than one second implies the possible importance of irregularities in the magnetic field lines near the trapping boundary as a loss mechanism. To investigate whether wave-particle interactions with VLF chorus are responsible for the triggering of the relativistic electron microbursts we searched VLF wave data recorded at Siple Station at times when the satellite was near Siple or its conjugate point. VLF chorus events were generally not observed on the ground when microbursts were detected in nearby passes of a low altitude polar-orbiting satellite. The available data thus appear to indicate that many of the bursts may not be due to wave-particle interactions with VLF chorus. These results are contained in a reprint and in a preprint included in Appendix D.

6. Papers Sponsored By ONR Contract N00014-88-C-0033

W. L. Imhof, H. D. Voss, J. Mobilia, M. Walt, U. S. Inan and D. L. Carpenter, Characteristics of short-duration electron precipitation bursts and their relationship with VLF wave activity JGR 94, 10079, 1989.

D. W. Datlowe and W. L. Imhof, Cyclotron Resonance Precipitation of Energetic Electrons from the inner Magnetosphere JGR 95, 6477, 1990.

W. L. Imhof, H. D. Voss, J. Mobilia, D. W. Datlowe, J. P. McGlennon, and D. N. Baker, Relativistic electron enhancements; simultaneous measurements from synchronous and low altitude satellites. GRL 18, 397, 1991.

W. L. Imhof, H. D. Voss, J. Mobilia, D. W. Datlowe, and E. E. Gaines, The precipitation of relativistic electrons near the trapping boundary JGR. 96, 5619, 1991.

D. W. Datlowe and W. L. Imhof, Seasonal Variations of Energetic Electron Precipitation by Cyclotron Resonance with VLF Waves from a Ground-based Transmitter, (submitted to Radio Science).

W. L. Imhof and R. W. Nightingale, Relativistic Electron enhancements observed over a range of L-shells at both high and low altitudes (submitted to JGR).

W. L. Imhof, H. D. Voss, J. Mobilia, D. W. Datlowe, E. E. Gaines, J. P. McGlennon, and U. S. Inan, Relativistic Electron Microbursts (being prepared for submission to JGR)

7. PAPERS PRESENTED AT SCIENTIFIC MEETINGS

D. W. Datlowe and W. L. Imhof, Cyclotron resonance precipitation of energetic electrons from the inner magnetosphere, presented at 1988 Fall Meeting of AGU.

W. L. Imhof, H. D. Voss, J. Mobilia, E. E. Gaines and D. W. Datlowe, Energy selective precipitation of electrons near the trapping boundary, presented at 1989 Fall Meeting of AGU.

D. W. Datlowe and W. L. Imhof, The seasonal variation in the occurrence of cyclotron resonance precipitation of energetic electrons by VLF transmitters, presented at 1989 Fall Meeting of AGU.

D. W. Datlowe and W. L. Imhof, Long term variations in the equatorial plasma density near L = 1.65 measured by resonant precipitation of energetic electrons, presented at 1990 Fall Meeting of AGU.

W. L. Imhof, H. D. Voss, J. Mobilia, D. W. Datlowe, and E. E. Gaines, The precipitation of relativistic electrons near the trapping boundary, presented at 1990 Fall Meeting of AGU.

D. W. Datlowe, W. L. Imhof and H. D. Voss, Detection of kilometer scale structures at the polar cap boundary by combining satellite x-ray images with in situ energetic electron flux profiles, to be presented at 1991 Fall Meeting of AGU.

H. D. Voss, J. Mobilia, W. L. Imhof, Thunderstorm effects in space observed with the SEEP S81-1 satellite, presented at AAAS Meeting in San Francisco, January 1988.

J. Mobilia, H. D. Voss, W. L. Imhof, Global lightning Observations and associated effects as measured from the S81-1/SEEP satellite, presented at AAAS Meeting in San Francisco, January 1988

H. D. Voss, Lightning with associated LEP and electric fields observed from the SEEP/S81-1 satellite, presented at 1988 Fall Meeting of AGU.

APPENDIX A

THE PRECIPITATION OF LOWER ENERGY ELECTRONS IN MICROBURSTS

Characteristics of Short-Duration Electron Precipitation Bursts and Their Relationship With VLF Wave Activity

W. L. Imhof, H. D. Voss, J. Mobilia, and M. Walt

Lockheed Palo Alto Research Laboratory, Palo Alto, California

U. S. Inan and D. L. Carpenter

STAR Laboratory, Stanford University, Stanford, California

Energetic (>6 keV) electron data from the SEEP payload on the low altitude (~200 km) polar orbiting S81-1 satellite indicate a high rate of occurrence of short duration (<0.6 s) electron precipitation bursts. Characteristics of events observed at night (2230 MLT) versus daytime (1030 MLT) and at midlatitudes (2 < L < 3) versus higher latitudes (L > 3) were distinctly different in several ways. For 2 < L < 3 the daytime bursts occurred approximately uniformly in longitude and were equally distributed between the northern and southern hemispheres. The nighttime bursts in the same L shell range occurred approximately twice as often on a worldwide basis and were observed predominantly in the northern hemisphere and at longitudes of 260°E to 320°E. In a significant number of the nighttime events at 2 < L < 3 the median electron energy increased with time during the burst, but most of the other spectra showed no well-defined trend. During some of the nighttime bursts broad peaks were observed in the energy spectra, but these peaks were not so evident in the daytime bursts. On higher L shells, L > 3, narrow electron precipitation bursts (<0.3 s duration) were frequently observed poleward of the plasmapause, more often near noon than near midnight and much more frequently than at 2 < L < 3. Comparison of the electron data with simultaneous VLF wave data from Palmer (L = 2.4) and Siple (L = 4.3) stations in Antarctica indicated a varying degree of association of electron bursts with whistlers and chorus emissions. Several of the electron bursts observed at nighttime and at 2 < L < 3 were correlated with lightning-generated whistlers observed at Palmer Station. When daytime bursts at higher latitudes (L > 3) were observed on satellite passes within ±50° of the Siple meridian, chorus was invariably detected at Siple, but correlation of electron bursts with individual chorus spectral elements was not evident. The lack of such correlation may be due to the limited spatial extent of flux tubes excited by individual chorus elements which are possibly generated without mutual coherence in multiple high altitude magnetospheric locations. Within one hour of all four of the satellite passes within 400 km of Siple with the highest rate (≥ 10 individual bursts per pass) of burst occurrence, overhead electron precipitation was clearly detected by ground based sensors at Siple Station. Quasi-periodic bursts of several seconds duration were observed on one or more of the photometer, riometer, and magnetic pulsation sensors and many of these bursts were correlated with clustered VLF chorus bursts. Hence, there is at least association of chorus with electron precipitation.

INTRODUCTION

In a recent paper. *Imhof et al.* [1986], we considered the contributions of various VLF wave types to the loss rates into the atmosphere of electrons trapped in the slot region of the radiation belts. From that investigation, as well as earlier comparisons between nighttime bursts and whistler activity [*Voss et al.*, 1984], it was suggested on the basis of the longitude and L shell variations that some of the well-defined bursts at nighttime were associated with lightning generated whistlers and some of those in the daytime may have been caused by other wave types such as chorus. However, the daytime electron precipitation events were not compared with simultaneous measurements of waves or with ground-observed signatures of particle precipitation, nor were many features of the electron precipitation such as the dynamic energy spectra and the time profiles intercompared between the daytime and nighttime events.

Over the years burst precipitation at mid and high latitudes and its association with wave activity has been studied from the perspectives of satellites and rockets and from the

viewpoints of ground stations and balloons. On Injun 3, *Oliven and Gurnett* [1968] made simultaneous measurements of electron bursts (of duration less than one second) and VLF chorus emissions at high latitudes. They found that electron precipitation bursts were always accompanied by chorus, but chorus bursts were not always accompanied by electron precipitation bursts. It was not generally possible to find a one-to-one association between individual electron precipitation bursts and individual chorus emissions. In a more recent experiment precipitation events of electrons 0.63 to 20 keV lasting from 1 to 2 s were observed from the HILAT satellite and interpreted by *Hardy and Burke* [1987] as arising from the interaction of VLF waves (possibly chorus) with plasma sheet electrons.

With the SEEP payload on the S81-1 spacecraft, *Voss et al.* [1984] found one-to-one correspondence between a series of nighttime electron bursts in the northern hemisphere near L = 2.5 and a series of whistlers recorded at Palmer Station. Antarctica in the south. In rocket experiments, *Rycroft* [1973] recorded a burst of electron precipitation at the time of a two-hop whistler recorded nearby on the ground, and *Goldberg et al.* [1987] observed X ray bursts that were coincident with lightning detected by nearby ground stations.

Burst precipitation associated with discrete waves such as whistlers or chorus has been detected at ground stations by photometers and radiowave receivers and on balloons by X ray detectors. For bursts inside the plasmasphere. the correlated waves have generally been lightning-associated whistlers. and the lightning-induced electron precipitation (LEP) events have been detected by observing perturbations (Trimpi effects) on subionospherically propagating VLF waves [e.g.. *Helliwell et al.*, 1973; *Inan and Carpenter*, 1986, 1987]. Poleward of the plasmapause the waves have usually been VLF chorus emissions. some of which showed evidence of being triggered by whistlers. Correlated bursts of X rays and whistler-triggered chorus were observed at Siple Station. Antarctica (*L* = 4.3) and were reported by *Rosenberg et al.* [1971] and by *Foster and Rosenberg* [1976]. Precipitating electrons with energies between ~70 and 250 keV were interpreted to be the primary contributors to the observed X ray flux. The typical VLF burst consisted of 3 to 5 rising elements of 0.1 seconds duration separated by ~0.15 s and was confined to the frequency range 1.5 to 3.8 kHz. In later experiments at *L* = 4.3 a detailed correlation was found in two events between electron microbursts and chorus elements of rising frequency observed at ionospheric conjugate points of the geomagnetic field [*Rosenberg et al.*, 1981]. Recently. the subionospheric signal from the Siple. Antarctica. experimental VLF transmitter received at several Antarctica stations has been used to detect wave-associated precipitation effects poleward of the plasmapause (*Carpenter et al.*, 1985: *Hurren et al.*, 1986].

To extend our understanding of the burst precipitation process. we have surveyed electron precipitation on a global basis and where possible compared the electron data with ground measurements of simultaneous wave activity and ionospheric effects. The present paper describes preliminary work of this kind. based upon electron measurements aboard the polar orbiting S81-1 satellite. Burst phenomena are studied both at midlatitudes (*L* = 2 to 3) and at higher *L* shells extending beyond the plasmapause. The temporal and energy spectral characteristics of nighttime and daytime bursts are investigated. and VLF wave data recorded at Siple and Palmer Stations in Antarctica are searched for wave activity that may be associated with the electron bursts.

DESCRIPTION OF INSTRUMENTATION

The stimulated emission of energetic particles (SEEP) experiment on the three-axis stabilized S81-1 spacecraft contained an array of cooled silicon solid state detectors to measure electrons and ions [*Voss et al.*, 1982]. The data were acquired over the period from May 28. 1982 until December 5. 1982. The S81-1 satellite was in a sun synchronous 1030 and 2230 local time polar orbit (inclination = 96.3°) at 170 to 280 km altitude. traveling southward during the daytime. The electron spectrometers were oriented at various angles to the local vertical. Data are presented from only two of the spectrometers. The spectrometer TE2 at 90° zenith angle (approximately 90° pitch angle for the data presented) had an acceptance angle of ±20° and a geometric factor of 0.17 cm^2 sr. The pulse-height analyzer for the data presented had a range of 6 to 930 keV with energy steps of 3.62 keV. The instrument ME1 at a zenith angle of 0° (approximately 30° pitch angle for most of the data presented) had an acceptance angle of ±30°. a geometric factor

of 2.47 cm^2 sr. a threshold energy of 45 keV. and an energy resolution of about 20 keV. Total integral counting rates above several thresholds in each of the spectrometers were recorded during successive 0.064 second intervals. and pulse height address of the first count in each successive 0.004-s interval was recorded for TE2 and for ME1.

In the data analysis *L* values were calculated using the Goddard Space Flight Center (GSFC 12/66) geomagnetic field model [*Cain et al.*, 1967] for the Epoch 1980.

OVERVIEW: ELECTRON BURSTS OBSERVED OVER A WIDE RANGE OF LATITUDES

Narrow bursts of electron precipitation with total durations of less than 0.6 s were observed in the SEEP experiment over a wide range of latitudes including *L* = 2 to 5. The latitudinal distribution of such bursts for a particular orbital pass is illustrated in the lower and middle panels of Figure 1. A strong and isolated electron precipitation burst was observed at *L* = 2.47. equatorward of the plasmapause. which at this time was estimated to have been at *L* = 3.6 from ground-based whistler data. At *L* = 2.8 there were some weaker events. but otherwise no strong burst activity until *L* = 3.6. beyond which burst activity substantially increased. Bursts were detected frequently. at time separations of less than 10 s. In this and many other satellite passes on which short bursts were observed. electron burst activity was concentrated above a well-defined *L* value near *L* = 4 which we associate with the plasmapause or its near vicinity in the poleward direction.

Throughout the SEEP pass illustrated in Figure 1. Siple Station (*L* = 4.3. 76°S. 276°E) recorded strong chorus emissions in the band ~0.5 to 1.5 kHz. Spectrograms of the wave activity during subintervals are shown at the top of Figure 1; they are restricted to 2-s recording intervals between 3-s pulses from the Siple Station experimental VLF transmitter. One-to-one correlations between the electron bursts at *L* > 3.6 and chorus structure were not observed. Such correlations were not necessarily expected. in view of the substantial longitude separation of the spacecraft and ground station (~26° or ~700 km at *L* ~ 4.3) and the fact that only a subset of magnetospheric chorus waves (i.e.. ducted signals) are observed on the ground. Whistler propagation to Palmer Station (*L* ~ 2.4. 65°S. 296°E) was observed at rates of 20 to 40 per minute during synoptic recordings that both preceded and followed the SEEP pass. The satellite track at *L* = 2.5 was ~1100 km to the east of Palmer. and while no ground recording was made during the overpass. a causal relation between whistlers and the burst activity at *L* = 2.47 and near *L* = 2.8 is considered likely.

ELECTRON PRECIPITATION BURSTS AT MID-LATITUDES

In the midlatitude range. *L* = 2 to 3. daytime and nighttime bursts were identified by the following selection criterion: a factor of 2 increase in the integral (>45 keV) flux observed with both the ME1 detector (at 0° zenith angle) and the TE2 detector (at 90° zenith angle) and a total pulse length (full-width-at-half maximum. including rise time. width. and decay) of less than 0.6 s. (Many "weaker" bursts and longer bursts were observed. but they are not considered here). Multiple bursts with a repetition period of a few tenths of a second were considered part of the same event. To be classified as distinct events. pulses had to be separated by
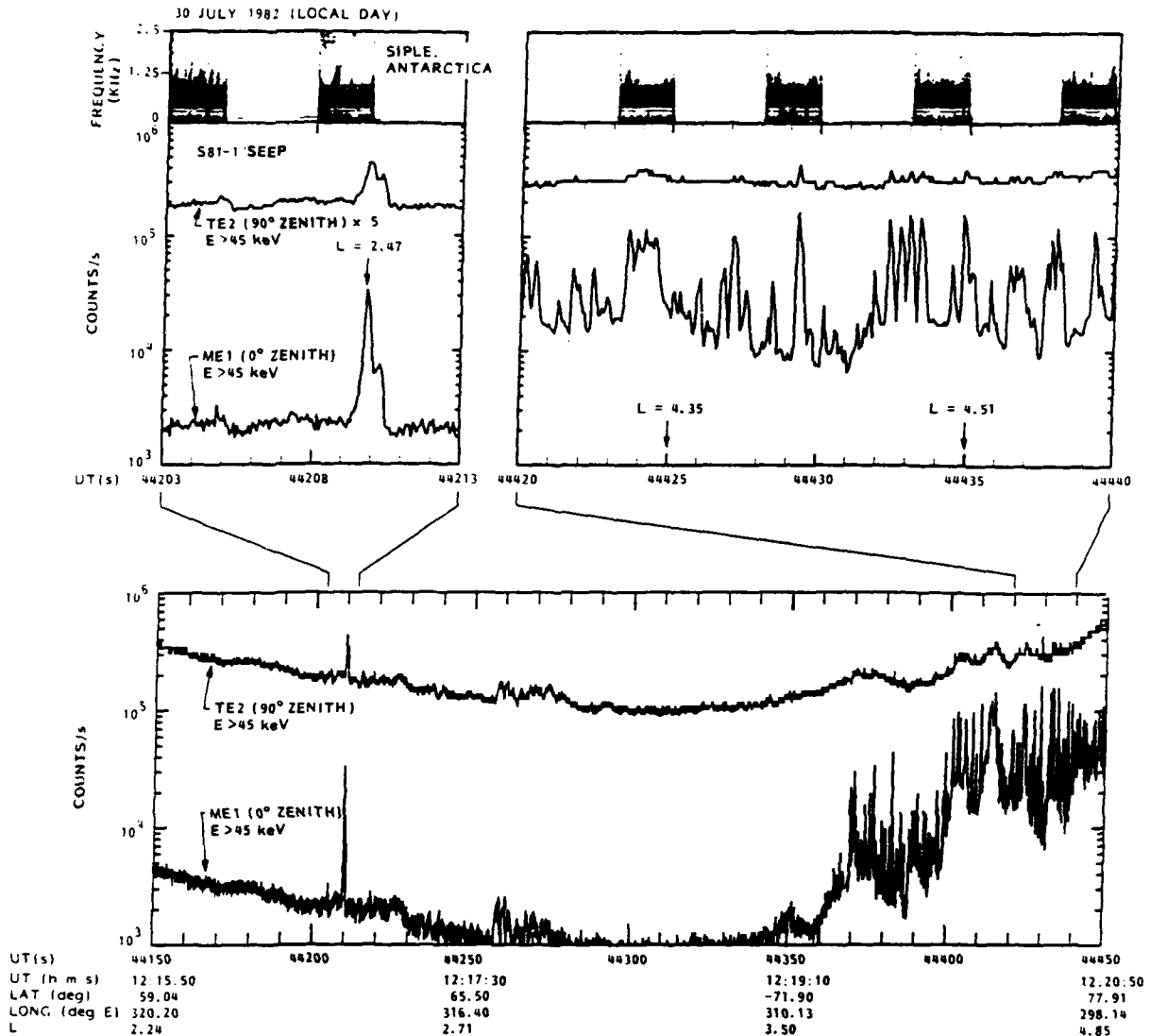
Fig. 1.   Counting rate versus time for the ME1 (>45 keV) and TE2 (>45 keV) detectors during a daytime pass of the S81-1 satellite. Also shown is the frequency-time record acquired at Siple Station. Nonrecording times are blank.

more than 7 s. With such criteria at mid-latitudes, 59 events at night and 26 in the daytime were found from the 6-month data set. With a broader criterion, one second rise time and 3-second decay time, 222 electron bursts at $L = 2$ to 3 had been selected [Imhof et al., 1986] from this data set which had a comparable number of daytime (4854) and nighttime (4773) satellite passes.

As an example the detailed time and energy characteristics of a nighttime burst at $L = 2.27$ are presented in Figure 2. The counting rates versus time are shown in the left-hand section for the ME1 and TE2 detectors for $E > 45$ keV. The listed start time of the plot is chosen to place the peak of the burst in the 90° detector at $t = 1$ second. In the right-hand section of Figure 2, the energies of individual electrons sampled by the TE2 detector at a maximum rate of one during each 0.004 s are plotted as a function of time for those periods when the counting rate was significantly above background. In addition, median energies are plotted as squares for each 0.064-s interval, and these squares are connected with straight lines.

The characteristics of eight representative bursts (four at night and four in the daytime) at $2 < L < 3$ are presented in Figure 3 with the same format as the previous figure. In the spectral presentations only the median energies for each 0.064 second interval are shown. The times and coordinates of the satellite during each of the observations are indicated. In these nighttime events an initial peak in the TE2 detector is followed by subsequent peaks separated by about 0.5 s. These peaks are believed to be due to multiple bounces (between hemispheres) of the electrons that have first interacted with the waves and then backscattered from the atmosphere [Voss et al., 1984]. In these plots the evidence for multiple bounces between hemispheres is stronger at night than during the day. Typically, for the nighttime bursts the counting rate in the ME1 spectrometer at 0° zenith angle is very weak on the first pulse in comparison to the TE2 detector near 90° pitch angle or to subsequent pulses in the ME1 spectrometer. This effect is discussed in more detail by Voss et al. [1984] and is attributed to changes in the electron
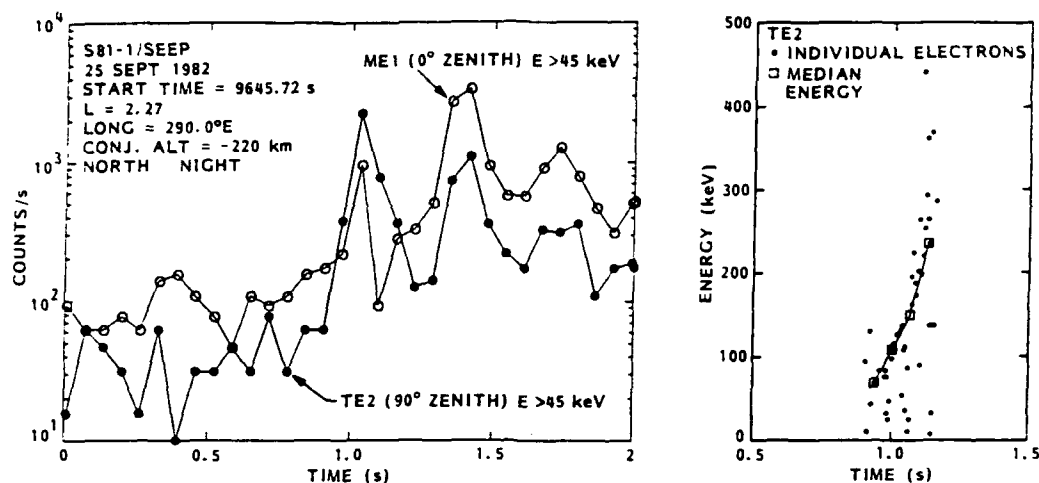
Fig. 2. Data from a representative isolated night burst. In the left-hand section is shown the counting rate versus time for the ME1 and TE2 detectors. In the right-hand section are shown the energies of individual electron counts and median energies during 0.064-s intervals in the TE2 detector.
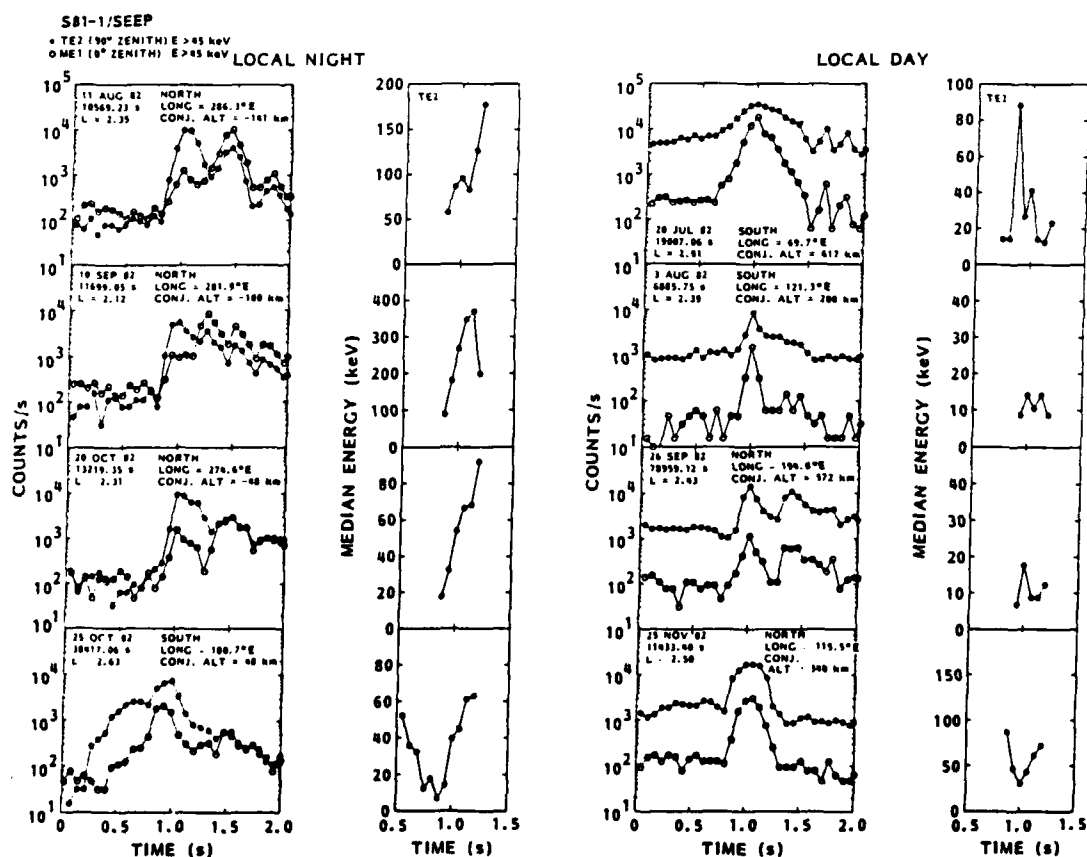

Fig. 3. Data from representative isolated night and day bursts at $L = 2$ to 3. In the left-hand section is shown counting rate versus time for the ME1 and TE2 detectors. In the right-hand sections are shown the median energies during 0.064-s intervals in the TE2 detector.

TABLE 1. Spectral Trends With Time for Narrow Bursts at
$2 < L < 3$

Median Energy Trends With Time During the Burst	Number of Daytime Cases	Number of Nighttime Cases
Rises	0	18
Falls	4	2
Falls, then rises	1	5
Rises, then falls	2	1
Not well defined	19	33
Total	26	59

pitch angle distribution when the initial pulse is reflected by atmospheric scattering.

In the right-hand portion of each panel in Figure 3 the median energies are plotted as a function of time beginning when the counting rate was significantly above background and extending for 0.192 s after occurrence of the peak flux. At nighttime the median energy often tended to increase with time during the first pulse. This behavior occurred in the

examples shown in the left-hand section of the figure, except for the October 25 case in which an unusually prolonged rise time perhaps unrelated to the burst itself, displayed a decreasing average energy. A detailed interpretation of the common trend, associated with the time variation of wave frequency in whistlers, is discussed by *Inan et al.* [1989]. Most of the daytime events (right-hand panels) showed little systematic spectral variation with time during the burst. A summary of the spectral trends with time during each of the 85 bursts reported here is given in Table 1. The trends were obtained by visual inspection and are listed as not well defined unless a clear-cut slope associated with the enhanced flux was apparent. Many of the "not well defined" cases can be attributed solely to the relatively low counting rate increase during the burst.

The time-integrated energy spectra of the electrons recorded during a 0.64 second interval spanning representative nightside and dayside bursts are shown in Figure 4. Background counting rates in each channel, taken to be equal to the rate preceding the burst, have been subtracted. In order to reduce the statistical scatter the 3.62-keV-wide energy channels are grouped by fives. A broad peak sometimes
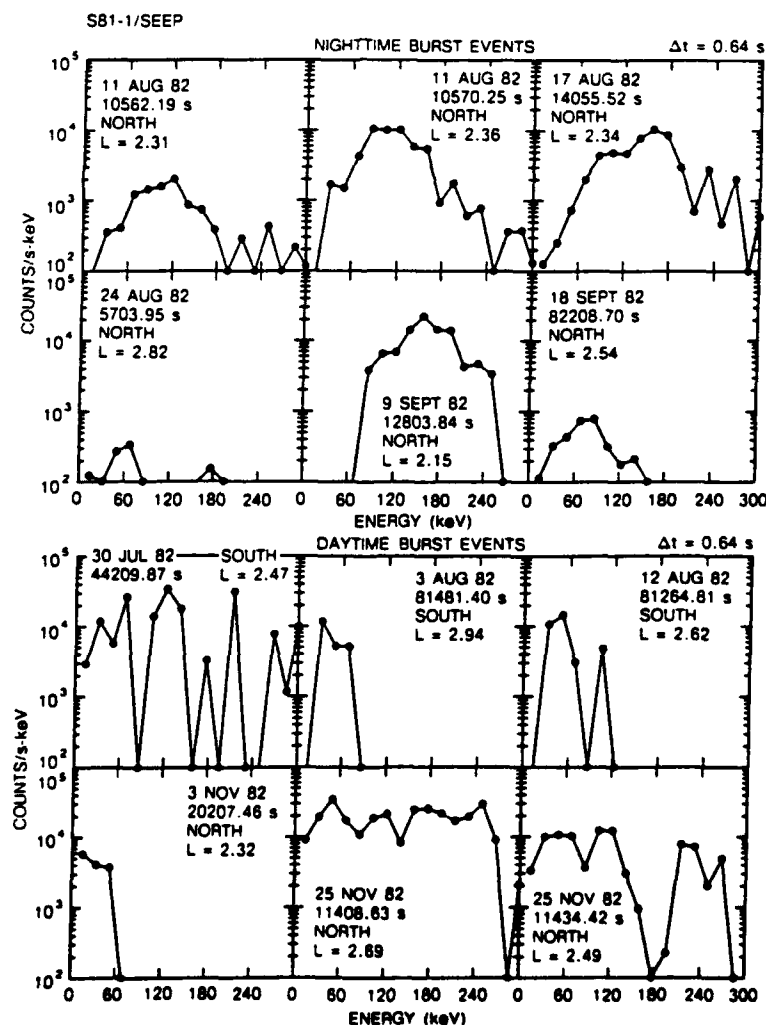

Fig. 4. Representative energy spectra measured during 0.64-s intervals in the TE2 detector for isolated nighttime and daytime electron bursts. The times listed are UT (s) start times for the intervals.
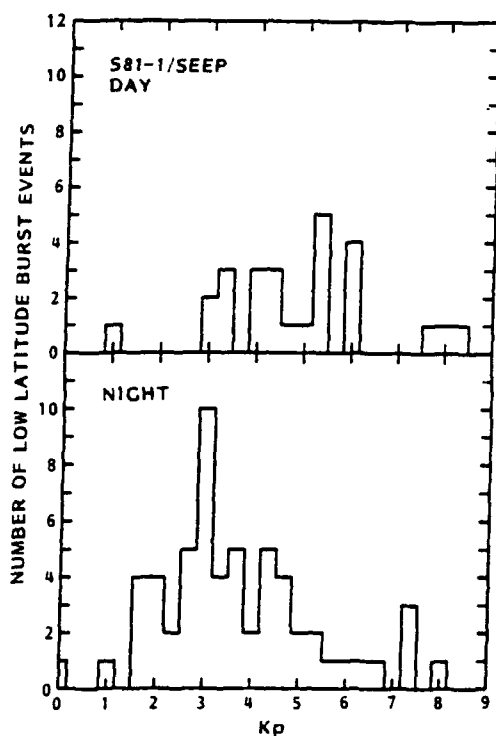
Fig. 5. The distributions in Kp values for the bursts at $L = 2$ to 3.

higher precipitation fluxes. The nighttime events were concentrated in the north at 260°E to 320°E longitude. This concentration is probably due to several factors, such as the distribution of lightning activity and the proximity of the South Atlantic Anomaly. The latter has the effect of reducing the flux normally present at the satellite altitude and allows small flux increases to satisfy the selection criteria. The east coast of the United States is a known region of high thunderstorm activity [Turman and Edgar. 1982; Mobilia et al.. 1985; Orville and Henderson. 1986], and this concentration of lightning flashes would lead to more electron burst events in this region at nighttime. However, ground-based observations of ionospheric effects of LEP bursts indicate a high level of event occurrence at longitudes of the western United States (e.g.. 240°E to 260°E) [Inan et al.. 1988].

In the nighttime ground-based measurements of ionospheric effects of LEP events also suggest that a comparatively high rate of events and generally larger fluxes should occur in the southern hemisphere near the longitudes of the South Atlantic Anomaly [Inan et al.. 1988]. The relatively small number of nighttime events observed in the south at 260°E to 320°E longitude can primarily be attributed to larger background fluxes of trapped electrons near the South Atlantic Anomaly and to the somewhat higher altitudes of the satellite in the southern hemisphere. We note that measurements of ionospheric effects are sensitive only to precipitating electrons while the sensitivity of the satellite-
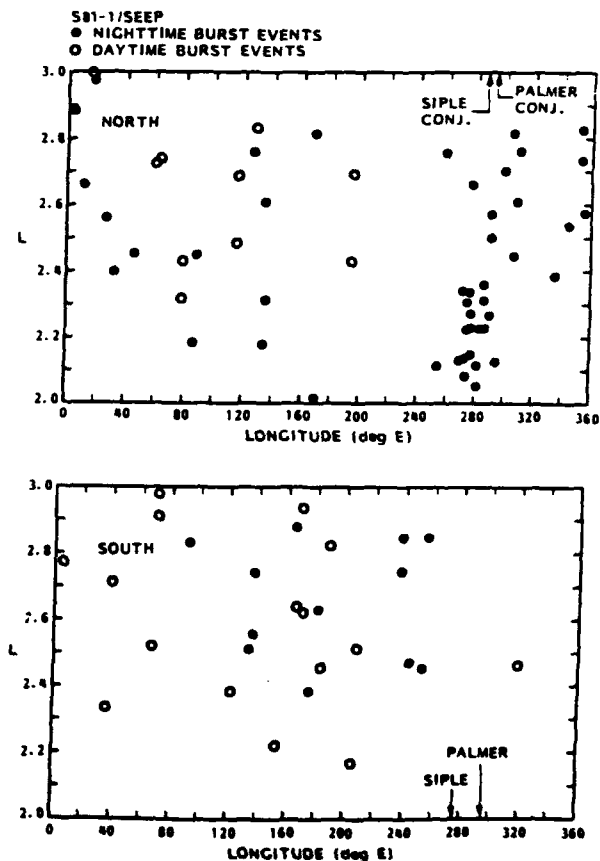
appears in the nightside energy spectra. but peaks are not so evident in the daytime spectra. The electron energies involved are generally consistent with those expected to arise from equatorial gyroresonant interactions within the plasmasphere with whistlers or outside the plasmapause with either whistlers or chorus emissions at frequencies up to a few kHz.

Histograms of the geomagnetic activity conditions (Kp) under which the dayside and nightside bursts at $L = 2$ to 3 were observed are presented in Figure 5. The occurrence of nightside events follows approximately the probability of occurrence of various Kp levels. In contrast. the daytime events show a tendency to occur with greater probability as disturbance levels increase from moderate to severe. A statistical comparison of the day and night distributions using the U-test of Wilcoxon. Mann. and Whitney shows that these two distributions are different. the probability that they are samples drawn from a common distribution being 0.005.

The L shell and longitude locations of the burst observations are presented in Figure 6 for each of the events at $2 < L < 3$. The daytime and nighttime events are plotted with open and closed circles. respectively. The coverage at the two local times was approximately equal. and a comparable number of passes was obtained at each longitude and L shell. As noted above. narrow bursts were identified only about half as often in the daytime as at night. The higher rate of event occurrence at night may result from increased ionospheric (D region) absorption during daytime at VLF frequencies [Helliwell. 1965]. Due to this effect. whistler wave intensities in the magnetosphere would be expected to be higher at night than during day thus leading to generally

Fig. 6. The longitude and L shell locations of each of the narrow bursts at $L = 2$ to 3 in the northern and southern hemispheres. The meridians of Siple and Palmer stations and their conjugate points are indicated.
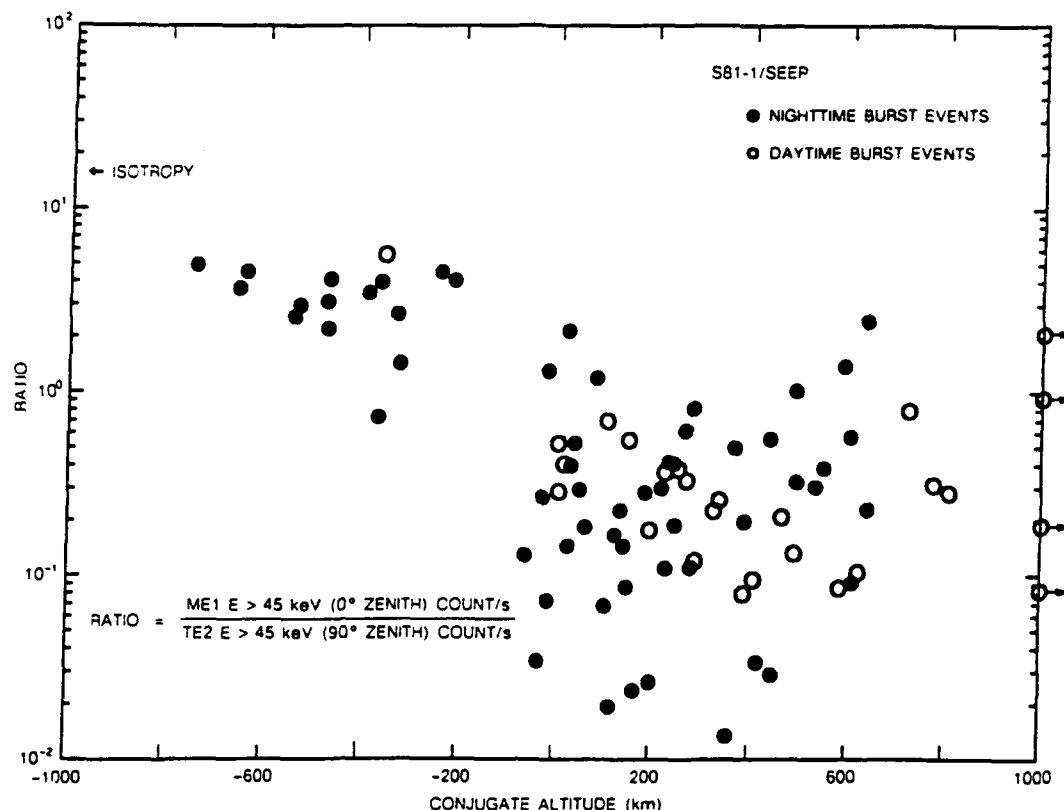
Fig. 7. Ratio of the net counting rate (with preburst rate subtracted) in the ME1 detector to that in the TE2 detector. plotted as a function of the altitude of the conjugate point. The ME1 spectrometer is at a zenith angle of 0° and typical pitch angle of ~30°. For the TE2 spectrometer these angles are 90° and ~90°. The ratio of counting rates for isotropy is indicated.

based burst detection also depends on the background of trapped flux. Our data also suggest a somewhat higher nighttime rate of occurrence in the south in the longitude range of 120°E to 260°E. The reasons for this effect are not known and statistics are not sufficient for any definitive conclusions. In contrast to the nighttime bursts. the daytime events display a slight preference for occurrence in the southern hemisphere but indicate no significant longitude variations within the limited statistical accuracies.

Let us next consider the pitch angle distributions associated with the electron precipitation bursts at different locations. A simple and convenient parameter representing the pitch angle distribution is the ratio of net counting rate (with preburst rate subtracted) in the ME1 detector (at ~30° pitch angle) to that in the TE2 detector (at ~90° pitch angle). Since one would expect this ratio to be influenced by the local atmospheric loss cone, the ratios are sorted by conjugate altitude, separately for day and night local times. The ratios are shown in Figure 7 during the 0.064-s interval at the time of the peak counting rate in the TE2 detector; they are plotted as a function of the conjugate point altitude. The ratio for pitch angle isotropy allowing for differences in the geometric factors of the two detectors is indicated. The ratios show considerable scatter but tend to decrease with increasing altitude of the conjugate point, and for large negative values of the altitude at the conjugate point the ME1/TE2 ratios indicate a more isotropic distribution. Even under the latter conditions the ratios are still less than those corresponding to isotropy. or equivalently the pitch angle

distributions show less flux near 30° than 90°. The variation of the pitch angle distribution with altitude of the conjugate point is similar for both daytime and nighttime events: this result may reflect the importance of atmospheric effects at both local times rather than any similarity in the precipitation mechanism.

It has not been possible to sort all of the daytime $L = 2$ to 3 events with respect to plasmapause location. The results of earlier studies of plasmapause radius as a function of geomagnetic activity [Carpenter and Park, 1973] suggest that the plasmapause was at $L < 3$ during some of the burst observations that occurred under relatively disturbed conditions. However. it is likely that a significant fraction of the daytime bursts occurred within the plasmasphere. as illustrated above for the case of Figure 1.

Most of the nightside events are believed to have occurred within the plasmasphere, based on considerations of magnetic activity (and in individual cases upon analyses of the correlated whistlers [e.g.. Voss et al.. 1984]). This inference is supported by the lower disturbance levels associated with these cases. and the fact that the plasmasphere radius at ~2230 MLT is on the average larger than it is in the post-dawn sector. where it tends to be near a diurnal minimum [Carpenter. 1966].

ELECTRON PRECIPITATION BURSTS AT HIGH LATITUDES

At $L > 3$ narrow electron precipitation bursts were detected much more frequently than at $L < 3$. Accordingly. an initial study was made of 87 satellite passes (61 in daytime.
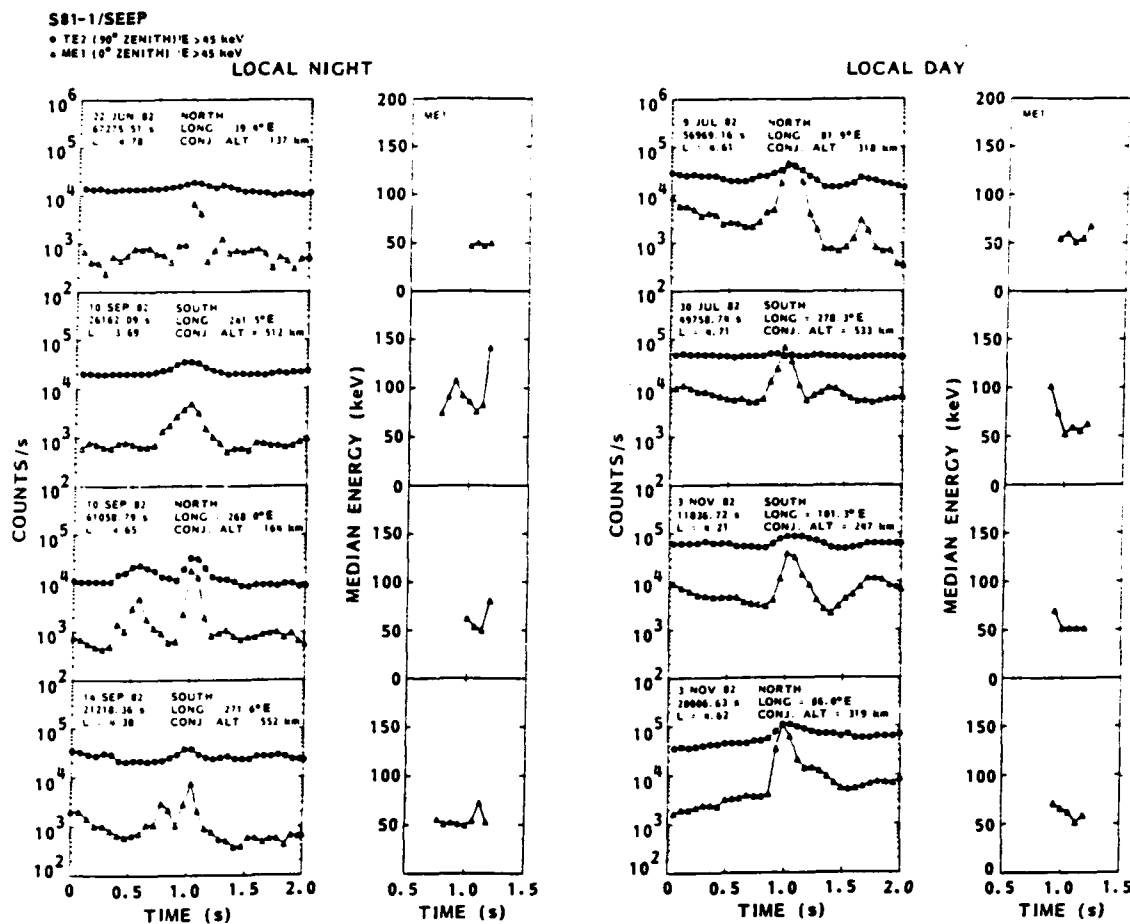
Fig. 8. Data from representative night and day bursts at $L = 4$ to 5. In the left hand sections are shown counting rate versus time for the ME1 and TE2 detectors. In the right-hand sections are shown median energies during 0.064-s intervals in the ME1 detector.

26 at night) from the period of May 28 to December 5, 1982. Many of the passes studied were processed because the satellite passed near (within $\pm 10°$) the meridians of Siple or Palmer station. (276°E and 296°E, respectively), but otherwise there was no special selection criterion. Narrow bursts at $L > 3$ were identified by the criterion that the ME1 detector show a counting rate increase of at least a factor of 2, that it be above 10^3 counts/second, and that the full width at half maximum of the counting rate peak be less than or equal to 0.3 s. No restrictions were placed on the appearance of another burst nearby in time.

Time profiles of the counting rates and median energies for peaks occurring at $L \sim 4$ to 5 are shown in Figure 8 for several dayside and nightside bursts. The listed start times of the plots are chosen to place the peak of the burst in the ME1 detector at $t = 1$ s. The energy spectra were taken from the ME1 spectrometer, since the events were much more prominent in that detector than in the TE2 spectrometer. In the ME1 detector individual pulse height addresses were recorded at a maximum rate of 16 per 0.064 s as with the TE2 detector. As in Figure 4, energy points are shown at times beginning when the counting rate was significantly above background and extending for three time frames (0.192 s) after the peak flux, provided that the counting rate in the

ME1 spectrometer was significantly above background. No consistent trend with time is evident in the median energies.

On 58 of 87 satellite passes, one or more narrow bursts were found at $L = 3$ to 5. The frequent clustering of bursts above some L value was indicated in Figure 1 and is further illustrated for day and night passes in Figure 9, where the counting rates in the ME1 detector are plotted as a function of time. On the top pair of panels, low L values are at the center of the page. In the daytime example at left, bursts are seen as narrow spikes extending above an envelope that drops sharply, by about an order of magnitude at $L \approx 3.5$, after which the count rate is low and steady. In the night example neither narrow bursts nor elevated counts at higher L were observed. In the middle pair of panels, higher L values are at the center of the page. Both passes show a relatively clear transition to a region of higher count rate and narrow burst activity at $L > \sim 3.4$. For both panels at the bottom of Figure 9, higher L is at the right. In the dayside case, an abrupt transition to strong burst activity occurs at $L = 4$, while the nightside case shows a complex structure throughout. Note, particularly in the middle and lower panels the tendency for narrow spikes to be superimposed upon or otherwise accompany fluctuations with time durations near 10 s.
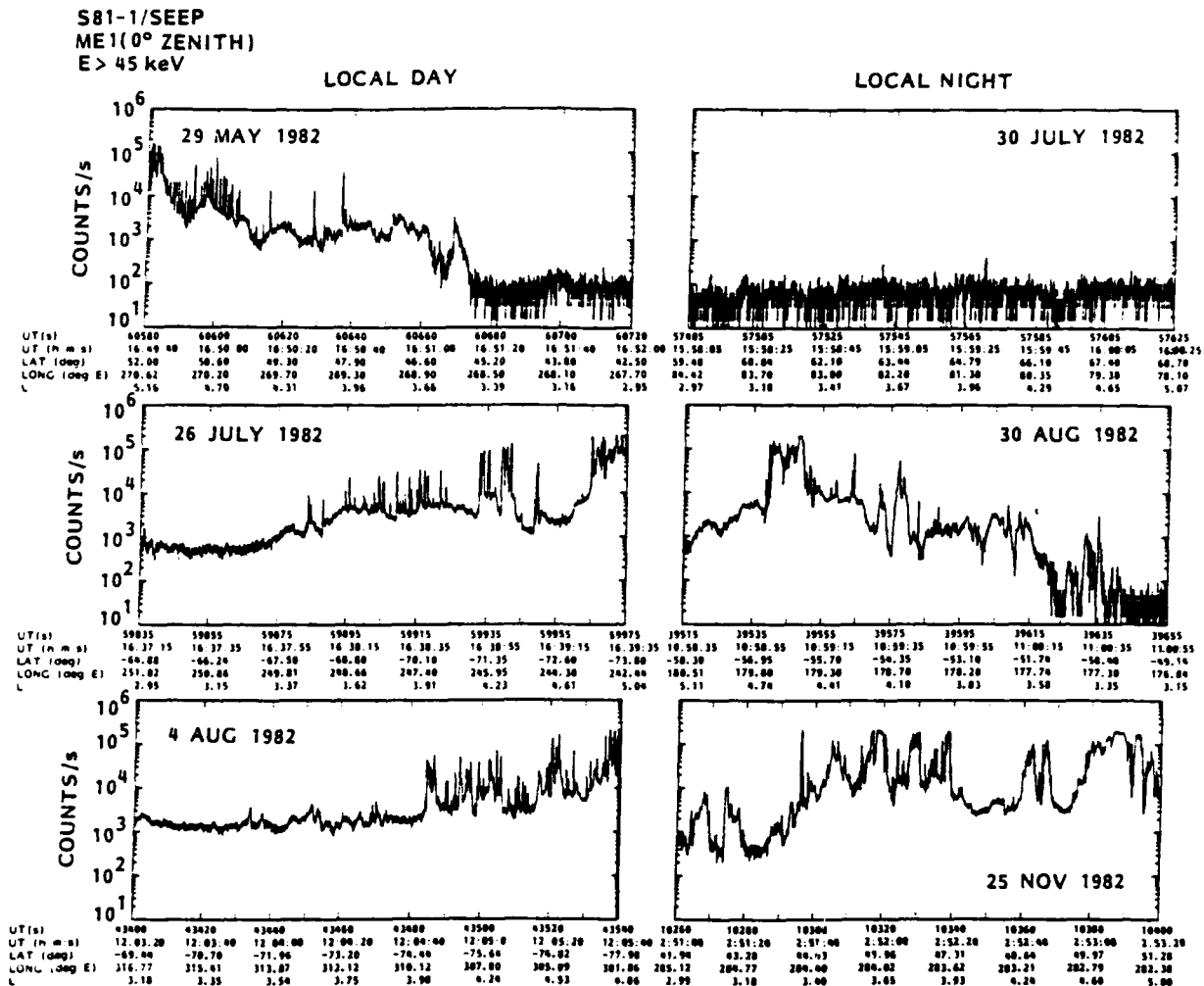
Fig. 9. Counting rate versus time for the MEI (>45 keV) detector during various passes of the S81-1 satellite.

Figures 10a and 10b show by solid dots the L values of bursts on those 44 of 61 passes on the dayside and 14 of 26 at night, respectively, during which at least one narrow burst was observed at L = 3 to 5. The times in seconds and longitudes for crossing L = 4 are given. The average frequency of occurrence of daytime bursts increased rapidly between L = 3.5 and 4. At night the distribution was more uniform, but Figure 10b suggests that this finding was dominated by a single case (November 25, illustrated at lower right in Figure 9). The comparatively higher levels of activity on the dayside are believed to be associated with the morningside peak in chorus activity in the magnetosphere [Burton and Holzer, 1974; Burtis and Helliwell, 1976].

SIMULTANEOUS WAVE MEASUREMENTS AND ELECTRON BURSTS

A substantial number of continuous ground recordings were made at Siple and Palmer, Antarctica, stations during SEEP passes at nearby longitudes. Unfortunately, many of the Siple recordings were only available for 2 s out of every 5 during times when the transmitter was off, as illustrated in Figure 1, and at Palmer there were few simultaneous record-

ings during dayside passes. However, in the case of nightside satellite observations at L = 2 to 3, a number of recordings were made at Palmer (L ≈ 2.4), and cases have previously been found in which whistlers occurred in close time coincidence with the electron bursts in the L = 2 to 3 range [Voss et al., 1984; McNerney et al., 1987]. An example occurred on September 9, 1982 and was presented by Voss et al. [1984]. Another example, from October 20, 1982, is shown in Figure 11. The upper two panels show the 0 to 10 kHz dynamic spectrum and 2 to 3 kHz log amplitude of the VLF wave activity at Siple. As in the case reported by Voss et al. [1984], the satellite was in the northern hemisphere and at a longitude roughly 1600 km to the west of the conjugate point to Palmer Station. Arrows beneath the wave amplitude records show the times of the radio atmospherics of the lightning discharges for the five prominent whistlers, each of which preceded a surge in the electron count rate by ~0.5 s.

In the daytime, only one electron burst event at L = 2 to 3 was recorded near the meridian of Palmer Station or its conjugate, as indicated in Figure 6. This event, illustrated in Figure 1, occurred during a period when whistlers propagating in the L range 2.8 to 3.0 were recorded at rates of 20 to

S81-1 SEEP LOCAL DAY PASSES

DATE (1982)	TIME (UTs)	LONG (deg E)	LAT (N/S)
25 NOV	11265	122	N
3 NOV	20034	84	N
3 NOV	11038	101	S
26 SEP	85781	150	S
26 SEP	78833	197	N
22 SEP	35751	17	N
22 SEP	25067	63	N
12 AUG	81387	167	S
11 AUG	51059	279	S
7 AUG	76916	184	S
7 AUG	55848	260	S
6 AUG	56993	257	S
6 AUG	51690	177	S
6 AUG	46439	291	S
6 AUG	48817	286	S
6 AUG	43488	309	S
3 AUG	81600	165	S
3 AUG	55320	260	S
3 AUG	7023	118	S
1 AUG	57861	250	S
31 JUL	59030	249	S
30 JUL	49723	283	S
30 JUL	44403	304	S
30 JUL	42352	350	N
29 JUL	56256	256	S
29 JUL	50949	276	S
29 JUL	49023	319	N
28 JUL	46805	297	S
27 JUL	53456	265	S
27 JUL	48146	285	S
26 JUL	59922	246	S
26 JUL	49350	284	S
26 JUL	44019	306	S
25 JUL	45257	301	S
24 JUL	72891	200	S
24 JUL	51812	276	S
24 JUL	46516	296	S
24 JUL	44475	341	N
20 JUL	51447	276	S
18 JUL	53897	267	S
12 JUN	48675	320	N
29 MAY	60636	269	N
29 MAY	51807	277	S
28 MAY	53097	273	S

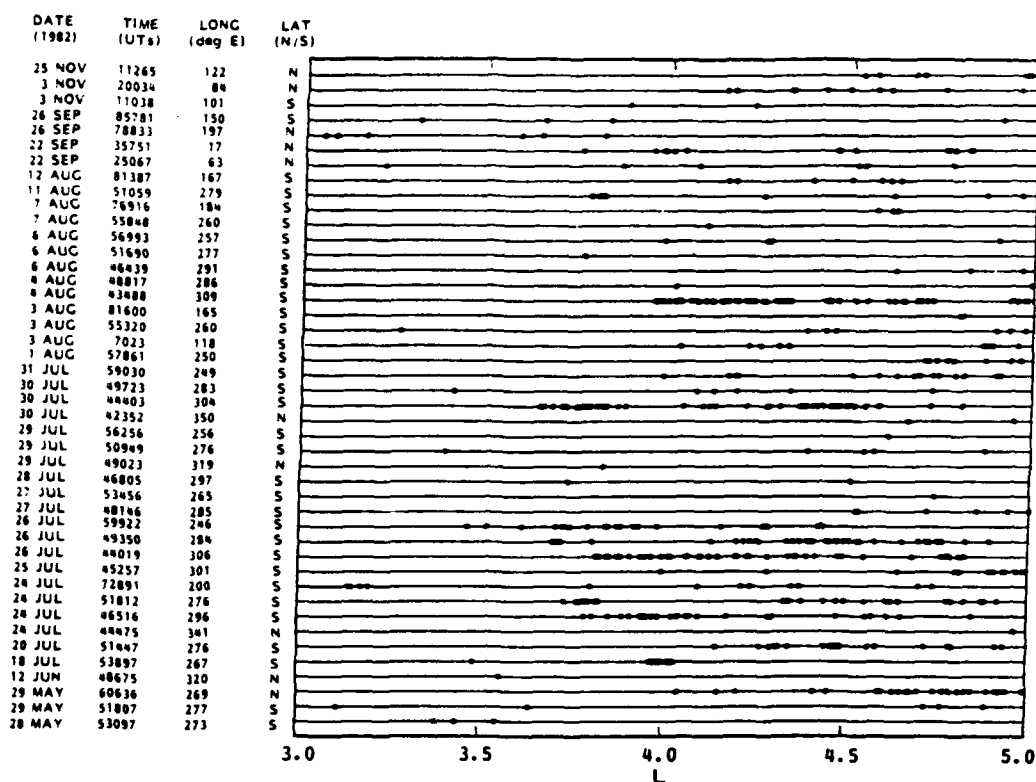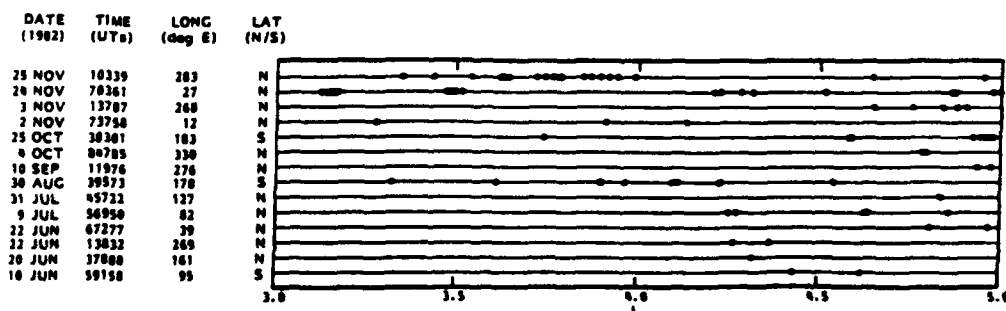3.0   3.5   4.0   4.5   5.0

L

Fig. 10a. Each narrow burst with a time width of 0.3 s or less plotted as a function of L during each of several orbits in which at least one narrow burst was observed over the range L = 3 to 5.

40 per minute at Palmer Station. It is likely that the weak burst events in Figure 1 near L = 2.8 were associated with this ducted whistler activity, and that the burst at L = 2.47 was induced by a particularly strong whistler component which propagated on a nonducted path originating close to a source lightning discharge.

The nightside and dayside particle observations at L > 3 were supported by a number of simultaneous wave recordings at Siple. Of 40 passes within ±50° of the Siple meridian on which one or more narrow bursts (<0.3 s) were detected, simultaneous ground recordings either continuous or on a 2 s out of 5 s basis were available during 17. For the remaining 23 passes, 1-min synoptic recordings either continuous or on a 2 s out of 5 s basis were available within several minutes of the SEEP pass. Thirty-three of the forty passes were on the dayside, and during or near each of these, chorus activity was observed at Siple. An example is that of Figure 1, in which discrete chorus elements appear against a relatively continuous band of background noise.

In many of the 33 dayside cases there was also whistler activity, with triggering of chorus bursts in the 1 to 4 kHz range by whistler components propagating outside the plasmapause. This type of spectral record is interpreted as evidence that the plasmapause L value was equatorward of

S81-1/SEEP LOCAL NIGHT PASSES

DATE (1982)	TIME (UTs)	LONG (deg E)	LAT (N/S)
25 NOV	10339	203	N
24 NOV	70361	27	N
3 NOV	13707	268	N
2 NOV	73738	12	N
25 OCT	38301	183	S
4 OCT	84785	330	N
10 SEP	11976	276	N
30 AUG	39573	178	S
31 JUL	45733	137	N
9 JUL	56950	82	N
22 JUN	67277	39	N
22 JUN	13832	269	N
20 JUN	37888	161	N
10 JUN	59158	95	S

3.0   3.5   4.0   4.5   5.0

L

Fig. 10b. Each narrow burst with a time width of 0.3 s or less plotted as a function of L during each of several orbits in which at least one narrow burst was observed over the range L = 3 to 5.
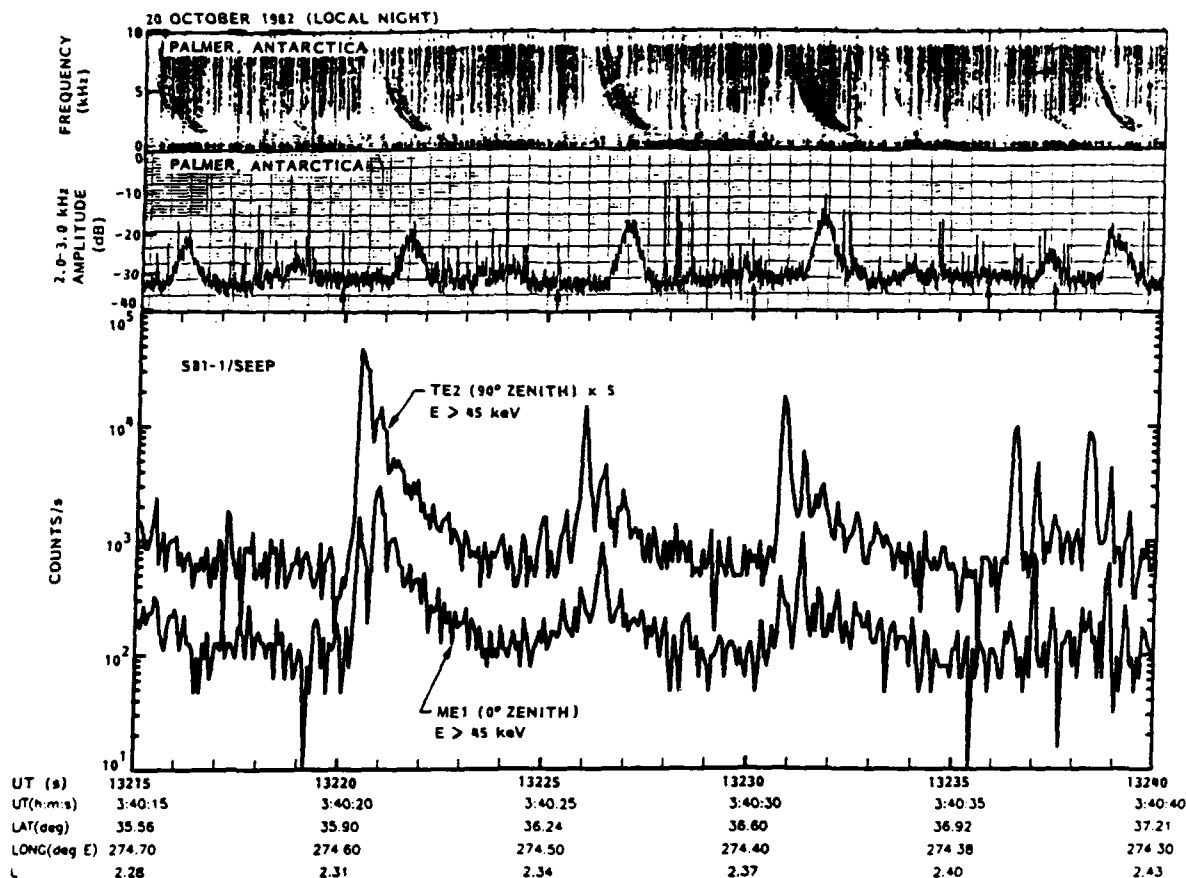
Fig. 11. In the top sections are shown the frequency-time record and the integrated wave intensity as recorded at Palmer Station. Arrows beneath the wave amplitude records show the times of the causative atmospherics of the five principal whistlers. In the bottom section the counting rates in the ME1 (>45 keV) detector at 0° zenith angle and the TE2 (>45 keV) detector at 90° zenith angle are plotted as a function of time. Ephemeris information for the satellite pass is provided at the bottom of the figure.

Siple [e.g.. Helliwell et al., 1980], as it was found to be for the pass of Figure 1. Both the dispersion properties of the whistlers surveyed and the high Kp levels associated with many of the dayside passes suggest that in most of these cases. the plasmapause was actually at $L < 4$ [e.g., Carpenter. 1966: Carpenter and Park, 1973]. Thus. the bulk of the narrow electron bursts observed on the dayside at $L > 3$ are inferred to have occurred poleward of the plasmapause and in the low density region where chorus is a major form of natural wave activity [Burtis and Helliwell, 1976].

For reasons discussed below, it was not anticipated that the individual chorus waves associated with electron bursts would be readily identifiable on ground records. In fact. such an identification was not achieved in the 17 cases for which simultaneous wave and particle data were available. Figure 12 shows the electron precipitation data from a dayside pass close to Siple (within ~2° at $L = 4.3$). The simultaneous 0 to 5 kHz VLF spectrum at Siple is illustrated in 2-s segments, showing two active frequency bands and numerous discrete rising chorus elements. Also shown is an amplitude record representing integrated field strength in a 300-Hz band centered at 1.5 kHz. A one-to-one correlation between chorus peaks and electron bursts is not evident. but the durations in time of the VLF amplitude enhancements are comparable to those of the electron bursts.

To illustrate the complex relations between the wave and electron data during the 40 passes within ±50° of the Siple meridian. we show in Figure 13 and 14 two of the four cases when continuous ground VLF recordings at Siple (a synoptic record of 53-s duration). were available during the satellite pass.

Figure 13 shows a dayside case in which the satellite crossed $L = 4.3$ about 20° east of Siple (~540 km). High burst activity was observed on the satellite, while the wave activity included pulsating (~10 s) clusters of chorus elements within a band below ~1 kHz and sporadic 2 to 3 kHz bursts, some of which were found to be triggered by whistlers.

Figure 14 shows another dayside case from ~20° west of Siple. In this case there was a prominent band near 1 kHz with many associated rising elements. Many of these risers appear to be part of a less steady higher-frequency band at 2.5 kHz.

While one-to-one correlations of narrow electron bursts with ground observed waves proved elusive. a close relation appears to have existed between a high rate of narrow bursts on the satellite at $L > 3$ in daytime and the observation of precipitation-induced ionospheric perturbations overhead Siple of the type reported previously by Rosenberg et al. [1971]. Helliwell et al. [1980], and Arnoldy et al. [1982]. In
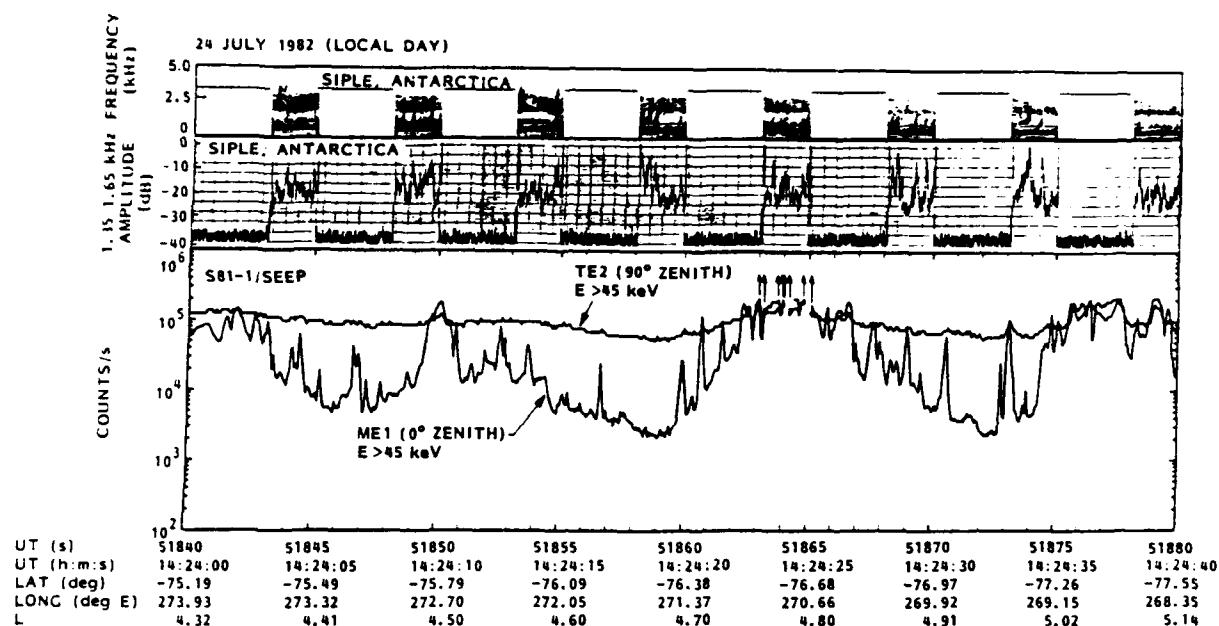
Fig. 12. In the top sections are shown the frequency-time record and the integrated wave intensity as recorded at Siple Station. In the bottom section the counting rates in the ME1 (>45 keV) detector at 0° zenith angle and the TE2 (>45 keV) detector at 90° zenith angle are plotted as a function of time.
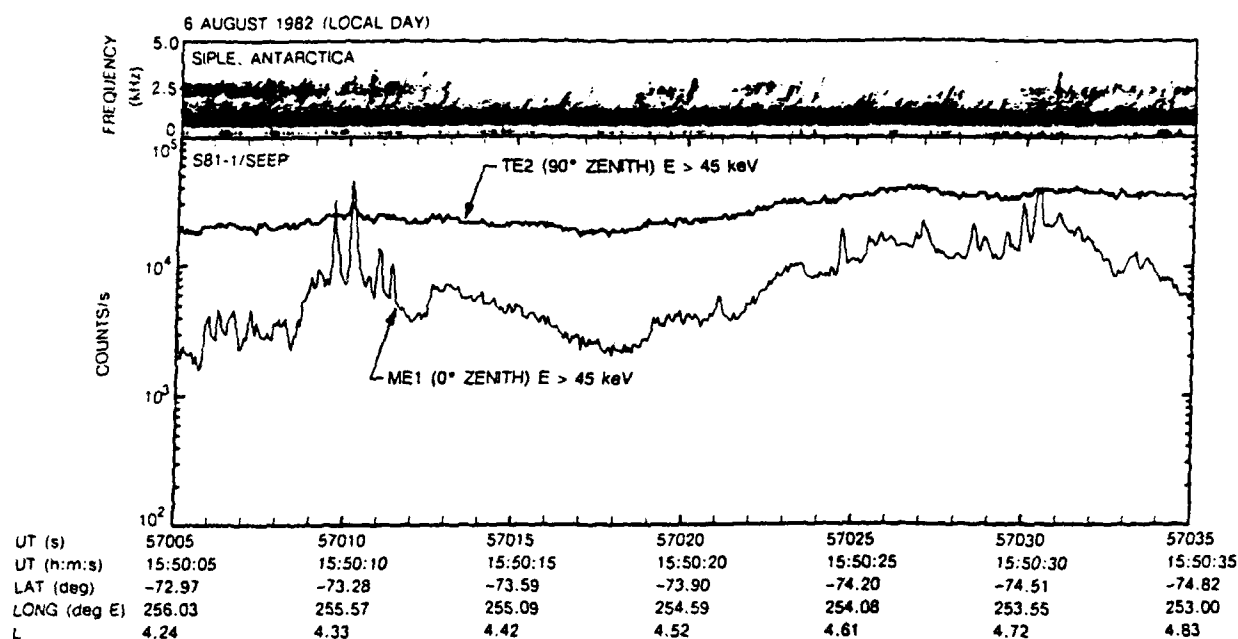
ground records of photometers, riometers, wave magnetometers, and VLF receivers, this precipitation often appears in the form of quasi-periodic pulsations lasting from one to several seconds and separated by 5 to 30 s. On several occasions, such pulsations have been clearly linked to burstlike clusters of VLF chorus elements, some of which were triggered by whistlers [Rosenberg et al.. 1971; Helli-

well et al., 1980], and a few case studies have shown a link between the fine structure within multielement chorus bursts and X ray microbursts [Rosenberg et al.. 1981], as well as a connection between individual chorus elements and brief (<1 s) optical pulsations [Tsuruda et al.. 1981].

During 9 of the 61 dayside passes studied. the satellite was in the southern hemisphere and crossed L = 4 within ~8° or less
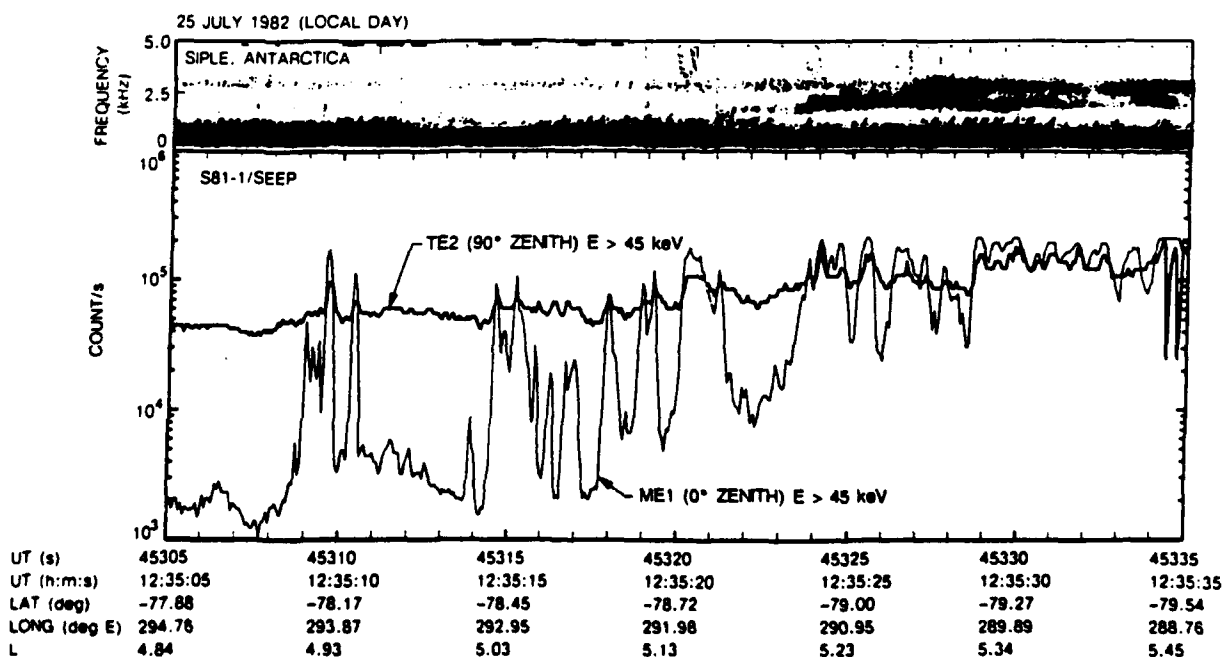
Fig. 13. In the upper section is shown the frequency-time record as recorded at Siple Station. In the bottom section the counting rates in the ME1 (>45 keV) detector at 0° zenith angle and the TE2 (>45 keV) detector at 90° zenith angle are plotted as a function of time.

6 AUGUST 1982 (LOCAL DAY)

SIPLE, ANTARCTICA

S81-1/SEEP

TE2 (90° ZENITH) E > 45 keV

ME1 (0° ZENITH) E > 45 keV

UT (s)	57005	57010	57015	57020	57025	57030	57035
UT (h:m:s)	15:50:05	15:50:10	15:50:15	15:50:20	15:50:25	15:50:30	15:50:35
LAT (deg)	−72.97	−73.28	−73.59	−73.90	−74.20	−74.51	−74.82
LONG (deg E)	256.03	255.57	255.09	254.59	254.08	253.55	253.00
L	4.24	4.33	4.42	4.52	4.61	4.72	4.83

Fig. 14.   In the upper section is shown the frequency-time record as recorded at Siple station. In the bottom section the counting rates in the ME1 (>45 keV) detector at 0° zenith angle and the TE2 (>45 keV) detector at 90° zenith angle are plotted as a function of time.

of the Siple longitude (and thus passed within ~220 km of the station). In 5 of these 9 cases. the number of short bursts detected between $L = 3$ and $L \approx 5$ was relatively small (1, 3, 5, 5, 6), and in only one of these cases was overhead burst precipitation clearly indicated at Siple. However, in the remaining four cases. there were 10 or more narrow electron bursts recorded on the SEEP payload (10, 18, 24, 35), indicating a high temporal rate of activity. In all four of these cases, overhead perturbations of several seconds duration were clearly detected at Siple, as indicated by correlated changes in the 2 to 4 kHz integrated amplitude and one or more of the outputs of a riometer, photometer, and magnetometer. These precipitation episodes, lasting 1 to 3 hours, were detected either during the SEEP pass or within less than one hour before or after the pass. In all four cases, the activity had been recognized by the Siple Station observer.

Figure 15 shows portions of the Siple station analog chart

used to monitor the outputs of multiple sensors. The record is from July 24, 1982. and represents an interval within 10 min of the nearly overhead SEEP pass illustrated in Figure 12. The charts indicate that this type of activity had been underway for at least 30 min prior to the SEEP pass and that it continued for at least 90 min afterward. Peak to peak correlations exist between many of the changes on the VLF and optical records. although the VLF surges are broader. probably due to contributions from magnetospheric wave paths outside the field of view of the vertical looking photometer.

DISCUSSION

Our study suggests that narrow (<1 s) burst activity is a global phenomenon. occurring at essentially all longitudes and at latitudes both within and beyond the plasmasphere. At $L = 2$ to 3 there appears to be some clustering of the

SIPLE, ANTARCTICA   24 JULY 1982
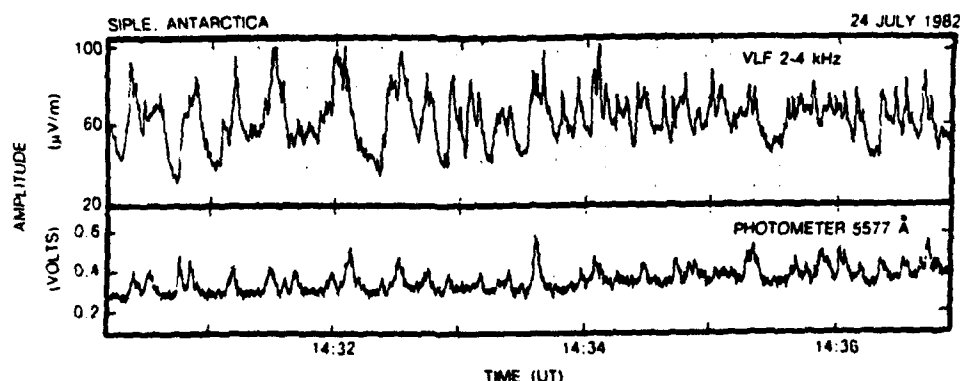
VLF 2-4 kHz

PHOTOMETER 5577 Å

Fig. 15.   Portions of the Siple Station analog chart for July 24. 1982. showing VLF amplitude in the 2 to 4 kHz band and the intensity of the 5577-Å line excited by precipitating electrons.

activity in local time, longitude, and hemisphere, due to the mixed effects of whistler source activity, day-night differences in ionospheric absorption of VLF waves, magnetic field topology, and instrument sensitivity. Our study further suggests that the bulk of the narrow bursts occurred as the result of interaction with transient VLF waves. This conclusion is supported by the electron observations themselves, which showed energy spectra and time and pitch angle signatures that were generally consistent with previous theoretical and experimental studies of particle scattering by VLF waves. The burst events at $L = 2$ to 3 were rare by comparison to the $L = 3$ to 5 activity, both in terms of the number of passes on which one or more events were detected and the occurrence of multiple events on a given pass. This feature is believed to be linked to the quasi-continuous nature and wide spatial distribution of chorus activity above $L = 3$, and to the concentration of this chorus activity outside the plasmapause, where trapped particle fluxes tend to be larger than those near the slot region. In comparison ducted whistlers tend to occur irregularly, at highly variable average rates and are most common on paths within the plasmasphere [Carpenter and Sulic, 1988].

The absence of one-to-one correlations between electron bursts and chorus elements and the presence of such correlations with whistlers can be partially understood as follows. In the case of a whistler the lightning source usually excites multiple ducted paths and also illuminates magnetospheric regions in which energy propagates in the nonducted mode. Because of the spatially distributed and both ducted and nonducted nature of this propagation, whistler components received at a ground station will mark the occurrence of a whistler, without in fact being that specific part of the whistler-mode energy involved in producing an observed particle event. On the other hand, in the case of chorus, there may be no mutual coherence between chorus elements originating spontaneously at various high altitude locations distributed in L value and longitude. Thus, if on ground records, a chorus element is to serve as a marker of a particular satellite-observed electron burst, the element must be a propagated component of the actual driving wave. Meanwhile, however, it will tend to be mixed with wave contributions from high altitude regions whose ionospheric projections are not being probed at that time by the satellite. However, if chorus bursts are whistler-triggered over a distributed region, a large measure of spatial coherence will be present and there should be increased probability of detecting correlations. This type of burst has been observed in several of the ground and balloon-based correlations reported to date [Rosenberg et al., 1971; Helliwell et al., 1980].

If the chorus elements associated with a series of electron bursts are nonducted, they are not likely to be observed on the ground at all because of wave absorption and reflection within the magnetosphere [Kimura, 1966; Edgar, 1976]. Nonducted chorus may have been a factor in both the $L > 3$ and $L < 3$ electron bursts observed on the dayside. At $L < 3$ nonducted chorus of the special type reported by Poulsen and Inan [1988] may have been involved as well as whistlers and ducted chorus events. The Poulsen and Inan chorus was found to occur at $2 < L < 4.5$, preferentially in the dawn sector under relatively disturbed conditions and within a frequency band whose limiting frequencies varied with satellite L value. On many satellite records it was the dominant

natural wave activity in an L range spanning the plasmapause.

Several-second-long precipitation bursts were observed overhead Siple during (or within one hour of) all four of the nearby SEEP passes on which more than 10 bursts were observed. We suggest that the satellite was sampling the electron population associated with the ground-observed activity. The narrow ~0.3-s bursts observed on SEEP were possibly due to individual spontaneous or whistler-triggered chorus elements of particularly high amplitude, while the wider, order of 10-second surges on the satellite may have been caused by the integrated effects of chorus elements closely spaced in time. While these surges may be related to the ground observations of several-second-long bursts, the connection is not yet clear. Dayside cases were found in which broader electron bursts, not qualifying as narrow events, were observed in the $L = 2$ to 3 range as the satellite passed close to the meridian of Siple (276°E) and Palmer (296°). In these cases, strong VLF chorus was detected at Siple ($L \simeq 4.3$) and Palmer ($L \simeq 2.4$), but one-to-one correlations between the envelopes of the wave and electron burst activity could not be established.

It is of interest to review the similarities and differences between the mid- and high-latitude bursts. Perhaps the most pronounced difference is that at midlatitudes the narrow bursts were often isolated, whereas at high latitudes they frequently occurred in trains. The evidence suggests that the midlatitude events occurred within the plasmasphere, with some possible exceptions on the dayside. In contrast, the more numerous high-latitude events occurred poleward of the plasmapause. After the initial burst the midlatitude events often showed secondary pulses that can be attributed to the bouncing of an electron bunch between hemispheres. At mid-latitudes the narrow events occurred more often near midnight than noon, apparently because of the combined effects of greater nighttime lightning activity and lower nighttime wave absorption in the ionosphere. At high latitudes the daytime activity was greater, apparently because of the dayside concentration of magnetospheric chorus activity.

Only the nighttime bursts at mid-latitudes frequently displayed a pronounced increase in median energy with time, consistent with electron scattering by a whistler train. Peaks in the energy spectra often occurred at night, but were seldom present in the daytime. Chorus is believed to be associated with the high-latitude events both at noon and midnight, and with perhaps some of the midlatitude bursts near noon, whereas the nighttime events at mid latitudes are believed to be associated with whistlers.

REFERENCES

Arnoldy, R. L., K. Dragoon, L. J. Cahill, Jr., S. B. Mende, and T. J. Rosenberg, Detailed correlations of magnetic field and riometer observations at $L = 4.2$ with pulsating aurora, *J. Geophys. Res.*, 87, 10.449, 1982.

Burtis, W. J., and R. A. Helliwell, Magnetospheric chorus: Occurrence patterns and normalized frequency, *Planet. Space Sci.*, 24, 1007, 1976.

Burton, R. K., and R. E. Holzer, The origin and propagation of chorus in the outer magnetosphere, *J. Geophys. Res.*, 79, 1014, 1974.

Cain, J. C., S. J. Hendricks, R. A. Langel, and W. V. Hudson, A proposed model for the international geomagnetic reference field, *J. Geomagn. Geoelectr.*, 19, 335, 1967.

Carpenter, D. L., Whistler studies of the plasmapause in the magnetosphere, 1, Temporal variations in the position of the knee and some evidence on plasma motions near the knee, *J. Geophys. Res.*, 71, 693, 1966.

Carpenter, D. L., and C. G. Park, On what ionospheric workers should know about the plasmapause-plasmasphere, *Rev. Geophys.*, 11, 133, 1973.

Carpenter, D. L., and D. M. Sulic, Ducted whistler propagation outside the plasmapause, *J. Geophys. Res.*, 93, 9731, 1988.

Carpenter, D. L., U. S. Inan, F. W. Pascual, and A. J. Smith, A new VLF method for studying burst precipitation near the plasmapause, *J. Geophys. Res.*, 90, 4383, 1985.

Edgar, B. C., The upper and lower frequency cutoffs of magnetospherically reflected whistlers, *J. Geophys. Res.*, 81, 205, 1976.

Foster, J. C., and T. J. Rosenberg, Electron precipitation and VLF emissions associated with cyclotron resonance interactions near the plasmapause, *J. Geophys. Res.*, 81, 2183, 1976.

Goldberg, R. A., S. A. Curtis, and J. R. Barcus, Detailed spectral structure of magnetospheric electron bursts precipitated by lightning, *J. Geophys. Res.*, 92, 2505, 1987.

Hardy, D. A., and W. J. Burke, Observations of auroral electron precipitation produced by VLF waves (abstract), *Eos Trans. AGU*, 68, 1440, 1987.

Helliwell, R. A., *Whistlers and Related Ionospheric Phenomena*, Stanford University Press, Stanford, Calif., 1965.

Helliwell, R. A., J. P. Katsufrakis, and M. L. Trimpi, Whistler-induced amplitude perturbation in VLF propagation, *J. Geophys. Res.*, 78, 4679, 1973.

Helliwell, R. A., S. B. Mende, J. H. Doolittle, W. C. Armstrong, and D. L. Carpenter, Correlations between λ4278 optical emissions and VLF wave events observed at $L \sim 4$ in the Antarctic, *J. Geophys. Res.*, 85, 3376, 1980.

Hurren, P. J., A. J. Smith, D. L. Carpenter, and U. S. Inan, Burst precipitation-induced perturbations on multiple VLF propagation paths in Antarctica, *Ann. Geophys.*, 4, 311, 1986.

Imhof, W. L., H. D. Voss, M. Walt, E. E. Gaines, J. Mobilia, D. W. Datlowe, and J. B. Reagan, Slot region electron precipitation by lightning, VLF chorus, and plasmaspheric hiss, *J. Geophys. Res.*, 91, 8883, 1986.

Inan, U. S., and D. L. Carpenter, On the correlation of whistlers and associated subionospheric VLF/LF perturbations, *J. Geophys. Res.*, 91, 3106, 1986.

Inan, U. S., and D. L. Carpenter, Lightning-induced electron

precipitation events observed at $L = 2.4$ as phase and amplitude perturbations on subionospheric VLF signals, *J. Geophys. Res.*, 92, 3293, 1987.

Inan, U. S., T. G. Wolf, and D. L. Carpenter, Geographic distribution of lightning-induced electron precipitation observed as VLF/LF perturbation events, *J. Geophys. Res.*, 93, 9841, 1988.

Inan, U. S., M. Walt, H. D. Voss, and W. L. Imhof, Energy spectra and pitch angle distributions of lightning-induced electron precipitation: Analysis of an event observed on the S81-1 (SEEP) satellite, *J. Geophys. Res.*, 94, 1379, 1989.

Kimura, I., Effects of ions on whistler mode ray tracing, *Radio Sci.*, 1, 269, 1966.

McNerney, P. C., U. S. Inan, W. L. Imhof, H. D. Voss, and M. Walt, A satellite-ground study of lightning induced electron precipitation events and their association with whistlers and VLF perturbations (abstract), *Eos Trans. AGU*, 68, 1222, 1987.

Mobilia, J., H. D. Voss, and W. L. Imhof, Lightning observations from the SEEP/S81-1 satellite (abstract), *Eos Trans. AGU*, 66, 1001, 1985.

Oliven, M. N., and D. A. Gurnett, Microburst phenomena, 3, An association between microbursts and VLF chorus, *J. Geophys. Res.*, 73, 2355, 1968.

Orville, R. E., and R. W. Henderson, Global distributions of midnight lightning: September 1977 to August 1978, *Mon. Weather Rev.*, 114, 2640, 1986.

Poulsen, W. L., and U. S. Inan, Satellite observations of a new type of discrete VLF emission at $L < 4$, *J. Geophys. Res.*, 93, 1817, 1988.

Rosenberg, T. J., R. A. Helliwell, and J. P. Katsufrakis, Electron precipitation associated with discrete very low-frequency emissions, *J. Geophys. Res.*, 76, 8445, 1971.

Rosenberg, T. J., J. C. Siren, D. L. Matthews, K. Marthinsen, J. A. Holtet, A. Egeland, D. L. Carpenter, and R. A. Helliwell, Conjugacy of electron microbursts and VLF chorus, *J. Geophys. Res.*, 86, 5819, 1981.

Rycroft, M. J., Enhanced energetic electron intensities at 100 km altitude and a whistler propagating through the plasmasphere, *Planet. Space Sci.*, 21, 239, 1973.

Tsuruda, K., S. Machida, T. Oguti, S. Kobubun, K. Hayashi, T. Kitamura, O. Saka, and T. Watanabe, Correlations between the very low frequency chorus and pulsating aurora observed by low-light-level television at $L = 4.4$, *Can. J. Phys.*, 59, 1042, 1981.

Turman, B. N., and B. C. Edgar, Global lightning distributions at dawn and dusk, *J. Geophys. Res.*, 87, 1191, 1982.

Voss, H. D., J. B. Reagan, W. L. Imhof, D. O. Murray, D. A. Simpson, D. P. Cauffman, and J. C. Bakke, Low temperature characteristics of solid state detectors for energetic X-ray, ion and electron spectrometers, *IEEE Trans. Nucl. Sci.*, NS-29, 164, 1982.

Voss, H. D., W. L. Imhof, M. Walt, J. Mobilia, E. E. Gaines, J. B. Reagan, U. S. Inan, R. A. Helliwell, D. L. Carpenter, J. P. Katsufrakis, and H. C. Chang, Lightning-induced electron precipitation, *Nature*, 312, 740, 1984.

D. L. Carpenter and U. S. Inan, STAR Laboratory, Stanford University, Stanford, CA 94305.

W. L. Imhof, J. Mobilia, H. D. Voss, and M. Walt, Lockheed Missiles and Space Laboratory, Dept. 91-20, Bldg. 255, 3251 Hanover St., Palo Alto, CA 94304.

APPENDIX B

PRECIPITATING ELECTRONS WITH PEAKED ENERGY SPECTRA

Cyclotron Resonance Precipitation of Energetic Electrons From the Inner Magnetosphere

D. W. Datlowe and W. L. Imhof

Lockheed Palo Alto Laboratory. Palo Alto, California

Cyclotron resonance between trapped energetic electrons and VLF waves produces pitch angle scattering which leads to electron precipitation in the inner magnetosphere. Previous experiments have shown that in the drift loss cone at L values from 1.5 to 1.8 the energy spectrum of the electrons above 50 keV is often dominated by a single narrow peak. The center energy of this peak varies with L in a manner characteristic of cyclotron resonance between the electrons and monochromatic VLF waves in the vicinity of the geomagnetic equator. The source of the waves is probably VLF communication or navigation transmitters. We report here the results of a study of 680 occurrences of these peaks detected by the low altitude polar orbiting satellite S81-1. The present data. from altitudes between 170 and 270 km. show the resonance peaks only in two restricted longitude zones centered at 110°E and 300°E; this result contrasts with the previous measurements at higher altitudes, which detected peaks over a wide range of longitudes. The majority of nighttime events were near transmitter locations where the cyclotron resonance condition was met by electrons with pitch angles near the edge of the loss cone. Detailed study of the events occurring near 110°E reveals a 27-day periodicity in the frequency of occurrence; peaks are most often observed during minima in solar/geomagnetic activity. The peaks observed at nighttime in both longitude zones have a possible seasonal variation, being most frequent when it is wintertime at the site of the VLF transmitters responsible for the precipitation.

INTRODUCTION

Peaks in the spectrum of energetic (~100-keV) electrons are often observed by low altitude satellites in the inner magnetosphere. *Imhof et al.* [1973] reported that the spectrum of electrons observed in the inner magnetosphere may be narrowly peaked, and that the energy of that peak increases rapidly with decreasing L value. The energy of the peak follows approximately the L dependence which is expected from first-order cyclotron resonance between the electrons and fixed frequency VLF waves [*Brice,* 1964]. Therefore these peaks are attributed to resonant interactions between trapped electrons and ground-based transmitters as a source of nearly monochromatic waves [*Imhof et al.,* 1974; *Vampola and Kuck,* 1978].

Electron spectra with peak energies which follow cyclotron resonance relation are most prominent in the range from $L = 1.6$ to $L = 1.9$ [*Imhof et al.,* 1974, Figure 2]. The peaks are found in the region of quasi-trapped electrons, particles which are locally trapped but will precipitate into the atmosphere as their drift motion carries them eastward. The peaks have been observed over the longitude range from 60°E to 300°E [*Vampola and Kuck,* 1978, Figure 5; *Imhof et al.,* 1978]. Within this longitude range, no apparent clustering of either the frequency of occurrence or the intensity of these events has been reported. Peaks at higher L values (L ~ 2.5) have been detected by these experiments, but we will confine the present discussion to peaks at L values below 2.0.

Five different satellite programs have observed these peaks, starting in 1968 on OV1-14 and OV1-19 [*Vampola and Kuck,* 1978]. 1971-089A and P72-1 [*Imhof et al.,* 1974], on S3-3 [*Vampola,* 1987], and on P78-1 [*Imhof et al.,* 1981]. Some of these instruments have had high spectral resolution

but limited pitch angle resolution, while others have had fine pitch angle resolution but broad energy channels. The experiments are in agreement that pitch angle scattering by ground-based transmitters is responsible for the occurrence of these peaks. However, the published results do not agree on probable longitudes of the interactions which scatter the electrons or on the frequencies of waves causing the interactions.

We report here on a survey of 680 occurrences of cyclotron resonance peaks observed by an electron spectrometer on the Stimulated Emission of Energetic Particles (SEEP) payload on the S81-1 satellite. The SEEP electron data were acquired from May to December 1982; because of uniform temporal and spatial coverage during that time we have been able to search for periodicities and long term (~7 month) variations in the precipitation which may have occurred during the observing period. We report for the first time a 27-day variation which is anticorrelated with solar activity, attributable to changes in the coupling of the ground-based transmitters to the interaction region. We also have found a long term or seasonal variation in the frequency of occurrence of the peaks.

These observations differ from the previous experiments because the vehicle was at much lower altitude. Proximity to the atmospheric scattering layer restricts the distance an electron may have drifted since scattering into the drift loss cone. With these data we are able to localize the cyclotron resonance peaks which are recorded during satellite nighttime to two longitude zones. One zone of occurrence of peaks is in the eastern hemisphere from 90°E to 150°E. The second region is primarily in the western hemisphere and spans the longitude range from 100°W to 20°E. The clustering of peaks at certain longitudes, and the occurrence of the most intense ones at the longitudes of known VLF transmitters. permits us to identify NWC at 114°E and NAA/NSS near 290°E as significant contributors to the precipitation.

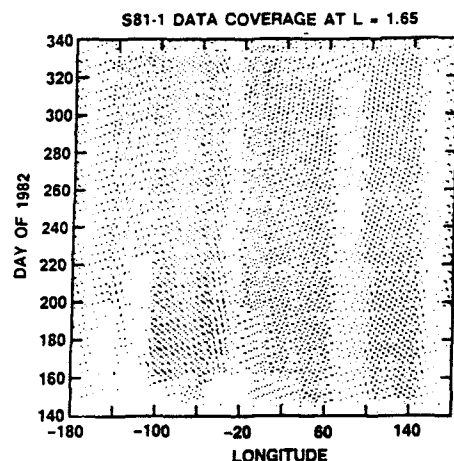6478   DATLOWE AND IMHOF: RESONANCE PRECIPITATION OF ELECTRONS

Fig. 1. SEEP data coverage. Each point in this plot represents the time and geographic longitude of data coverage at L = 1.65. The vertical coordinate is the day of 1982 (142–339), and the horizontal coordinate is the geographic longitude.

INSTRUMENTATION

The S81-1 satellite was in a polar orbit, ranging in altitude from 170 to 290 km. The orbit was Sun synchronous, covering local times 1030 and 2230; the vehicle passed over any given place on the ground twice per day, once in daylight and once at nighttime. The spacecraft was three-axis stabilized.

The payload contained an array of instrumentation, but all of the observations reported here came from a single electron spectrometer, referred to as TE2. The spectrometer was a solid state detector, covering the range 6–1000 keV in 256 pulse height channels. The detector system was cooled to achieve high energy resolution, and spectral broadening by detector noise was very small. The geometric factor was 0.17 cm^2 sr. The field of view was always centered at 90° from the zenith, looking horizontally, and therefore it measured the flux of particles mirroring at the altitude of the satellite. We can calculate the equatorial pitch angle of the observed particles using the ratio of the local magnetic field to the equatorial magnetic field for the same field line.

The data acquisition period was from May 24 to December 5, 1982. During this time interval the SEEP particle detectors returned data for 68% of the approximately 12,600 possible crossings of L = 1.65. A high degree of coverage is required to search for time variations without introducing any bias due to periodicities in the sampling. The uniformity of the sampling is demonstrated in Figure 1, which shows the data coverage as a function of longitude and time. Each dot on the plot represents an observation in the data base searched for events. It is evident from the plot that after June 1 (day 152) the longitude coverage was largely uniform, with somewhat less coverage near 25°W, 70°E, and 150°E. The uniformity in the temporal direction of the plot will be important later, as it is essential for detecting the 27-day and long-term variations. The apparent patterns in the plot are due to the fact that the orbital period divided almost evenly into three days; the patterns are the slow drift from the remainder. A 1-day

gap in the data coverage on day 217 (August 5) is evident in the figure.

Special color video displays were created to permit efficient scanning of the TE2 spectra during the many passes. We have surveyed the entire set of data from the TE2 electron detector for cyclotron resonance peaks, at all longitudes and for both day and night. However, only peaks in the range of L = 1.5 to L = 2.0 were recorded: peaks at other magnetic latitudes, if present, were not included in this survey. In all, 680 occurrences of cyclotron resonance peaks were identified both at satellite daytime and satellite nighttime. In this paper we will consider only the 361 events which occurred at satellite nighttime.

ENERGY SPECTRA

The cyclotron resonance condition [Brice, 1964] is given by the equation

$$\omega - k \cdot v = m\Omega \qquad (1)$$

In this formula, ω is the VLF wave angular frequency, k is the VLF wave vector, v is the electron velocity vector, Ω is the cyclotron angular frequency, and m is the order of the resonance. Evaluation of the wave vector k introduces the wave normal angle and the index of refraction for the whistler mode. The index of refraction in turn depends on the electron cyclotron angular frequency Ω, the plasma frequency ω_p, and the transmitter frequency. We note that at the L values of our observations the transmitter frequencies (~20 kHz) are much smaller than the equatorial cyclotron frequency (~200 kHz) or the equatorial plasma frequency (~500 kHz). For numerical calculations we have used the form of the equations in Koons et al. [1981]. Details of the calculation of the resonant energy in the relativistically correct form will be found in the appendix.

The SEEP TE2 detector directly measured the flux of electrons mirroring at the altitude of the satellite as a function of energy. We calculate the equatorial pitch angle of locally mirroring electrons from the ratio of local to equatorial magnetic fields at the point of observation. Typical values for the equatorial pitch angles may be 20°–30° depending on satellite location, with a spread of the order of 1° due to the acceptance angle of the collimator.

The basic evidence that the electron scattering is due to the cyclotron resonance condition comes from the variation of the central energy of the peaks with L value [Imhof et al., 1974]. A sequence of electron spectra at different L values shows a variation in the energy of the peak. The variation is sufficiently characteristic, and the interaction sufficiently strong, that sequences of this type may be readily identified in surveys of electron data. Figure 2 is an example of a series of electron spectra which show the effect. The figure consists of eight individual electron spectra, in chronological order, from L = 1.95 to L = 1.69. Each spectrum shows a peak, starting at ~40 keV for the highest L value to ~180 keV for the lowest L value. The spectra acquired outside this L value range on the same pass did not show any evidence of peaks. To show the spectra over the full range of L values, the figure shows 8-s accumulations of data. Since the center energy of the peak shifts on a time scale comparable to 8 s, the width of the peaks is broadened by the accumulation. For example, in a 1-s accumulation the peak at L = 1.72 has a full width at half maximum (FWHM) of 16 keV at an

S81-1/SEEP
ELECTRON SPECTRUM
27 AUGUST 1982

FLUX (ELECTRONS/cm²·s·sr·keV)

1.69
1.72
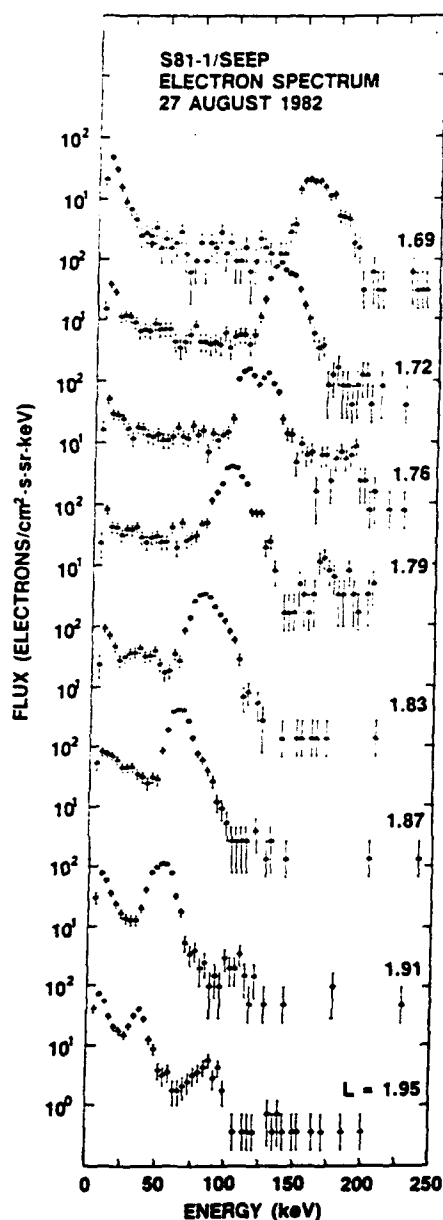1.76
1.79
1.83
1.87
1.91
L = 1.95

ENERGY (keV)

Fig. 2. Electron spectra from August 27, 1982. This figure shows eight individual electron spectra. Each point represents the flux in an individual channel 3.7 keV wide, and the counting statistics are indicated by the vertical error bars. The L value, from 1.69 to 1.95, is indicated at the right of each trace.

energy of 130 keV, but the 8-s accumulation in the figure shows a 25-keV FWHM. The most intense peak flux was about 225 electrons (el) $(cm^2 \ s \ keV \ sr)^{-1}$ at an energy of about 100 keV ($L = 1.78$), about 100 times more intense than the detector background at that time and location.

The variation in energy with L value is most easily visualized with the aid of a contour plot. Figure 3 shows the same data as contours of electron flux. The flux is a function of L value and the equatorial parallel energy of the observed electrons. As with all of the spectra, we assume that the electrons are locally mirroring at the altitude of the satellite, and we calculate the equatorial pitch angle θ from the ratio of

the local magnetic field to the equatorial magnetic field. The parallel energy at the equator is given by

$$E_{\parallel} = E \cos^2 \theta \qquad (2)$$

Figure 4 shows three additional examples of electron data with prominent cyclotron resonance peaks. In all four cases shown, the satellite was in the eastern hemisphere at longitudes near 120°E, and at nighttime.

The calculated resonance condition is shown as a dashed line in Figures 3 and 4, where we have used a transmitter 22.3-kHz frequency. This calculation assumes that the interaction region is near the geomagnetic equator and that the VLF waves propagate along the magnetic field. The physical quantities required to evaluate the wave vector are modelled using the geomagnetic field model of Olsen and Pfitzer [1974] and the plasma density model of Chiu et al. [1979]. The equatorial plasma density is subject to fluctuations, so it must be understood that mean values are used in the calculations. Since there was no simultaneous measurement of the VLF waves in the interaction region, transmitter frequency must be an assumption.

The variation in the intensity of electrons with L value in the figure shows that the contours of electron flux agree with the calculated resonance condition, confirming our assertion that cyclotron resonance interactions are present. This variation does not however confirm our choice of wave normal angle, transmitter frequency, or density model. In the appendix we show the sensitivity of the calculated resonance energy to the assumed values of these parameters. We summarize the appendix by noting that all of the choices give curves of comparable shape, but resonance energies different by a factor of 2 are entirely within the range of possible parameters. The appendix also shows that only first-order resonance ($m = 1$) gives values in agreement with the data.

In the figures, variation with L value of the data points is more rapid than the calculated variation with L. Examination of a large number of comparable plots indicated that this is generally the case in the SEEP data. Likewise the data values shown in Imhof et al. [1974] often vary more rapidly than the curve which the authors calculated. Possible explanations for the difference include wave normal angles which depend on L value and density gradients which are smaller than in the model used; however, low altitude electron measurements alone do not provide enough information to answer this question.

From the agreement between the electron data and the calculated locus of the cyclotron resonance condition, we can see that the 22.3-kHz frequency of NWC is a good choice. Because so many model-dependent quantities are included in the calculation, we cannot use this agreement to identify 22.3 kHz as the wave frequency. The primary evidence we have for identifying the VLF transmitters which are the origin of the cyclotron resonance peaks is geographic: the locations where the peaks occur most frequently and the locations where the most intense peaks have been detected.

LOCATIONS OF THE EVENTS

Due to the offset of the axis of the geomagnetic field from the geographic center of the Earth, there is a set of drift shells which intersect the top of the atmosphere in the region
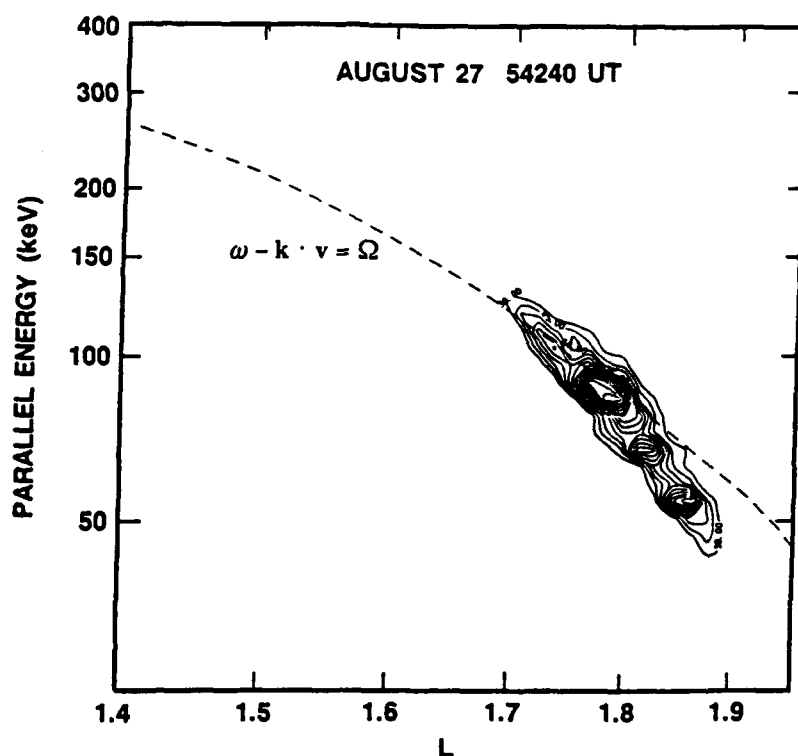
Fig. 3. Contour plot of the electron flux versus L value. The contours represent electron flux as a function of L value and $E_{\parallel}$. The contours are spaced linearly in steps of 15 el $(cm^2 \, s \, sr \, keV)^{-1}$, with a minimum contour of 30 $(cm^2 \, s \, sr \, keV)^{-1}$. The dashed line indicates the cyclotron resonance condition for $f = 22.3$ kHz.

of the South Atlantic Anomaly. An electron may be temporarily trapped on these drift shells. However, on a time scale of hours, electrons drift eastward until the drift shell dips into the top of the atmosphere and the electrons are precipitated. On L shells where this can occur, the range of pitch angles over which electrons are quasi-trapped by this process is called the drift loss cone, where the background electron flux is quite low. Thus any process which produces even a small amount of pitch angle scattering of electrons into the drift loss cone is clearly visible.

The existence of a drift loss cone is very important for detecting cyclotron resonance effects. Pitch angle scattering which leaves the electron in the stably trapped population may require precise pitch angle distribution measurements in order to detect the effect. On the other hand, a transition from the stably trapped population into the quasi-trapped population can be detected on the basis of intensity measurements alone. The 680 SEEP cyclotron resonance events considered here were detected in the quasi-trapped electron population.

At certain locations in the orbit of a low altitude satellite the point where electrons mirror in the opposite hemisphere (the conjugate point) is below the ~100-km atmospheric scattering layer. For an electron to be detected over these geographic locations, it must have been scattered within the last few bounce periods (order of seconds). In this region, called the bounce loss cone, the SEEP satellite has detected transient events, such as lightning-induced precipitation [Voss et al., 1984] and precipitation by on-off modulated VLF transmissions [Imhof et al., 1983].

At magnetic L values less than 10, the S81-1 satellite spent about 71% of the time observing the quasi-trapped electron flux. The conjugate point to the satellite was below 100 km, and locally mirroring electrons were in the bounce loss cone, about 18% of the time. The remaining 11% of the time the satellite was in the region of stably trapped particles, primarily in the South Atlantic Anomaly.

Figure 5 shows a map of the locations of the 680 observed events. To show each event in a uniform manner, all events are plotted at $L = 1.65$, although individual events span a range of L values, and some may not show detectable flux at $L = 1.65$. Furthermore, we have separated the events into spacecraft night and day, as the two groups of events have significantly different longitude distributions. Physically, the night/day difference is expected on the basis of the greater attenuation of VLF waves in the ionosphere during the daytime.

The cyclotron resonance events fall into two restricted regions on the map, in contrast to the more widespread distributions reported by earlier satellites, which were at higher altitudes. The first zone runs from 90°E to 150°E, and peaks are observed only at night in this region. In this zone the mirror points for electrons are at approximately the same height in both the north and south. Thus a particle scattered into the drift loss cone can be seen at either end of the field line. In this zone, electrons mirroring at the altitude of the satellite have equatorial pitch angles in the range 21.2°–23.4°.

The second zone runs from 90°W to the prime meridian. Cyclotron resonance interactions occurring at almost any longitude could scatter electrons into drift shells which
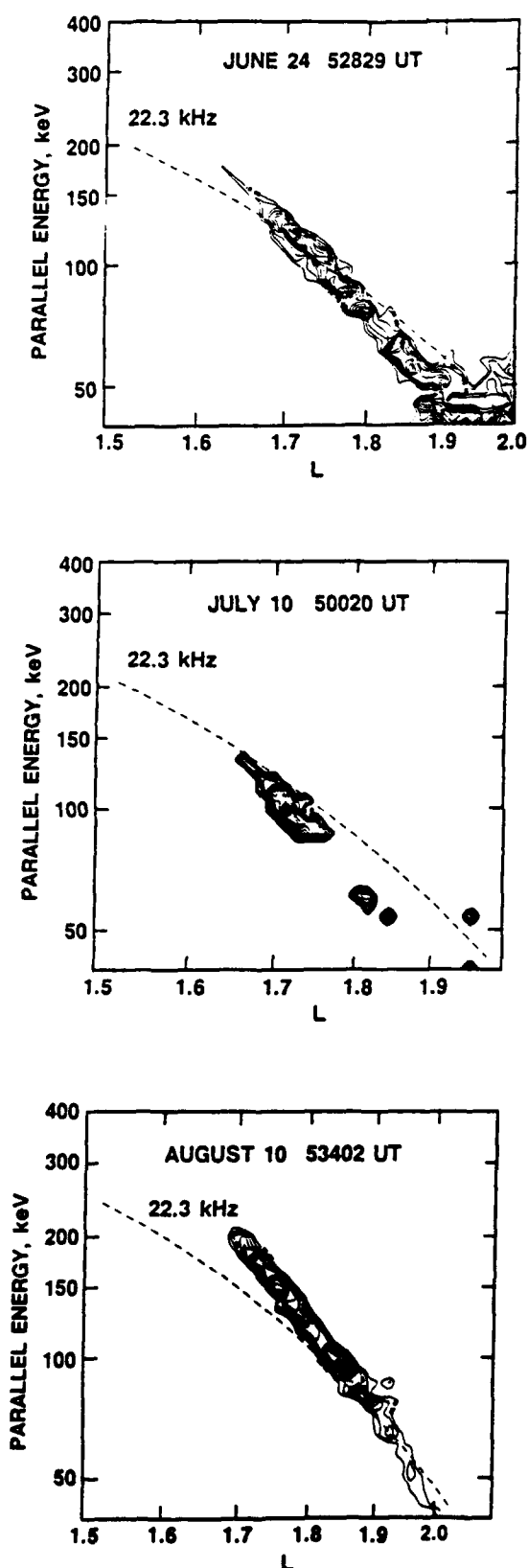
permit them to reach the second zone. Events are seen both during satellite day and satellite night in zone 2, although the region is broader in extent at night than during the day. In the western hemisphere zone, events are observed primarily in the south. In this region, the equatorial pitch angle of electrons mirroring at the altitude of the satellite ranges from 25° to 33°. Due to the larger equatorial pitch angle, the peaks in this western zone are more intense than their counterparts in the eastern hemisphere.

In Figure 5 we have also indicated the locations of major VLF communication transmitters. The locations of these transmitters are taken from *Inan et al.* [1984]. For reference, the location of Siple station, in Antarctica, is also indicated. The shaded regions on the map indicate the observing locations for which the conjugate point to the satellite was below 100 km.

We can relate the locations of the observed peaks directly to the characteristics of the drift loss cone. Figure 6 compares the equatorial pitch angles of the observed events to the equatorial pitch angle of an electron mirroring at the atmospheric scattering layer, here taken as 100 km. The lines show the calculated equatorial pitch angle for $L = 1.65$ using the magnetic field model of *Olsen and Pfitzer* [1974]; the continuous line is for electrons mirroring in the south, and the dashed line for electrons mirroring in the north. The lines are plotted only at longitudes where the calculated mirroring altitude in the conjugate hemisphere is also above 100 km. The plot shows that electrons at equatorial pitch angles greater than 32° are stably trapped. Electrons with equatorial pitch angles between 21° and 24° will drift into the atmosphere between 120°E and 180°E in the northern hemisphere; electrons with equatorial pitch angles between 24° and 32° will drift into the atmosphere between 260°E and 335°E in the southern hemisphere.

Cyclotron resonance peak events are indicated in the figure by individual symbols. The close tracking of the calculated curves and the peaks in the locally mirroring electrons is a consequence of the low altitude of the satellite. A satellite at the same longitudes but higher altitudes may see events in the drift loss cone (at $L = 1.65$) as long as the equatorial pitch angle of locally mirroring particles is less than 32°. The data for day and night events are shown separately.

A number of features are evident from this plot. First, the cluster of night events near 120°E must be due to a source in that vicinity. For example, electrons scattered into the drift loss cone at 60°E must have a pitch angle greater than 25°. Electrons drifting eastward from that point mirror at altitudes above the satellite until they reach the longitude of about 260°E. Accordingly, the source of the events near 120°E must be in the proximity of that region.

It is also evident from the figure that eastward of 140° the conjugate point for electrons in the south is below 100 km; accordingly the absence of points over eastern Australia (at $L = 1.65$) is expected. The loss of electrons can be tracked in the north to approximately 160°E.

If the electrons which make up the cyclotron resonance peaks have been scattered from the stably trapped population, then to reach an equatorial pitch angle of ~22° they must have been scattered by at least 10° in pitch angle. We take this as evidence for the hypothesis that the scattering is not a transient event, but a continuous process built up over many scatterings.

Fig. 4. Additional examples of cyclotron resonance peaks with $f = 22.3$ kHz. (Top) June 24, 52829 s UT, 118°E, 27°S. (Center) July 10, 50020 s UT, 120°E, 46°N. (Bottom) August 10, 53402 s UT, 116°E, 27°S.

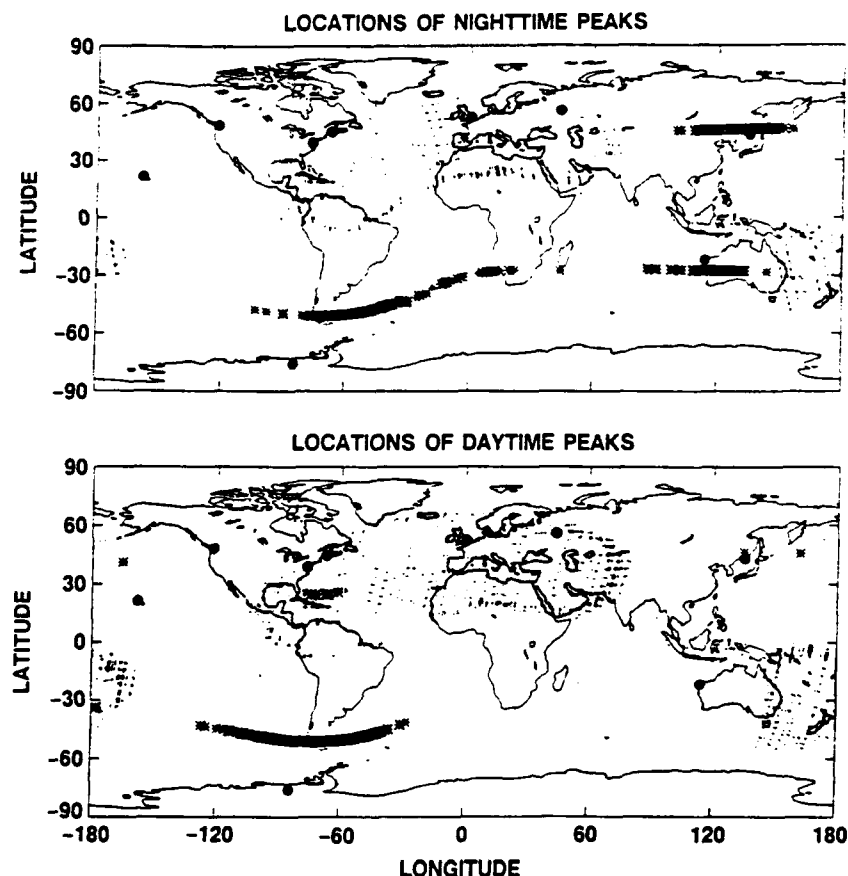## LOCATIONS OF NIGHTTIME PEAKS

LOCATIONS OF DAYTIME PEAKS

Fig. 5. Map of the locations of peaks recorded by SEEP. Each detection of cyclotron resonance peaks by SEEP is indicated by an asterisk. Major transmitters are indicated by solid circles, based on the listing in *Inan et al.* [1984]. The shaded areas indicate the two zones where the conjugate point to the satellite location is below 100 km.

The cyclotron resonance peak events observed during satellite daytime occur almost exclusively in the region where the equatorial pitch angle of the locally mirroring electrons is increasing with longitude. Note also that the easternmost end point of the daytime events is almost exactly the longitude of minimum altitude for electrons drifting with constant pitch angle. These facts lead to the suggestion that all of the cyclotron resonance interactions take place over transmitters in darkness, and that the daytime events consist of electrons which have drifted at least 120° in longitude to the point of observation.

PEAKS IN THE EASTERN HEMISPHERE

The prime focus of this study has been the events in the eastern hemisphere. From the color images of the electron data, 182 events were identified, and the locations of the satellite at those times were noted. Figure 7 shows, on an expanded scale, the distribution of the occurrence of these peaks. The data coverage was uniform between 80°E and 160°E in the north, with ~80 night passes in each 10° bin; in the south the coverage was also ~80 passes per bin between 100°E and 150°E, but outside this range there were fewer (~10) passes in each bin. The most prominent feature of this distribution is the very sharp onset in the bin from 110° to 120°E as one scans in the direction of electron drift. We take

it as no coincidence that the transmitter NWC is located close to the center of this bin, at 114°E. The transmitter RPS at 135°E may also contribute to this distribution.

The strongest evidence for NWC as the source of the waves which are precipitating the electrons comes from plotting the intensity of the peaks against longitude. To make a quantitative measurement, the event must have been sufficiently intense that a clear maximum could be identified in a contour plot similar to Figure 3. There were 149 events for which a suitable maximum contour could be identified; in the remaining 33 cases the flux was too small or the contours were too irregular to find a maximum. Since the flux and the energy of the peak change rapidly, on a scale comparable to the size of the energy and L value bins used to produce the plot, errors of up to 25% may occur in an estimate of the flux based on the maximum contour. The results are shown in Figure 8, which shows that the three most intense peaks occur within a few degrees of the longitude of NWC, as do most of the strong ones. We take this clustering of events about the station as definitive evidence that NWC is the source of the waves which produce the bulk of the events on this plot. A single strong event near 135°E may be a contribution from RPS, as may be the more easterly events. Nonetheless, we attribute the majority of the peaks to interactions with waves from NWC. The most intense event
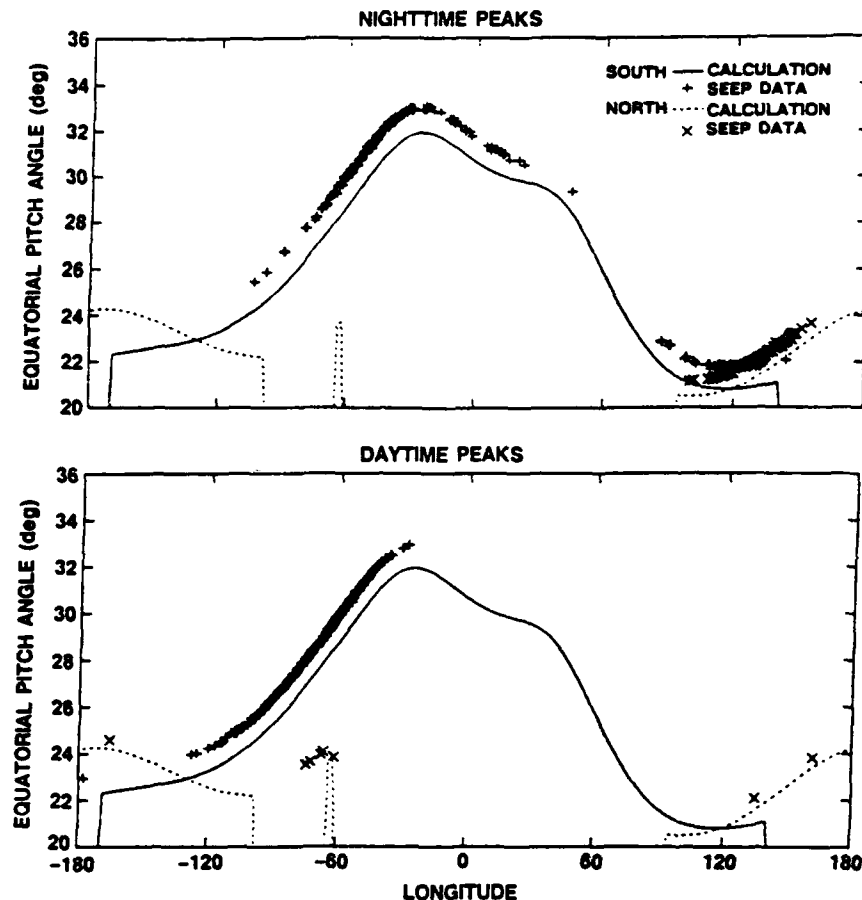
NIGHTTIME PEAKS

DAYTIME PEAKS

Fig. 6. Equatorial pitch angle of $L = 1.65$ electrons at the edge of the bounce loss cone versus longitude. The solid lines shows the calculated pitch angle for electrons mirroring at 100 km in the south, and the dashed lines show the same calculation for the north. The individual events are indicated by plus signs for the south and crosses for the north. Events detected in satellite nighttime and in satellite daytime are shown separately.

occurred on July 18; Figure 9 is a contour plot of electron flux versus parallel electron energy and L value of that event.

Peaks in the Western Hemisphere

The survey of cyclotron resonance peaks at nighttime also found 179 occurrences in the vicinity of South America and the South Atlantic. Seventy-seven percent (139/179) of the observed peaks occurred at longitudes from 30°W to 80°W, a range of 50°. This geographic region is important because it includes the conjugate points to several strong VLF transmitters in the United States. The routine detection of cyclotron resonance peaks in this geographic area is a unique feature of the low altitude of the S81-1 orbit. At the higher orbital altitudes of the vehicles mentioned in the introduction, intense fluxes of electrons in the South Atlantic Anomaly obscure the peaks, and they are rarely detected at those altitudes. Stated alternatively, in this zone a satellite must be at low altitudes to be in the region of quasi-trapped particles.

In the northern hemisphere at these same longitudes a satellite at the altitudes of S81-1 observes electron fluxes in the bounce loss cone, as the conjugate point is below sea level. No nighttime cyclotron resonance events were observed in this zone. The absence of cyclotron resonance

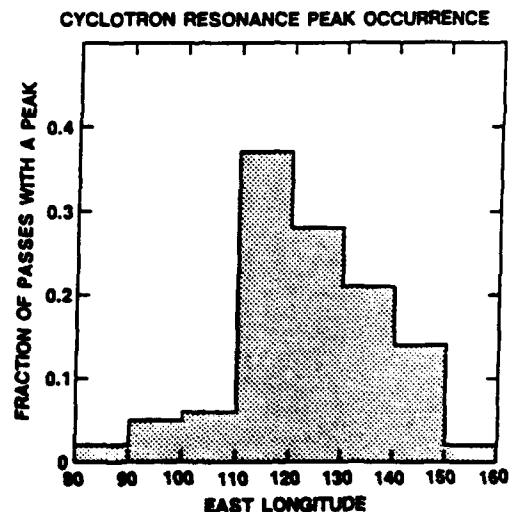## CYCLOTRON RESONANCE PEAK OCCURRENCE

Fig. 7. The distribution of occurrence of peaks versus longitude. The occurrence of peaks in the region around NWC is shown as a function of longitude. The data have been collected into bins 10° wide, and the number of peaks in each bin has been divided by the number of satellite passes through $L = 1.65$ in that longitude interval. In the bin from 110°E to 120°E, 60 peaks were detected in 163 passes, a ratio of 0.37.
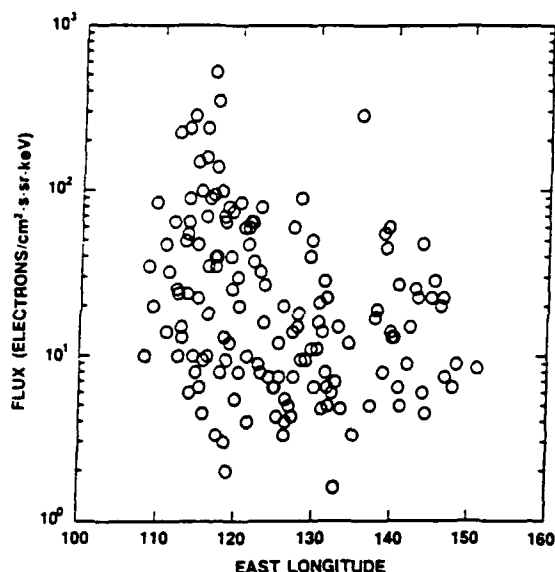
Fig. 8.   The intensity of peaks versus longitude in the region
near NWC. Each point represents the flux at the peak as a function
of longitude. The vertical scale is logarithmic from a flux of 1 el (cm^2
s sr keV)$^{-1}$ to 1000 el (cm^2 s sr keV)$^{-1}$. Contour plots of the same
type as in Figure 3 were searched for all events. Between fluxes of
1 and 10, the number of electrons within the highest contour is quite
small, and the flux determination is only approximate.

peaks in the bounce loss cone indicates that they are a
persistent phenomenon built up over many bounce periods.

In addition to cyclotron resonance peaks, the electro
spectra observed by SEEP at these longitudes contain peak.
of a different kind. These multiple peaks, with energies
which scale with L to maintain a constant drift period, were
first reported by *Imhof and Smith* [1965] and modelled by
Cladis [1966]. The SEEP observations of these peaks are
summarized in *Datlowe et al.* [1985]. The multiple peaks
represent a background against which the cyclotron reso-
nance precipitation must be observed. The superposition of
the two modes for scattering electrons into the drift loss cone
can create complex plots. Plate 3 of *Datlowe et al.* [1985]
shows two cases in which the combination of the two
scattering mechanisms plays an important role in the display
of flux versus L value and energy.

Figure 10 shows three examples of cyclotron resonance
peaks which were detected in this geographic region, using
the contour format. The line which gives the locus of
resonant energies for electrons is based on a transmitter
frequency of 17.8 kHz from the station at Cutler, Maine,
NAA. However, in the western hemisphere we found that no
single transmitter frequency gives satisfactory agreement in
the majority of cases. By contrast, in the eastern hemisphere
the 22.3-kHz frequency of NWC gives good agreement to the
observed contours in many cases.

The locations of the cyclotron resonance events are the
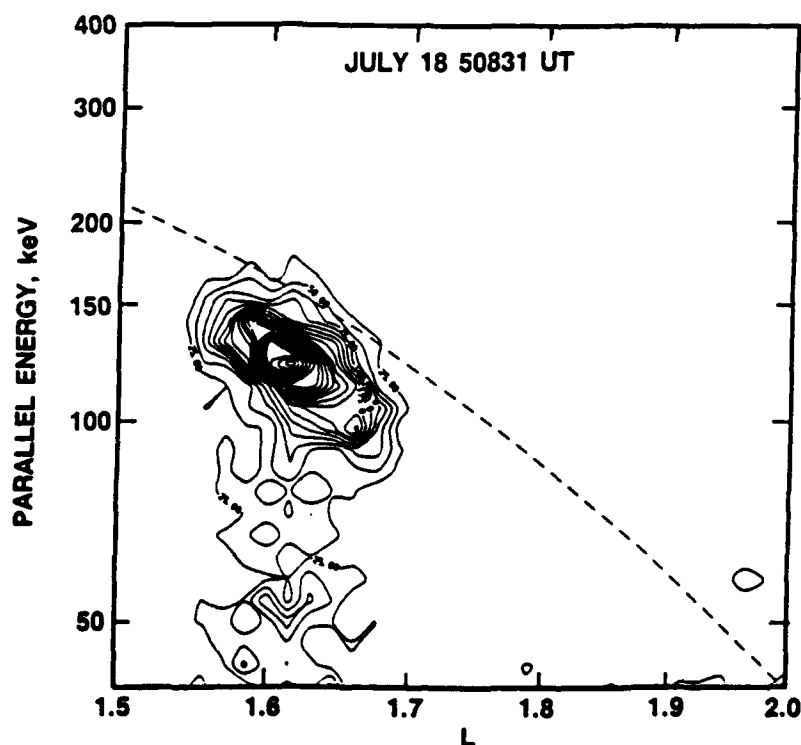basis for identifying the transmitters which are the sources of

Fig. 9.   Electron flux versus parallel energy and L value for the most intense event found at eastern longitudes. The
peak was detected on July 18, 1982, at 50831 s UT, at a satellite location of 116°E. The contours are spaced linearly in
steps of 25 el (cm^2 s sr keV)$^{-1}$, with a minimum contour of 25 (cm^2 s sr keV)$^{-1}$. The dashed line indicates the cyclotron
resonance condition for f = 22.3 kHz.

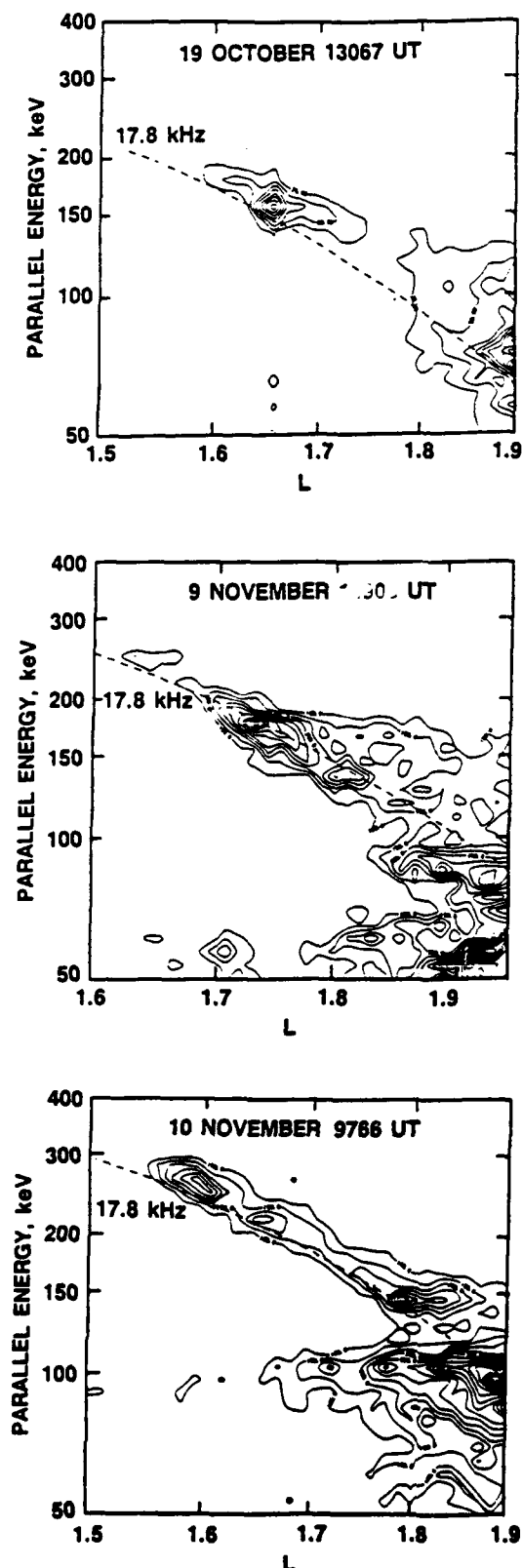the VLF waves. Contour plots such as Figure 10 were searched for all of the events to identify a peak flux for the electrons near $L = 1.65$. Because other phenomena contribute to the electron flux in this region, a maximum contour could be clearly identified only in intense events. Figure 11 shows the intensity as a function of longitude for 66 peaks in the range 260°E to 340°E. All of the peaks with fluxes above 100 el $(cm^2 \ s \ sr \ keV)^{-1}$ were found at longitudes between 280°E and 330°E. The significant feature is the sharp increase in the number of events near the conjugate point of NAA, which indicates that radiation from this transmitter is a significant source of precipitation.

The most intense peaks were detected at longitudes from ~310°E to ~325°E. This region is where the satellite is closest to the stably trapped particles and where the smallest pitch angle scattering will produce an event. The high intensity of these events is due more to the configuration of the geomagnetic field than to the locations of transmitters.

Between the longitudes of 20°W and 44°E, 28 cyclotron resonance events were found in the SEEP nighttime data. Only a few of these events were sufficiently intense and well separated from the background to allow quantitative estimates of the flux in the peaks. The most intense peak flux was ~65 el $(cm^2 \ s \ keV)^{-1}$ in an event located at a longitude of 12°E. Due to a lack of quantitative information about the events in this region, the source of the VLF waves cannot be identified at this time.

WHICH TRANSMITTERS?

The map of events observed by SEEP shows that the nighttime events were clustered in longitude about a few of the possible transmitters. Other transmitters with comparable transmission frequency and radiated power showed few if any events at $L = 1.65$. Using the list of communication transmitters of 250 kW or more radiated power in *Inan et al.* [1984], this section will break down the number of events which may be attributed to each.

NAA and NSS

Since NAA and NSS are located at 67°W and 76°W, respectively, the separation of these transmitters in longitude is too small to resolve on maps of cyclotron resonance events. *Arnoldy and Kintner* [1989] reported rocket observations of electrons directly precipitated by these two transmitters near the site of NSS. Of the 179 precipitation events observed by SEEP in the western hemisphere at night, about 3/4 were observed near the conjugate points of these transmitters. In addition, many observed peaks give good agreement with the 17.8- or 22.4-kHz frequencies of these stations. The SEEP data strongly suggest that these transmitters precipitate energetic electrons.

NLK

There are no nighttime precipitation peaks in the SEEP data at $L = 1.65$ which are near the longitudes of NLK (122°W) or its conjugate point. Evidently this transmitter does not precipitate electrons in the regions explored by the present experiment.

Fig. 10. Examples of cyclotron resonance peaks in the western hemisphere region. (Top) October 19, 13067 s UT, 288°E, 51°S. (Center) November 9, 10905 s UT, 296°E, 51°S. (Bottom) November 10, 09766 s UT, 301°E, 50°S. The dashed line indicates the cyclotron resonance condition for $f = 17.8$ kHz (NAA).

NPM

This station is located in Hawaii at 158°W. There were no nighttime cyclotron resonance events observed by SEEP within 10° geographic longitude of this station.
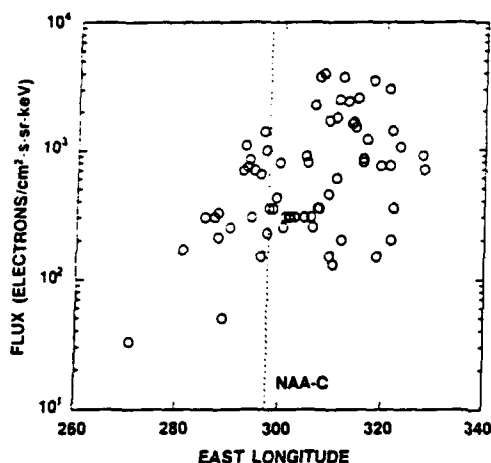
Fig. 11. The intensity of peaks versus longitude in the western hemisphere. Contour plots of the same type as in Figure 10 were searched for all events. There were 66 events with clearly defined peaks well separated from other electron flux components. Each point on this plot represents the peak flux as a function of longitude. The vertical scale is logarithmic from a flux of 10 el $(cm^{-2} \, s \, sr \, keV)^{-1}$ to 10^4 el $(cm^{-2} \, s \, sr \, keV)^{-1}$. Due primarily to the larger equatorial pitch angle of the measured particles, this flux scale is a factor of 10 higher than the scale used in Figure 8.

NWC and RPS

As indicated earlier, we attribute the bulk of the peaks in the eastern hemisphere to the transmitter at NWC (114°E). If we attribute the peaks in the northern hemisphere between 130° and 150° to RPS (135°E), then RPS accounts for 20% of the peaks observed in this region.

UMS

In a series of papers, Vampola has asserted that UMS is a major contributor to cyclotron resonance precipitation [Vampola and Kuck, 1978; Vampola, 1987; Vampola and Adams, 1988]. The results are based on data from the OV1-19 and S3-3 satellites. They used a technique of mapping electrons from the point of observation to the point of the resonance interaction using very high resolution pitch angle data. We note that in all of the published cases [see Vampola and Kuck, 1978, Figure 5] the points of detection range from 120°E, the vicinity of NWC, to 280°E, but the inferred transmitter location is 44°E, that of UMS.

The range of longitudes over which precipitation by UMS can be detected by a low altitude satellite is limited. From Figure 6, an electron mirroring at an altitude of 100 km and at a longitude of 44°E has an equatorial pitch angle of 28.4° for $L = 1.65$. Any electron scattered into the drift loss cone by waves from UMS must have a larger equatorial pitch angle at $L = 1.65$. These electrons will drift eastward at altitudes higher than the SEEP satellite. SEEP can detect these electrons as daytime events near 297°E, where the mirror altitude is again ~100 km.

There was only one isolated SEEP cyclotron resonance event at $L = 1.65$ which we can attribute to UMS. located at a longitude of 44°E. We conclude that UMS is not a significant contributor to the set of nighttime events detected by SEEP at $L = 1.65$.

Looking at the map of transmitter locations it would

appear to be a puzzle why some transmitters are effective in precipitating electrons and others are not. For example. NWC in Australia and NPM in Hawaii are both in the inner magnetosphere and both transmit at about the same frequency, yet only NWC is a major source of events observed from the orbit of S81-1. However, the transmitters which are prominent in the SEEP data have one thing in common: these transmitters are near the locations where the observations were made at the edge of the bounce loss cone. This finding shows that the effect is most prominent where the cyclotron resonance condition is met by pitch angles near the edge of the bounce loss cone.

CORRELATION WITH SOLAR ROTATION

It is of interest to search for any temporal changes in the cyclotron resonance peaks which might be synchronized with the 27-day period of solar rotation. Variations in the solar output will influence cyclotron resonance in two ways: either by shifting the resonant electron energy for a given transmitter frequency by altering the equatorial cold plasma. or by increasing the attenuation of the VLF waves penetrating the ionosphere. Equatorial plasma variations may be either density changes related to the diffusive equilibrium scale height [Chiu et al., 1979] or composition changes [Lennartsson, 1989]. These variations will modify the agreement between the calculated resonance line and the actual L-dependent variation of the electron energy and will be a relatively subtle effect. Marked changes in the attenuation through the ionosphere will be reflected in the frequency of occurrence of the resonance peaks. and this can be tested by a more direct procedure.

To search for an effect, we have selected seven solar rotations of electron data from days 151–339 of 1982 and performed a superposed epoch analysis. As an indicator of solar activity, we have used the 10.7-cm microwave index from Solar Geophysical Data. In this time interval a 27-day folding period gives the strongest modulation of the F10.7 index, so we have used this period (from a Sun synchronous satellite, only whole day folding periods can be used). As an indicator of the cyclotron peaks, we have plotted the fraction of satellite passes in which a peak was identified in the data. Figure 12 shows the result. The number of peaks in the eastern hemisphere used in this plot is 169. It will be seen on the plot that the frequency of peaks is significantly higher from day 10 to day 18 than on the remaining days of the cycle. For comparison, the figure also shows the average of the solar 10.7-cm flux index over the same seven cycles. Clearly, the observed peaks are most frequent at times of minimum solar activity. The correlation is significant at the 99% (3σ) level.

A similar search was carried out using the Dst and Kp geomagnetic indices. In the case of Dst there may be an anticorrelation with the fraction of passes in which peaks were observed; however, statistically the result is only significant at the 95% (2σ) level. A comparable search using the Kp index gave a null result.

A search for 27-day variations in the peaks observed over the western hemisphere did not turn up any prominent correlation, either in the daytime or nighttime peaks. Evidently the effect is unique to the observing conditions at Australian longitudes.

What we have shown is that during the time of the SEEP

observations there was a 27-day periodicity in the occurrence of cyclotron resonance peaks, and that this variation was out of phase with the solar $F10.7$ index. This epoch was a time of high solar microwave flux, so it is quite possible that at times near solar minimum the cyclotron resonance peaks would not show any 27-day periodicity.

LONG TERM (SEASONAL) VARIATION

A long term variation in the frequency of occurrence of peaks is evident in the data from the OV1-19 satellite reported by *Vampola and Kuck* [1978]. Cyclotron resonance precipitation was observed less often after about day 270 of 1969. The OV1-19 experiment identified cyclotron resonance precipitation using narrow temporal peaks in the counting rates in broad energy channels. A seasonal variation in the median energy of the observed peaks at $L = 1.65$ was reported by *Imhof et al.* [1978] based on data taken in the period from November 1971 to August 1972. They found at the 2σ level, that the energy of the peaks at $L = 1.65$ was lower in the summer months. They did not report any long term variation in frequency of occurrence. As a shorthand we use the term seasonal variation, even though none of the experiments has used a body of data which extended over a full year.

A long term variation in the occurrence of the cyclotron resonance precipitation has been detected by the SEEP electron spectrometer. Peaks in the eastern hemisphere occur more frequently in the time interval from June to September; very few of the 182 peaks occur in October, November, or the start of December. We note also that in this region the dominant transmitter, NWC, is in the south. In the other region of peak occurrence, from 100°W to 20°E, the opposite seasonal variation is observed. We note that all of the high power VLF transmitters which are likely candidates are located in the northern hemisphere.

Figure 13 displays the time trends in the format used by *Vampola and Kuck* [1978]. Time (day of year) runs upward in the plot, and longitude of the observation runs horizontally. Each triangle represents one event; the uniformity of the coverage was demonstrated in the same format in Figure
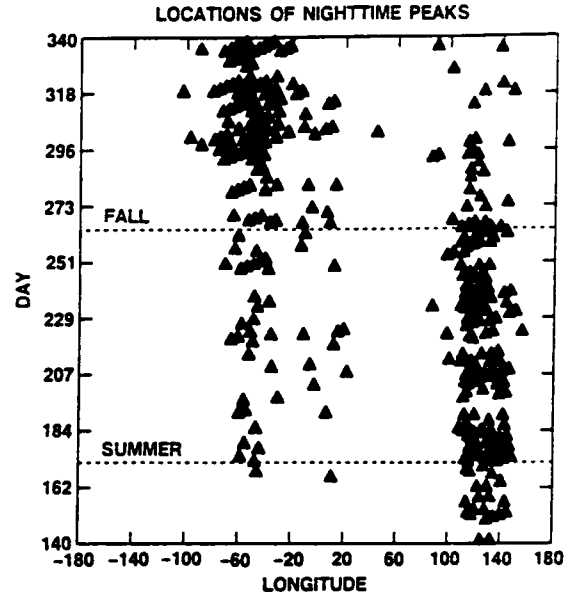

Fig. 13. Distribution of the occurrences of peaks versus geographic longitude and day of 1982, in the format of Figure 1. Each triangle represents one event.

1. Only nighttime events are plotted, but north and south are both included.

Although the frequency of occurrence of peaks in a particular location varies with time, the occurrence of peaks at all longitudes does not change markedly. If the transmitters which are contributing to the precipitation process change with time, then we could expect a change in the energies of the peaks with time, corresponding to the resonant energies of the different transmitters. This type of effect might have been the origin of the spectral variation reported by *Imhof et al.* [1978].

A time span of seven months is too short to determine if this variation repeats from one year to the next. When a data base of several years of observations may become available, we suggest that the question of seasonal variations will be well worth investigating.

CONCLUSIONS

We have surveyed over 680 occurrences of cyclotron resonance peaks observed at low altitude by the S81-1 SEEP experiment in 1982. Based on the data from 361 nighttime events we reach the following conclusions:

1. At altitudes from 190 to 270 km the occurrence of peaks tends to cluster in regions near high power VLF transmitters which may scatter electrons into the drift loss cone via the cyclotron resonance.

2. NWC in Australia and NAA/NSS in the United States are at the centers of the two main clusters and are likely to be the source of waves scattering the electrons. The Russian transmitters UMS and RPS play a less significant role at $L = 1.65$. The two stations NLK and NPM are in regions where cyclotron resonance peaks were not observed or were rarely observed. The relative importance of the particular stations may be quite different for experiments on satellites searching at other altitudes or at other L shells.

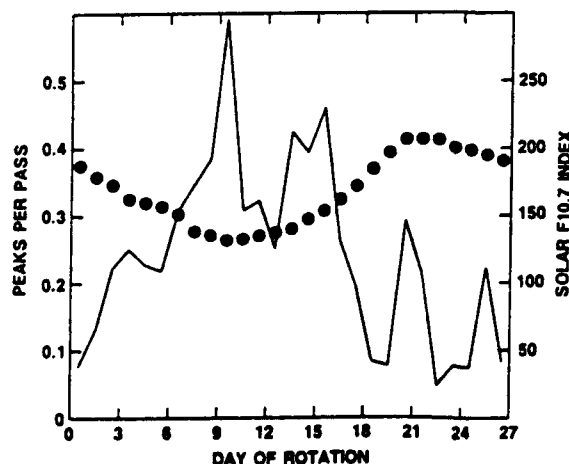3. The transmitters which have produced the majority of

Fig. 12. Superposed epoch analysis for the occurrence frequency of peaks, shown as a solid line. For reference, the averages over the same seven solar cycles of the daily $F10.7$ index are shown by solid circles.

the events detected by this experiment are located near the western edge of regions where the conjugate point to the satellite is below 100 km. This result shows that the events are most prominent in places where pitch angles near the edge of the bounce loss cone meet the cyclotron resonance condition.

4.   During days 151–339 of 1982 there was a clear 27-day modulation in the fraction of observations which showed peaks. There was a significant anticorrelation with the solar $F10.7$ index. The variation was found in the peaks between 108°E and 152°E, but not in the western hemisphere events.

5.   There was a long term variation in the frequency of occurrence of the nighttime peaks, with peaks most frequent when the likely source transmitters were in wintertime. This result shows the importance of a data set covering several years to establish conclusively the existence of a seasonal variation.

APPENDIX

The calculation of the resonance condition shown in Figures 3, 4, 9 and 10 uses the following relation (similar to equation (1)):

$$\omega - k \cdot v = m\Omega/\gamma$$

where ω is the angular frequency of the source of waves, k is the wave vector, v is the velocity of the electron, and the equatorial pitch angle of the electron is used to perform the dot product. Ω is the electron gyrofrequency, and m is a small integer representing the order of the resonance. We have retained the relativistic correction factor γ for the electron velocity and the gyrofrequency in the rest frame of the electron.

Evaluation of the wave vector k requires several quantities which are not measured by a low altitude particle detector system, and therefore a model must be used to specify the values. These quantities are required to calculate the index of refraction

$$\mu = \left[1. + \frac{\omega_p^2}{\omega(\Omega \cos \theta - \omega)} \right]^{1/2} \qquad (A1)$$

where ω_p is the plasma frequency, Ω is the electron gyrofrequency, and θ is the wave normal angle. In this appendix we show the sensitivity of the calculated resonance condition to variations in the model parameters. We take the approach of using the parameters of Figure 3 as a baseline. For each of the model parameters we show, on a separate plot, the variation in the calculated resonance condition for various possible values of the variable.

The electron gyrofrequency $\Omega = eB/mc$ is calculated from the equatorial magnetic field strength. We have used the model of *Olsen and Pfitzer* [1974]. In the inner magnetosphere the gyrofrequency can be calculated with some precision, and we take the uncertainty in this frequency to be too small to be of interest here. The magnetic field model is also used to calculate the equatorial pitch angle of the electrons. We have used the equatorial pitch angle of the locally mirroring electrons (the "final" pitch angle), but we might also have used the smallest equatorial pitch angle of the stably trapped population (the "initial" pitch angle) at each L value. Since the equatorial parallel energy is the quantity plotted in the figures, either choice gives nearly the

same result. At $L = 1.75$ the baseline calculation (pitch angle 19.6°) gives a resonant energy of 95 keV; using the limit of the stably trapped electrons (28.8°) the resonant energy is 2 keV less. The difference between the two resonance lii calculations is barely visible on the plots.

The wave normal angle θ is assumed to be zero in the baseline model. The angle may be as large as

$$\theta_c = \cos^{-1}(\omega/\Omega) \qquad (A2)$$

where the expression for the index of refraction is singular. At $L = 1.75$ the critical angle is 82°. Field-aligned propagation has been assumed in calculations of wave-particle interactions [*Inan et al.*, 1984], but wave normal angles as large as 63° have been derived in at least one ray tracing calculation [*Koons et al.*, 1981]. A wave normal angle of approximately 70° gives the largest resonant energies; at larger angles the singularity in the index of refraction decreases the calculated resonant energy. Figure A1 shows the variation in the resonance condition for eight wave normal angles: 0°, 10°, 20°, 30°, 40°, 50°, 60°, and 70°. The deviation of the 30° line from the baseline is small. The separation of the 50° line is about the same as the observed width of the contours. The 70° wave normal angle has increased the resonant energy at $L = 1.75$ from 95 keV to 170 keV. Thus the choice of wave propagation along the magnetic field introduces an uncertainty of less than a factor of 2.

If the wave propagation were confined to a single duct, we would expect that cyclotron resonance interactions would only be observed over a very limited range of L values. The left panel of Figure 10 (October 19) shows a sharp burst of electrons at $L = 1.65$, which might be expected from a localized region of enhanced wave intensity. The satellite need not pass through the duct, as the scattered electrons will drift eastward from the duct to the point of observation. But profiles similar to October 19 are not common in the SEEP data set. The extended range over which cyclotron resonance precipitation is observed in most cases argues for unducted propagation of the VLF waves.

We have used the transmission frequency of NWC, 22.3 kHz, in plotting the baseline resonance condition. Figure A2 shows the effect of several choices of frequency. The traces at 20 kHz and 25 kHz represent a 20% frequency change and fall along the data contours. The frequencies of 27.5 and 17.1 kHz are not ruled out by the data; 17.1 kHz is the listed frequency of RPS, which is at about the same longitude as NWC. Omega-H transmits at these same longitudes operating at 10.2–13.6 kHz [*Inan et al.*, 1984]. The corresponding resonant energies in the figure seem well separated from the data points, so that it is unlikely that Omega transmitters are the source of the precipitation. At $L = 1.75$ the baseline resonant energy is 95 keV; a transmitter frequency of 17.1 kHz raises it to 133 keV, and a transmitter frequency of 27.5 kHz lowers it to 70 keV. This is a reasonable range for the uncertainty in the source transmitter frequency.

The final quantity in the equations which is not measured by this experiment is the equatorial cold plasma density. Various models for this density have been published. In addition, there may be short term variations of a factor of 3 related to geomagnetic activity [*Webb and Lanzerotti*, 1977] and long term solar cycle variations [*Chiu et al.*, 1979]. The baseline model is the solar maximum/nighttime model from *Chiu et al.* [1979]. We show the calculated resonant energy
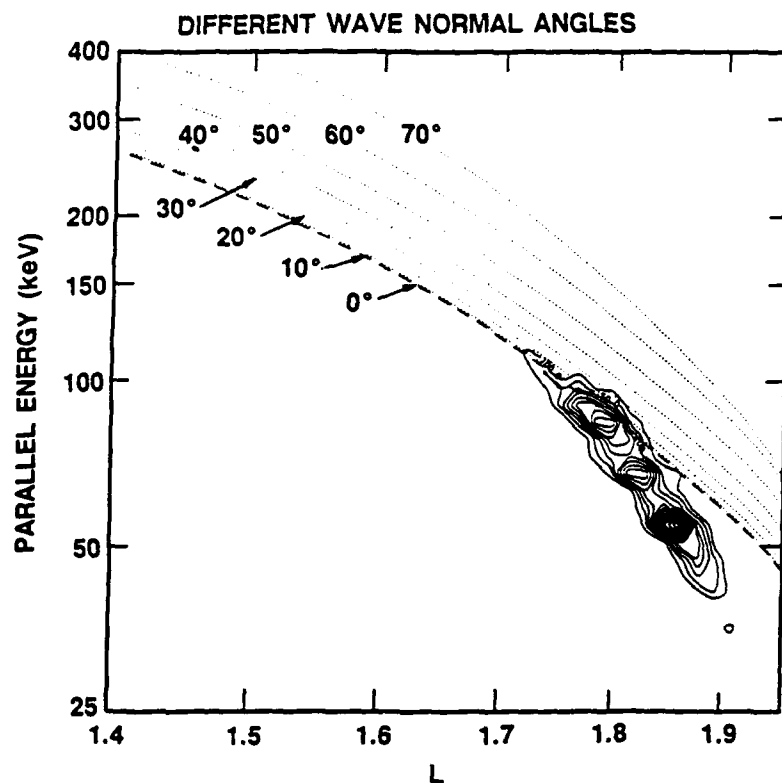
DIFFERENT WAVE NORMAL ANGLES

Fig. A1.   Wave normal angle. The resonance condition has been calculated for wave normal angles from 0° to 70° in 10° increments.

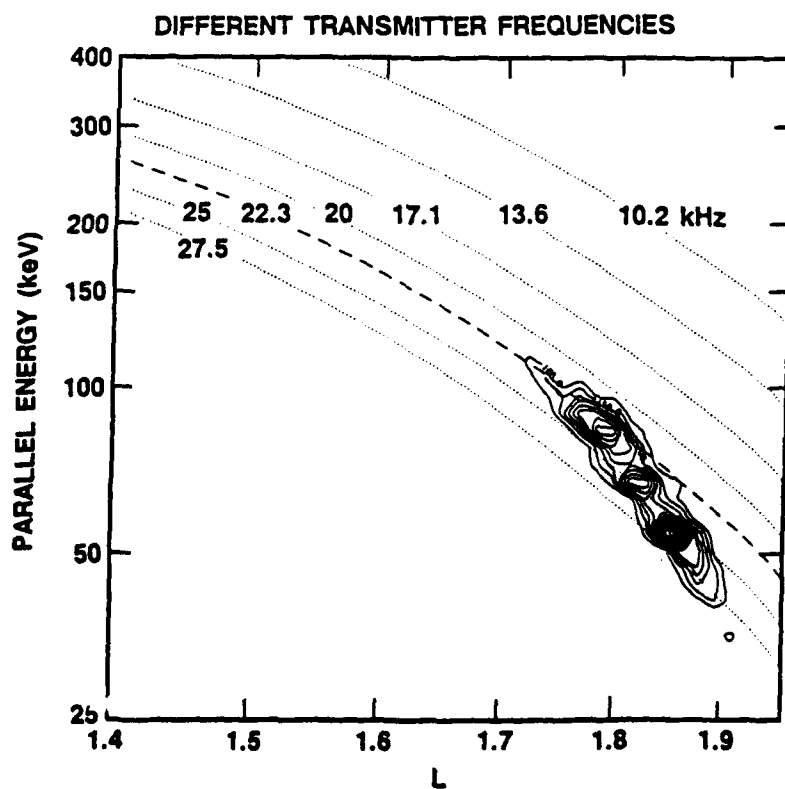## DIFFERENT TRANSMITTER FREQUENCIES

Fig. A2.   Transmitter frequency. The resonance condition has been calculated for wave VLF wave frequencies of 10.2 kHz, 13.6 kHz, 17.1 kHz (RPS), 20 kHz, 22.3 kHz (NWC), 25 kHz, and 27.5 kHz.
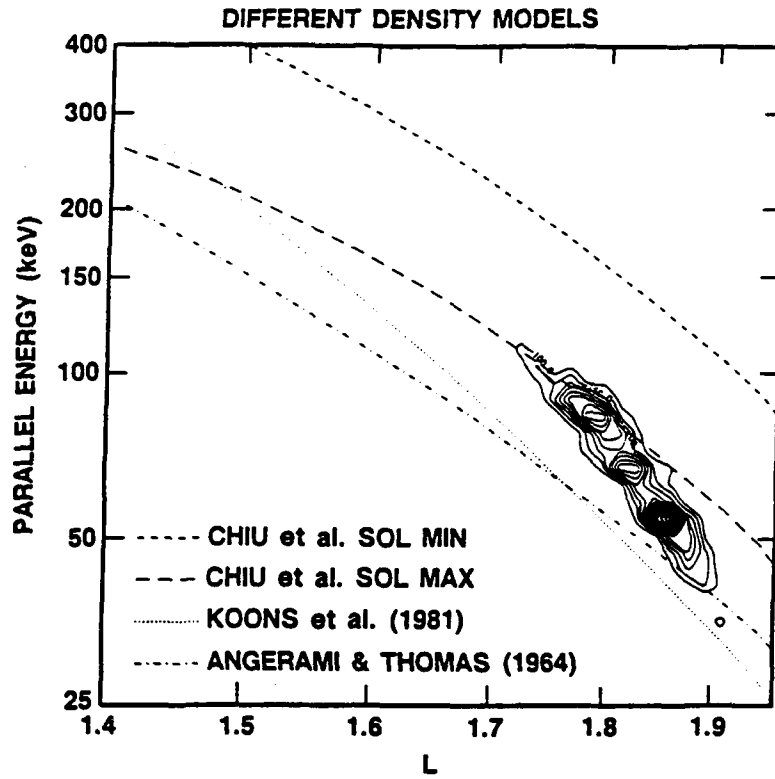
DIFFERENT DENSITY MODELS

Fig. A3. Density models. Reference case (long-dashed line) *Chiu et al.* [1979] "solar maximum" model. Short-dashed line: *Chiu et al.*, [1979] "solar minimum" model. Dotted line: *Koons et al.* [1981]; $N = 10^4(1.2/L)^{1.8}$. Dot-dash line: *Angerami and Thomas* [1964]; $N = 3000(2/L)^4$.

ORDER OF RESONANCE
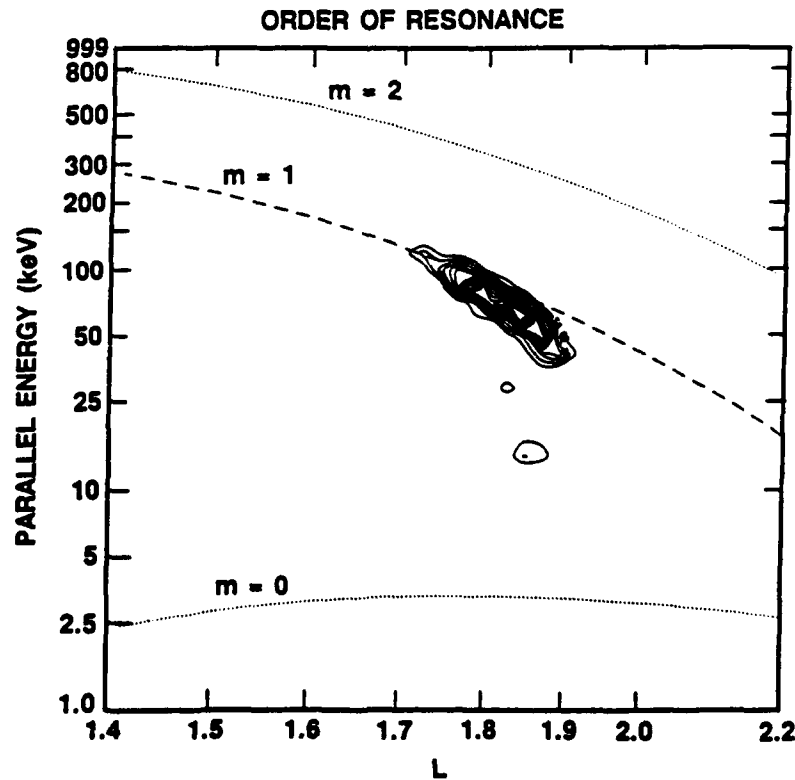
Fig. A4. Mode. The resonance condition $M = 0$, 1, and 2. The range of energies and L values is expanded on this plot.

versus L value for three other density models in Figure A3. For comparison, the solar minimum/nighttime model from the same Chiu et al. paper gives resonant energies significantly above the data points. The models of *Koons et al.* [1981] and *Angerami and Thomas* [1964] have been used in conjunction with studies of cyclotron resonance peaks. The calculated resonance energies from these models fall below the observed data points. The range of density functions given in the models and the possibility of short term variations make the equatorial density the largest uncertainty in the calculations of the resonant energy.

We have assumed first-order cyclotron resonance in the calculation. Figure A4 shows the electron resonant energies for $m = 0$, 1, and 2 in equation (1). To keep the values within the boundaries of the plot, the vertical scale has been expanded to cover the range 1 keV to 1 MeV. It is clear from the plot that the first order, $m = 1$, is the observed value. Above $L = 2.2$ the values of the resonant energy calculated with our assumed transmitter frequency, wave normal, and plasma density, are very small. At $L = 2.4$ the calculated resonant energy is equal to the 6-keV threshold of the SEEP TE2 spectrometer, and therefore it is not possible to identify first-order "peaks" above that L value with the TE2 instrument.

To summarize, the ranges of possible parameters lead to the following ranges of possible values for the resonant energies at $L = 1.75$: (1) Varying the wave normal angle from field aligned to 70° increases the resonant energy from 95 to 170 keV. (2) Lowering the transmitter frequency from 22.3 kHz to 17.1 kHz raises the resonant energy from 95 keV to 133 keV. Raising the transmitter frequency to 27.5 kHz lowers the resonant energy to 70 keV. (3) Different density models vary by a factor of 2 in the calculated resonant energy. (4) The order of the resonance is $m = 1$ in the observed cases.

Other possible factors, such as off-equatorial contributions and transmitter bandwidth, are beyond the scope of the present investigation.

REFERENCES

Angerami, J. J., and J. O. Thomas, Studies of planetary atmospheres. 1, The distribution of electrons and ions in the Earth's exosphere, *J. Geophys. Res.*, *69*, 4537, 1964.

Arnoldy, R. L., and P. M. Kintner, Rocket observations of the precipitation of electrons by ground VLF transmitters, *J. Geophys. Res.*, *94*, 6825, 1989.

Brice, N., Fundamentals of very low frequency emission generation mechanisms, *J. Geophys. Res.*, *69*, 4515, 1964.

Chiu, Y. T., J. G. Luhmann, B. K. Ching, and D. J. Boucher, Jr., An equilibrium model of the plasmaspheric composition and density, *J.Geophys.Res.*, *84*, 909, 1979.

Cladis, J. B., Resonance acceleration of particles in the inner radiation belt, in *Radiation Trapped in the Earth's Magnetic Field*, edited by B. M. McCormac, pp. 112–115, D. Reidel, Hingham, Mass., 1966.

Datlowe, D. W., W. L. Imhof, E. E. Gaines, and H. D. Voss, Multiple peaks in the spectrum of inner belt electrons, *J. Geophys. Res.*, *90*, 8333, 1985.

Imhof, W. L., and R. V. Smith, Low altitude measurements of trapped electrons, *Phys. Rev. Lett.*, *14*, 85, 1965.

Imhof, W. L., E. E. Gaines, and J. B. Reagan, Dynamic variations in intensity and energy spectra of electrons in the inner radiation belt, *J. Geophys. Res.*, *78*, 4568, 1973.

Imhof, W. L., E. E. Gaines, and J. B. Reagan, Evidence for the resonance precipitation of energetic electrons from the slot region of the radiation belts, *J. Geophys. Res.*, *79*, 3141, 1974.

Imhof, W. L., J. B. Reagan, and E. E. Gaines, The energy selective precipitation of inner zone electrons, *J. Geophys. Res.*, *83*, 4245, 1978.

Imhof, W. L., E. E. Gaines, and J. B. Reagan, Observations of multiple, narrow energy peaks in electrons precipitating from the inner radiation belt and their implications for wave-particle interactions, *J. Geophys. Res.*, *86*, 1591, 1981.

Imhof, W. L., J. B. Reagan, H. D. Voss, E. E. Gaines, D. W. Datlowe, J. Mobilia, R. A. Helliwell, U. S. Inan, J. Katsufrakis, and R. G. Joiner, Direct observation of radiation belt electrons precipitated by the controlled injection of VLF signals from a ground-based transmitter, *Geophys. Res. Lett.*, *10*, 361, 1983.

Inan, U. S., H. C. Chang, and R. A. Helliwell, Electron precipitation zones around major ground-based VLF signal sources, *J. Geophys. Res.*, *89*, 2891, 1984.

Koons, H. C., B. C. Edgar, and A. L. Vampola, Precipitation of inner zone electrons by whistler mode waves from the VLF transmitters UMS and NWC, *J. Geophys. Res.*, *86*, 640, 1981.

Lennartsson, W., Energetic (0.1- to 16-keV/e) magnetospheric ion composition at different levels of solar F10.7, *J. Geophys. Res.*, *94*, 3600, 1989.

Olsen, W. P., and K. A. Pfitzer, A quantitative model for the magnetospheric magnetic field, *J. Geophys. Res.*, *79*, 3739, 1974.

Vampola, A. L., Electron precipitation in the vicinity of a VLF transmitter, *J. Geophys. Res.*, *92*, 4525, 1987.

Vampola, A. L., and C. D. Adams, Outer zone electron precipitation produced by a VLF transmitter, *J. Geophys. Res.*, *93*, 1849, 1988.

Vampola, A. L., and G. A. Kuck, Induced precipitation of inner zone electrons, *J. Geophys. Res.*, *83*, 2543, 1978.

Voss, H. D., W. L. Imhof, M. Walt, J. Mobilia, E. E. Gaines, J. B. Reagan, U. S. Inan, R. A. Helliwell, D. L. Carpenter, J. P. Katsufrakis, and H. C. Chang, Lightning-induced electron precipitation, *Nature*, *312*, 740, 1984.

Webb, D. C., and L. J. Lanzerotti, Temporal variations in slant total plasmasphere content and their relationship to the ring current intensity in the plasmapause, *J. Geophys. Res.*, *82*, 5201, 1977.

D. W. Datlowe and W. L. Imhof, Lockheed Palo Alto Laboratory, Department 91-20, Building 255, 3251 Hanover Street, Palo Alto, CA 94304.

Seasonal Variations of Energetic Electron Precipitation by Cyclotron Resonance with VLF Waves from a Ground-based Transmitter

Dayton W. Datlowe and William L. Imhof
Lockheed Palo Alto Research Laboratories
3251 Hanover Street
Palo Alto, California

Abstract

We report here for the first time the detection of a seasonal variation in the occurrence of peaks in the spectra of energetic ~ 100 keV electrons precipitating from the inner radiation belt. Narrow spectral peaks have been previously reported; because the peak energy varies in a characteristic way with magnetic L value and because the nighttime peaks occur near certain powerful ground based VLF transmitters, they have been been interpreted as the result of cyclotron resonance between the waves and the electrons. The spectra reported here were observed from the low altitude polar orbiting satellite P78-1 at midnight local time. The data, acquired over the 5 year period from March 1979 to July 1984, are the first multi-year data set used to study cyclotron resonance peaks. The geographical distribution of the events is strongly clustered around the 22.3 kHz VLF transmitter NWC in Australia. At a magnetic L-value of 1.65 the peak in the energy of the electron spectrum is typically close to the expected 170 keV, but the energy of the peaks changes with L-value more rapidly than expected. Binning the data into seasons, we find that the events occur 2.5 times more often during the six months from day 80 to 263 than during the remainder of the year, and that the seasonal difference is statistically significant at a high level. Since the observed change is in the frequency of occurrence of the peaks and not in the mean energy of the peaks, we attribute the effect to a seasonal change in ionospheric transmission of VLF waves rather than a seasonal change in the equatorial cold plasma density.

Seasonal Variations of Energetic Electron Precipitation by Cyclotron Resonance with VLF Waves from a Ground-based Transmitter

Dayton W. Datlowe and William L. Imhof

Introduction

Precipitation of energetic electrons from the inner radiation belt in narrowly peaked spectra has been observed by a number of satellites. In a series of spectra recorded by a single satellite the energy of the peaks varies with L-value in a characteristic way, according to the condition for cyclotron resonance [*Brice*, 1964] with waves at a single VLF frequency. Since the cyclotron resonance condition is met, and because the peaks observed at satellite night time cluster around particular VLF transmitters [*Datlowe and Imhof*, 1990], the peaks are interpreted as the result of cyclotron resonance with VLF waves from ground based transmitters [*Inan et al.*, 1984].

Six different satellite experiments have reported data on cyclotron resonance precipitation of electrons. The first reports of the phenomenon were based on observations from P71-2 and P72-1[*Imhof, Gaines, and Reagan*, 1973, 1974]. Later *Vampola and Kuck* [1978] reported observations from the OV1-14 and OV1-19 satellites. Further results came from S3-3 [*Vampola*, 1987] and P78-1 [*Imhof et al.*, 1981]. These papers are in general agreement that pitch angle scattering by waves from ground based transmitters is the most likely origin of the peaks, but reached differing conclusions as to the relative importance of various known stations. A large

number of cyclotron resonance events were observed by the S81-1 satellite in 1982 [*Datlowe and Imhof*, 1990]. This survey was restricted to events at L=1.65, in the inner magnetosphere. A map of the locations of the events strongly favors the conclusion that one particular station, NWC (22.3 kHz) in Australia, is the major contributor to the precipitation in this L-value range. The low altitude (< 270 km) satellite S81-1 also frequently observed precipitation in the vicinity of NAA (17.8 kHz) and NSS (21.4 kHz) in the eastern United States, transmitters which are not prominent in the data from higher altitude satellites.

A seasonal variation in the median energy of the observed peaks was found by *Imhof et al.* [1978] in the period from November 1971 to August 1972; the energies of the peaks were reported to be lower in the summer months. The data from OV1-19 reported by *Vampola and Kuck* [1978] showed a sharp decrease in the number of observations in which cyclotron resonance effects were observed after day 270 of 1969. Plotting the S81-1 data in the same format, Datlowe and Imhof [1990] showed that the peaks in the eastern hemisphere (over NWC) were found mainly from May to September, while peaks from stations in the western hemisphere were observed primarily after September. They used the term"Seasonal Variation", although the data covered only seven months. To detect changes on these time scales without any ambiguity requires a uniform set of electron observations by the same detector system over a time span of years. Unfortunately, none of the previous investigations of cyclotron resonance precipitation covered as much as one year.

In this report we use for the first time a multi-year data set to search for a seasonal

variation in cyclotron resonance precipitation. The electrons were detected by the EEM-002 electron spectrometer on the P78-1 satellite. Although there are time gaps in the data available for this study, the period of observation spanned five years from March 1979 to July 1984.

Instrumentation

The P78-1 satellite was in a polar orbit with a nominal 600 km altitude. The orbit was sun synchronous in the noon-midnight plane, so that passes over a low latitude transmitter always occurred at noon or midnight local time. The spacecraft consisted of two parts, a large solar panel oriented toward the sun, and a wheel rotating every 5.5 seconds. The spin axis was oriented parallel to the plane of the equator, so that the scan was always in the north-south direction. The EEM-002 detector was mounted on the spinning section of the spacecraft with its center axis perpendicular to spin axis. In this orientation a complete pitch angle distribution was obtained on each spin of the satellite.

The EEM-002 electron spectrometer was a silicon solid state detector covering the energy range 68 to 1120 keV in 256 pulse height channels. The energy resolution was ~20 keV full width at half maximum. The opening half-angle of the detector was 15 degrees, and the geometric factor was 0.69 cm^2 sr. The combination of a 3.2 mg/cm^2 aluminum and Kapton entrance window and pulse height information gave excellent rejection of any local proton or heavy ion fluxes below an energy of 1 MeV. This system operated successfully from the day of launch, 24 February 1979, until the last day of the mission, on 13 September 1985, without significant degradation in

gain, resolution or efficiency.

Cyclotron Resonance Precipitation

The first order cyclotron resonance condition [*Brice*, 1964] is given by the equation

$$\omega - \mathbf{k} \cdot \mathbf{v} = \Omega / \gamma \qquad (1)$$

where ω is the VLF wave angular frequency, $\mathbf{k}$ is the VLF wave vector in the interaction region, $\mathbf{v}$ is the electron velocity vector, Ω is the electron cyclotron angular frequency, and γ is the relativistic factor. Evaluation of the wave vector $\mathbf{k}$ introduces the wave normal angle and the index of refraction. We calculate the index of refraction from the transmitter frequency, the cyclotron frequency, and the equatorial plasma density using the formulation of *Koons et al.* [1981]. The equatorial magnetic field is calculated from the model of *Olsen and Pfitzer* [1974] and the equatorial plasma density is calculated from the model of *Chiu et al.* [1979]. Calculation of the wave normal angle requires ray-tracing techniques which are beyond the scope of the present investigation, and in our calculations we have assumed propagation parallel to the magnetic field lines. The errors introduced by the various assumptions are discussed in detail in the appendix of *Datlowe and Imhof* [1990]. With these assumptions the calculation of the resonant velocity is the solution to a quadratic equation. However, for propagation nearly parallel to the magnetic field line an approximate solution for E_{res}, in terms of the equatorial plasma density n_0, the transmitter angular frequency ω, and the wave normal angle ϕ is as follows:

$$E_{res} \sim (n_0 \, \omega \cos^2 \phi \,)^{-1} \qquad (2)$$

The transmitter frequency is constant in time. Variations in the cold plasma density profile will make changes in the wave normal angle ϕ at the equator, but for small angles the changes in the resonant energy are small since the cosine is close to 1.0. Therefore the dominant factor responsible for changes in the observed resonant energy at a fixed location is the cold plasma density.

The Spacecraft Data

Precipitation of electrons according to the cyclotron resonance condition is readily recognized in the spectra of ~100 keV trapped electrons. To search for occurrence of cyclotron resonance peaks efficiently, color displays of the EEM - 002 electron spectra and pitch angle distributions were generated to survey the data to identify times of interest. Although the fluxes may be very weak, the characteristic variation in peak energy with L-value is readily visible on these images. The energy versus L-value variation of these features is the characteristic signature of the cyclotron resonance precipitation phenomenon in the P78-1 surveys. Where peaks were detected, spectra were plotted for each spin of the satellite; six such spectra from a satellite pass on 22 July 1982 are displayed in Figure 1.

To observe energy spectra, the incoming electron flux must be accumulated over a range of pitch angles, and therefore a small range of resonant energies. We have used pitch angles from 65 to 115 degrees, corresponding to locally mirroring (trapped) electrons. The analysis of this event involves scanning the spectra to record the energy of the peak in the electron spectrum as a function of the geomagnetic L value. The results of the scans are displayed in Figure 2. Each symbol represents the parallel

energy of the resonantly scattered electrons, which is calculated from the observed electron spectral peak energy times the square of the cosine of the pitch angle at the geomagnetic equator. We use the parallel energy as it is directly comparable to the results of the model, which is indicated as a dashed line in the Figure. Note that in the actual data the resonant energy varies with L-value more rapidly than predicted by the model. The same model was used by *Datlowe and Imhof* [1990] for the comparison of spectral information from the S81-1 satellite; in that data the resonant energy also changed with L-value more rapidly than the model predicted.

Unfortunately, for programmatic reasons data coverage is not uniformly available over the five years. After the first year of operations nighttime observations became much less frequent due to limited battery power. Also, after the first year the data were processed only at times which supported coordinated observing campaigns. We have made a systematic survey of all available data when the satellite was at L=1.65. Figure 3 is a map of the geographic latitude and longitude of 163 well observed events. Each event is marked at the latitude and longitude closest to L=1.65 in the series of spectra.

Previous observations with the S81-1 SEEP satellite showed that precipitation events of this type were commonly found in the vicinity of the VLF transmitter in Australia, NWC. The station is a communication transmitter located at 21°49'S and 114°10' E, radiating 1000 kW at a frequency of 22.3 kHz [*Inan et al.* 1984]. Continuous uninterrupted operation of the transmitter is assumed throughout our analysis.

Figure 4 shows the distribution in longitude of the events in the P78-1 data. All of the events are in the longitude range 68 to 208 degrees east, which is therefore the range of longitudes of passes counted as "Observations", and the majority of the events are in the range from 110 to 160 degrees east. The frequency of occurrence of events increases rapidly near the 114 degrees longitude of the NWC transmitter. The drift of energetic electrons due to the curvature and radial gradient of the geomagnetic field is eastward, so that many more events are found east of the transmitter than west of the transmitter. The absence of nighttime events eastward of 210 degrees is also significant: since the satellite always crosses the equator near local midnight, when P78-1 is at a longitude of 204 degrees it is approximately dawn at the site of the transmitter. This finding is consistent with the conclusion that the resonant scattering of trapped electrons takes place only when the VLF transmitter is in darkness.

An event is considered well observed if spectral plots showed well defined peaks and we could identify the energy of the cyclotron resonance peak at several L-values. In addition we required that the peak energy vary in a consistent way with L value; thus events with poorly measured peak energies were rejected. The breakdown by years is given in Table 1. For the purpose of counting the number of observations all available nighttime passes through this longitude range in both the north and south are included. Each observing day included several passes through the region of interest, so that the count of days with one or more observations is 261.

Table 1

Year	Obs	Days	Peaks	Per Cent
1979	526	188	111	21
1980	0	0	0	--
1981	0	0	0	--
1982	35	23	12	34
1983	46	33	22	48
1984	35	17	18	51
Total	643	261	163	25

To gather the statistics of a large number of events, we can parametrize the variation of peak energy with L value by an exponential:

$$E_{res}(L) = E_{1.65} \, exp \, [(1.65-L)/L_0] \qquad (3)$$

Since the range of L values with detectable peaks is small, linear correlations and power law functions also provided satisfactory fits; the goodness of fit criteria do not provide a basis for preferring power laws or exponentials. We choose the exponential form because the fitting parameter L_0 is readily interpreted as a scale height, the range of L values over which the resonant energy changes by a factor of $e = 2.7$. In the approximation that the cold plamsa density variation dominates the energy change, then the product of L_0 and the radius of the earth gives an estimate for the plasma scale height near L = 1.65.

For example, in the event shown in Figure 2 the fitted parameters are $L_0 = 0.294$ and the intercept at $L = 1.65$ is 177 keV. In comparison, if the same fitting is applied to the model (dashed line) in Figure 2, the parameters are $E_{1.65} = 175$ keV and $L_0 = 0.356$ although the exact values depend on longitude. This fitting procedure provides the selection criterion for a "well observed" event: if the data points represent a correlation between energy and L-value which is significant at less than 5σ, the event was rejected. This quality of fit criterion removes the weak or noisy events, for which the peak energies could not be well determined.

The results of the parameter fitting are shown in Figure 5, which is a scatter diagram of the resonant energy $E_{1.65}$ against the slope parameter L_0 for the 163 events. The 120 black dots represent events for which the range of L values with peaks included $L = 1.65$, and the hollow symbols represent the events for which the best fit was extrapolated to $L = 1.65$. The "cross hairs" represent the model line shown in Figure 2. It is evident from the plot that the calculated resonant energy is close to the median of the points, but that the observed slope parameter L_0 is smaller than the predicted 0.36 in most cases. This scatterplot does not show a statistically significant correlation between the parameters $E_{1.65}$ and L_0. The mean value for $E_{1.65}$ is 170 keV and the mean slope parameter L_0 is 0.28. There are also about 10 events with a slope parameter greater than 0.5, which is large enough to question the inclusion of these events in a list of cyclotron resonance peaks. We will discuss these events elsewhere. The frequency of occurrence of different values of $E_{1.65}$ and L_0 are show in Figure 6a and Figure 6b respectively.

Seasonal Variation in the Frequency of Occurrence

It has been suspected from previous experiments, S81-1 and OV1-19, that there may be a seasonal variation in frequency of occurrence of peaks. Since the present data are the first which explore a time period of more than one year, we can show for the first time that the annual variation is a statistically significant effect. Table 2 summarizes the data from 643 observations at L = 1.65. For consistency we have counted only the 163 "well observed" events; Figure 7 shows the results in histogram form.

Table 2

Season	Days	Passes	Events	PerCent	<Long.> deg	$E_{1.65}$ keV
Winter	1-80,>355	78	9	12	144	157
Spring	80-171	320	102	32	145	169
Summer	172-263	118	37	31	132	177
Fall	264-355	127	15	12	110	159
Total		643	163	25		

We use the day numbers which correspond to the familiar northern hemisphere seasons, although in fact the station NWC is located in the southern hemisphere. It is clear from the "PerCent" column that in the spring and summer, days 80 to 263, the events are found 2.5 times more often than in the fall-winter time frame. With an overall occurrence rate of 25%, we expect that the fall-winter period will produce 52 events in 205 observations, and the observed number is 24. In a binomial distribution with $p = 0.25$, the probability of 24 or fewer events in 205 trials is 2×10^{-6}. We conclude that the "seasonal variation" in the peaks observed near NWC is a statistically significant effect.

One potential bias in this analysis is a seasonal variation in the energy of the peaks as measured by $E_{1.65}$. For this reason the last column of the table gives the mean value of $E_{1.65}$ for each group. The Standard Deviation for this parameter is approximately 25 keV, which is comparable to the differences in the mean values. The point is that this difference in $E_{1.65}$ is too small to introduce observational biases due to different backgrounds or to reduced detector sensitivity at energies close to the detector threshold of 68 keV. Furthermore, from equation (2) we can infer that no seasonal variation in the equatorial plasma density n_0 has been detected.

Another potential bias is related to variations in the patterns of data coverage for the different observing times. Specifically, "Fall" data coverage occurred significantly westward of the other observing times. This is evident from the "<Longitude>" column of Table 2, which gives the mean longitude of the data coverage during each time interval. In the fall time period, data coverage was concentrated west of NWC, a region with fewer resonance peak events. We can remove this bias by narrowing the longitude range to 110 to 160 degrees; with this restricted range the number of passes is about the same for all longitudes. There were 215 observations at L = 1.65 and there were 112 well observed cyclotron resonance precipitation events detected. Table 3 shows the breakdown. Once again the percentage of events in the Fall/Winter time frame (24%) is significantly lower than in the Spring/Summer time frame (60%).

Table 3

Season	Passes	Events	PerCent	<Long.> deg	$E_{1.65}$ keV
Winter	30	6	20	133	154
Spring	124	74	60	134	169
Summer	42	26	62	135	176
Fall	19	6	32	127	168

Dividing the data into the 1979 epoch (67 events/138 passes) and into the 1982 to 1984 time frame (45 events/77 passes) produces the same results. Clearly the events in the vicinity of NWC are detected twice as often during the northern hemisphere spring and summer months.

An additional concern is that the apparent seasonal cycle may be accidental because solar or geomagnetic phenomena by coincidence may have had the same time scale during our observing period . We have sorted two published geomagnetic indices and two Solar activity indices into the four seasonal time bins. The geomagnetic indices are the Dst and Kp indices, and the Solar indices are the 10.7 cm microwave flux and the Sunspot number. Table 4 lists the mean and standard deviation for the days in each season. The result is that the differences in the average values of these indices across the four time bins is less than or comparable to the standard deviation of the indices.

Table 4

Season	Days	<Dst>	Sigma	<Kp>	Sigma	<F10.7>	Sigma	<Spots>	Sigma
Winter	28	-30.5	23.2	25.8	13.6	166.7	24.0	125.1	32.3
Spring	112	-23.0	25.9	30.8	14.5	167.9	30.4	118.3	38.2
Summer	61	-14.2	30.1	29.0	14.1	172.7	41.3	138.0	53.7
Fall	60	-15.4	20.0	21.8	13.6	209.9	47.3	169.0	58.2

The only marginal correlation is increased solar activity during the "Fall" period, but the "Winter" period also has a lower frequency of occurrence and the same solar activity indices as "Spring" and "Summer". Since the four indices do not correlate either with our time bins, or with the $E_{1.65}$ and L_0 parameters of the events individually, we conclude that the forces which drive these indices are not accidentally correlated with the seasons over the time period of the P78-1 observations.

Discussion

The most clear cut seasonal effect in the P78-1 electron data is the frequency of occurrence variation. Of the possible origins, an associated variation of the penetration of VLF waves through the ionosphere would be the most direct way in which the effect might occur. Seasonal changes in the cold plasma density might also be a factor. However, to the extent that $E_{1.65}$ is an indicator of the equatorial plasma density at L = 1.65, then the seasonal variation in this data set (Table 2) is very small and less than the standard deviation of the measurements. Accordingly we favor ionospheric attenuation as the origin of the seasonal effect. Since NWC is a station in the southern hemisphere, the attenuation is greatest during the local spring and

summer months.

We also note that the fraction of observations in which a cyclotron resonance peak
was detected increased from 21% in 1979 to 50% in 1983 and 1984. This same time
period coincides with a significant drop in Solar activity. For example, the yearly
mean value of the Solar 10.7 cm microwave index dropped from 192 in 1979 to 101
in 1984. This change suggests that there may be a solar cycle dependence.

Conclusions

1. Cyclotron resonance electron precipitation has been observed by the P78-1
EEM-002 electron spectrometer. The events are identified by spectral peaks which
vary in energy according to the cyclotron resonance condition.

2. The 163 well observed nighttime events cluster around the 22.3 kHz VLF station
NWC, indicating it is the source of the waves which interact with the energetic
electrons. Earlier work with the S81-1 instrument [*Datlowe and Imhof*, 1990] also
found clustering of events around NWC.

3. In the 163 events the mean value of the resonant energy at L=1.65 was observed to
be very close to the value of 170 keV predicted by the model. However the resonant
energy $E_{1.65}$ changes with L value more rapdily than predicted; the mean value of
the slope parameter L_0 is 0.28 as compared to a predicted value of 0.36.

4. We conclude that the seasonal variation in the frequency of occurrence of the
cyclotron resonance peaks, which was suggested by the earlier satellite data from
S81-1 and OV1-19, is statistically significant in the 5 years of available P78-1
electron data.

5. Since the energies of the peaks were constant to within statistical errors, we infer from equation (2) that no equatorial plasma density change was detected. Accordingly we conclude that ionospheric transmission changes are the origin of the seasonal frequency of occurrence variations.

Acknowledgments

References

Brice, N., Fundamentals of very low frequency emission generation mechanisms, *J. Geophys. Res. 69*, 4515, 1964

Chiu, Y. T., J. G. Luhmann, B. K. Ching and D. J. Boucher, Jr., An equilibrium model of the plasmaspheric composition and density, *J. Geophys. Res. 84*, 909, 1979

Datlowe, D. W., and W. L. Imhof, Cyclotron resonance precipitation ofenergetic electrons from the inner magnetosphere, *J. Geophys. Res., 95*, 6477, 1990.

Imhof, W. L., E. E. Gaines, and J. B. Reagan, Dynamic variations in intensity and energy spectra of electrons in the inner radiation belt, *J. Geophys. Res. 78* , 4568, 1973

Imhof, W. L., E. E. Gaines, and J. B. Reagan, Evidence for the resonance precipitation of energetic electrons from the slot region of the radiation belts, *J. Geophys. Res. 79*, 3141, 1974

Imhof, W. L., J. B. Reagan and E. E. Gaines, The Energy selective precipitation of inner zone electrons, *J. Geophys. Res. 83*, 4245, 1978

Imhof, W. L., E. E. Gaines, and J. B. Reagan, Observations of multiple, narrow energy peaks in electrons precipitating from the inner radiation belt and their implications for wave-particle interactions, *J. Geophys. Res. 86* , 1591, 1981

Inan, U. S., H. C. Chang, and R. A. Helliwell, Electron precipitation zones around major ground-based VLF signal sources, *J. Geophys. Res. 89*, 2891, 1984

Koons, H. C., B. C . Edgar, and A. L. Vampola, Precipitation of inner zone electrons by whistler mode waves from the VLF transmitters UMS and NWC, *J. Geophys Res.*, *86*, 640, 1981

Olsen, W. P., and K. A. Pfitzer, A quantitative model for the magnetospheric magnetic field, *J. Geophys. Res. 79* , 3739, 1974

Vampola, A. L., and G. A. Kuck, Induced precipitation of inner zone electrons, *J. Geophys. Res.* *83* , 2543, 1978

Vampola, A. L., Electron precipitation in the vicinity of a VLF transmitter, *J. Geophys. Res.* *92* , 4525, 1987

Vampola, A. L., and C. D. Adams, Outer zone electron precipitation produced by a VLF transmitter, *J. Geophys. Res.* *93* , 1849, 1988

CAPTIONS

Figure 1
Electron spectra from the EEM-002 instrument. Each individual spectrum is accumulated when the angle between the centerlineof the detector and the local magnetic field is between 65 and 115 degrees. The magnetic L-value is indicated at the right of each spectrum. To save space, only data from every second spin of the satellite is plotted.

Figure 2

Resonant energy is plotted versus L-value. The squares connected by solid lines represent the data points from Figure 1 and the dashed line gives the model calculation. To calculate the parallel energy, the energy of the peak from the previous Figure has been multiplied by the square of the cosine of the pitch angle of locally mirroring electrons .

Figure 3

Worldwide distribution of the events. The symbol $*$ gives the latitude and longitude of the one peaked spectrum in each set which was closest to L=1.65. Major VLF transmitters (*Inan et al.* 1984, Table 1) are designated by ●.

Figure 4

The fraction of satellite passes in which a peak was observed as a function of longitude.

Figure 5

Scatter plot of the fitting parameters. Each event is plotted according to it parallel energy at L=1.65 and the slope parameter L_0 from equation (3). The filled circles ● represent events with spectra at L=1.65, and the open squares ❑ represent events in which the fitting parameter $E_{1.65}$ is extrapolated from the correlation fit.

Figure 6
   A) Frequency of occurrence of the fitting parameter E_{res} for 163 events
   B) Frequency of occurrence of the fitting parameter L_0 for 163 events

Figure 7
The fraction of the P78-1 satellite observations which detected a cyclotron resonance peaks as a function of northern hemisphere season.
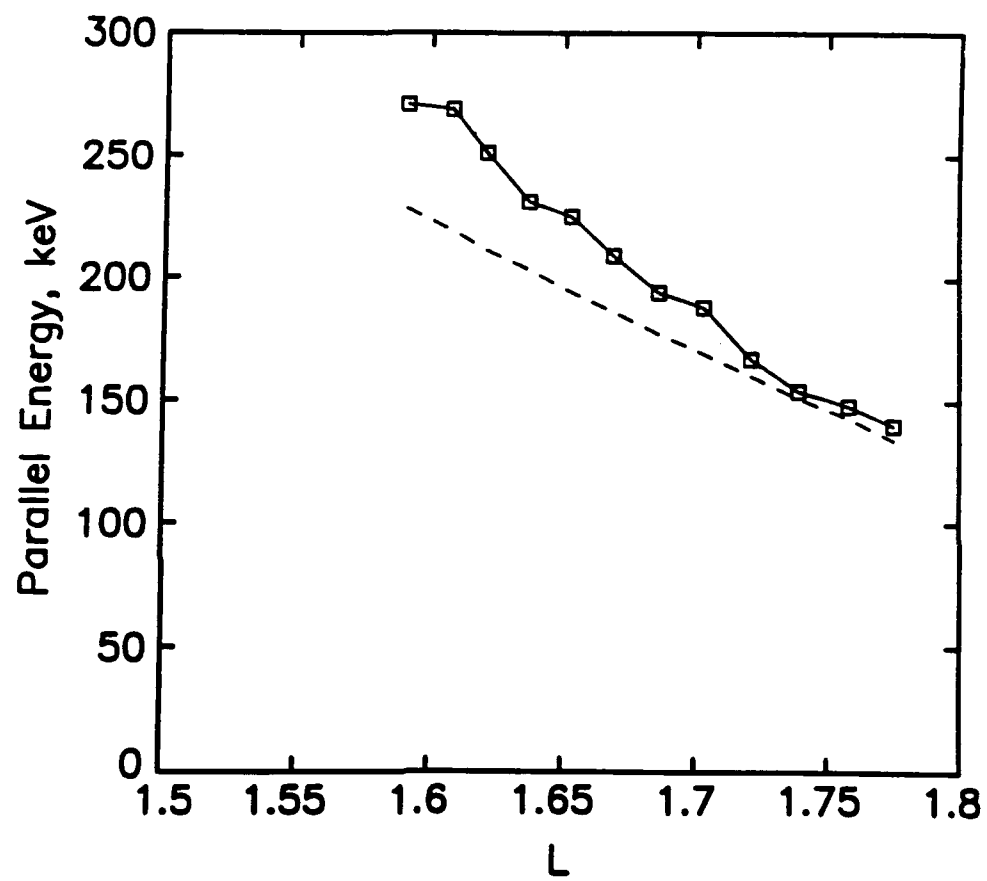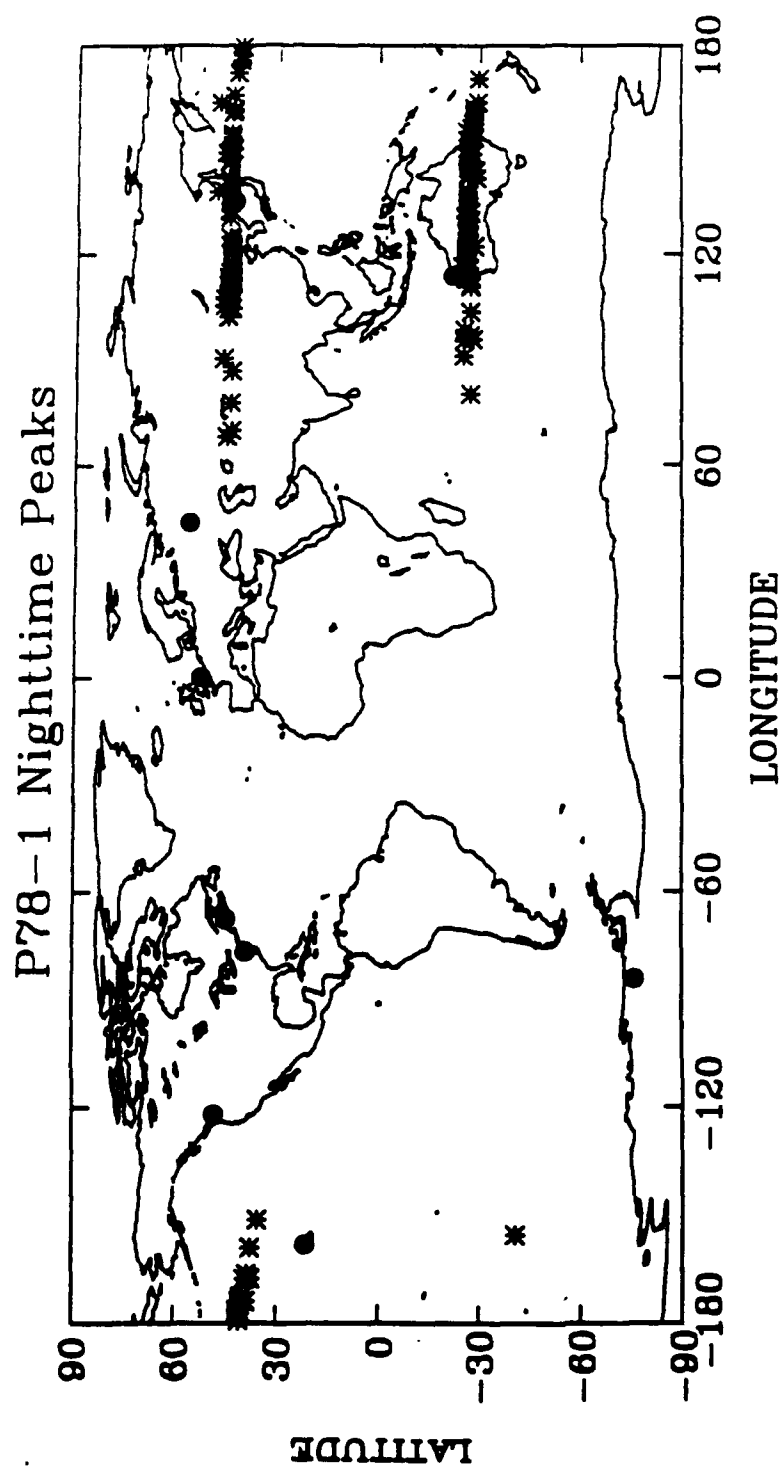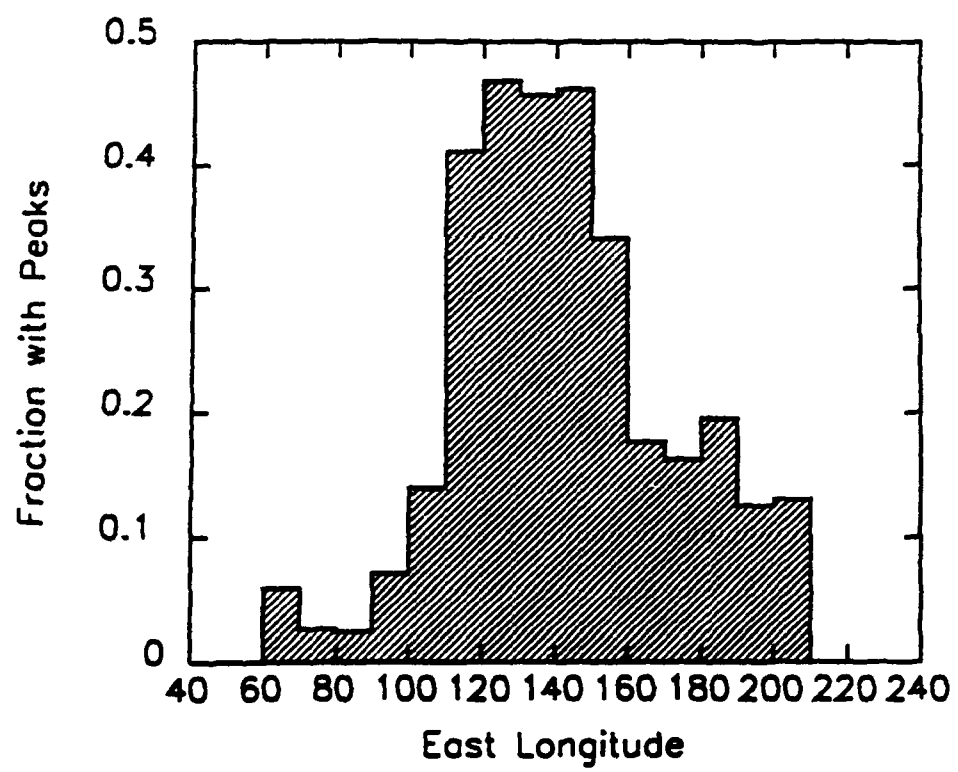
Figure 1

Figure 2

P78-1 Nighttime Peaks
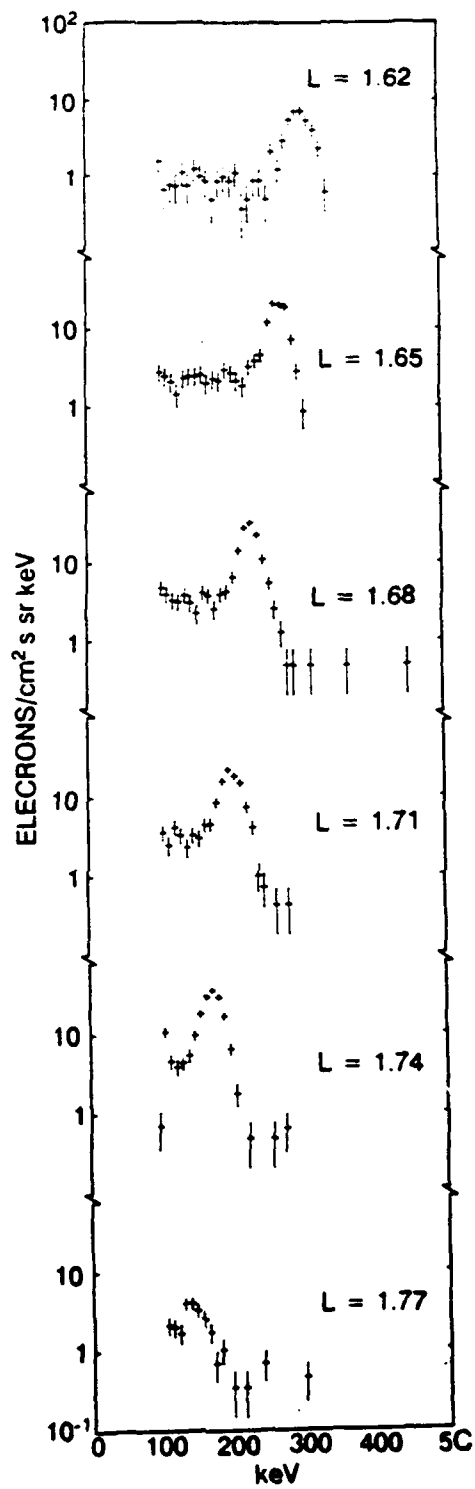
Figure 3

Figure 4

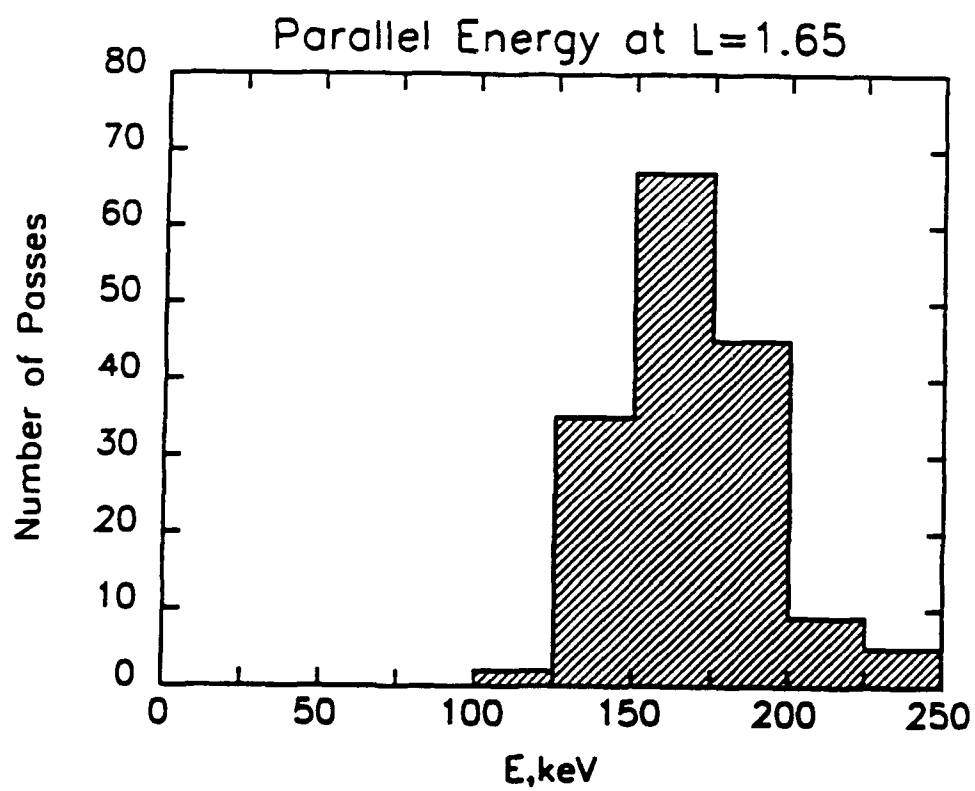Cyclotron Resonance at L=1.65
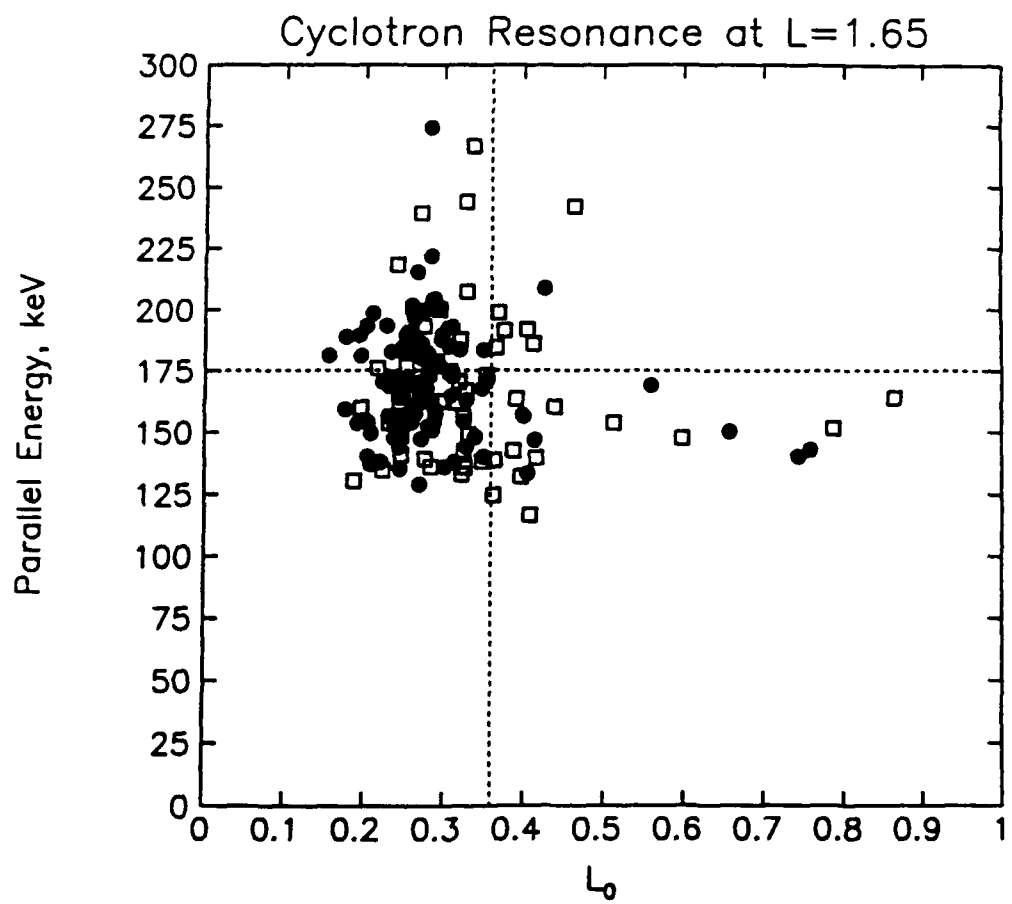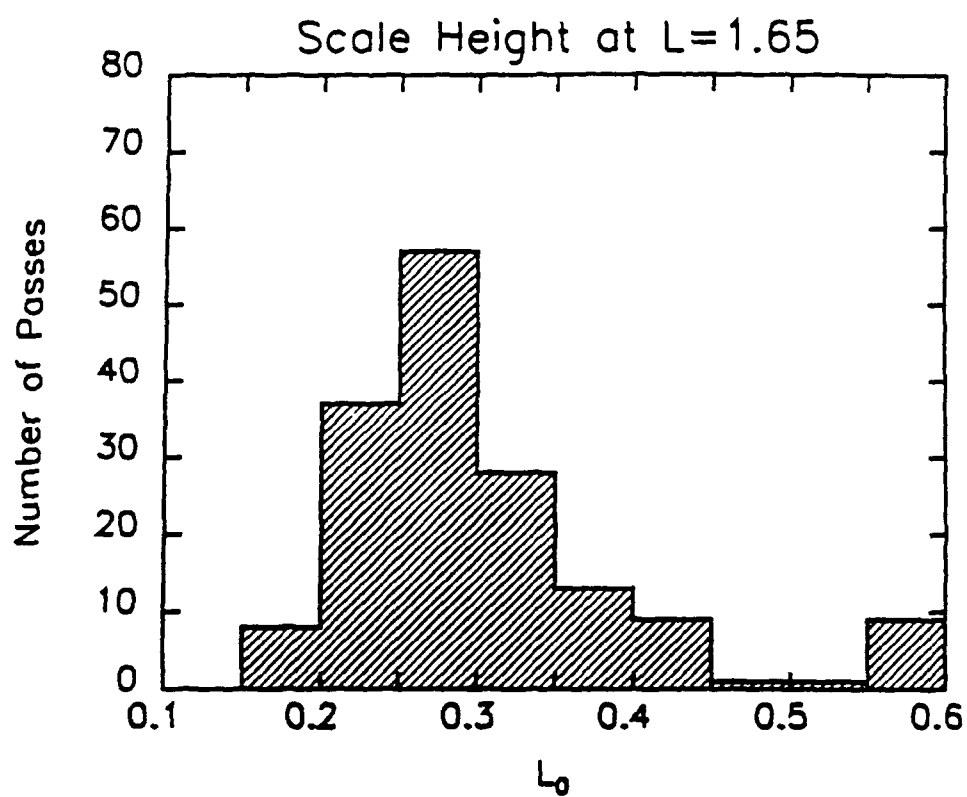
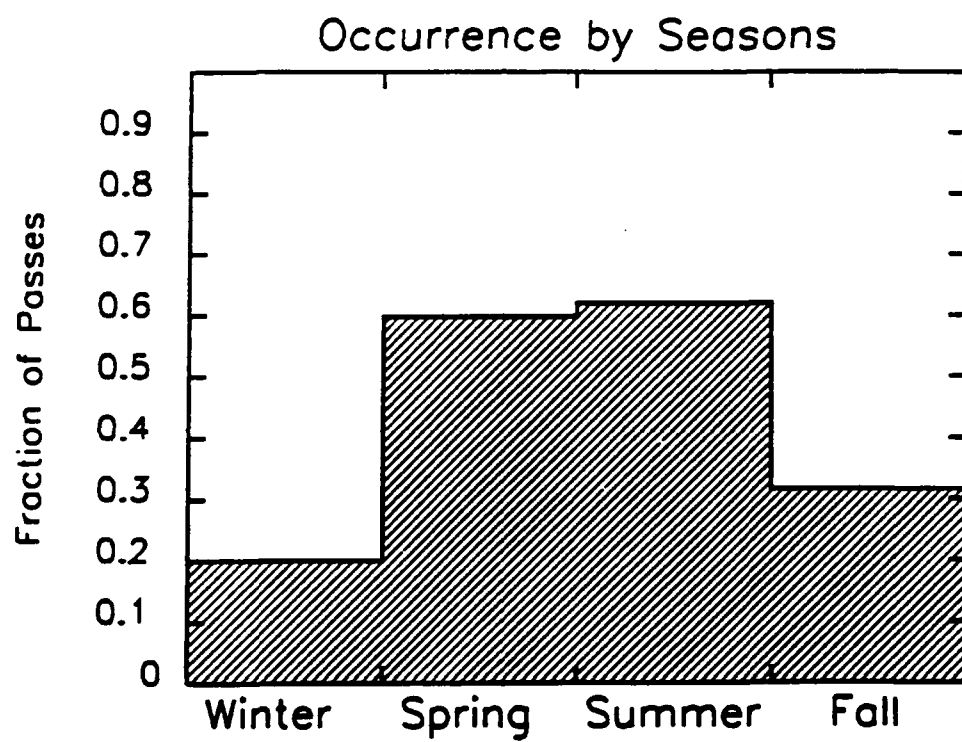Figure 5

Figure 6a

Figure 6b

Occurrence by Seasons

Figure 7

Cyclotron Resonance Precipitation of Energetic Electrons from the Inner Magnetosphere

D W DATLOWE and W L IMHOF (Lockheed Palo Alto Research Laboratory, Palo Alto, California 94304)

Cyclotron resonance between trapped energetic electrons and VLF waves produces pitch angle scattering which leads to electron precipitation in the inner magnetosphere. Previous experiments have shown that in the drift loss cone at L values from 1.5 to 1.8 the energy spectrum of the electrons above 50 keV is often dominated by a single narrow peak. The center energy of this peak varies with L in a manner characteristic of scattering by monochromatic VLF waves interacting in the vicinity of the geomagnetic equator, and the source of the waves is probably VLF communication or navigation transmitters. We report here for the first time the results of a study of 680 occurrences of these peaks detected by the low altitude polar orbiting satellite S81-1. The present data, from altitudes between 170 and 270 km. show the resonance peaks only in two restricted longitude zones centered at 110°E and 300°E, this result contrasts with the previous measurements at higher altitudes. which detected peaks over a wide range of longitudes. Detailed study of the events occurring near 110°E reveals a 27 day periodicity in the frequency of occurrence; peaks are most often observed during minima in solar/geomagnetic activity. The peaks are observed only at nighttime and have a possible seasonal variation, being more frequent from May to September. Since it is widely recognized that the transmission of VLF waves up through the ionosphere is best at night, if the seasonal varation is related to the number of hours of nighttime at the source, then the seasonal variation suggests that the transmitter which is precipitating these electrons is located in the southern hemisphere.

1. 1988 Fall Meeting

2. 001380622

3. D. W. DATLOWE
   Dept. 91-20, Bldg. 255
   Lockheed Palo Alto Research
   Laboratory
   3251 Hanover St.
   Palo Alto, CA 94304

4. (SM) Magnetospheric Physics

5. No special session
   2716 (precipitating particles)

6. Oral

7. None

8. Invoice 40.00
   P.O. ZAP-202970X
   Technical Information Center
   Lockheed Palo Alto Research
   Laboratory
   Dept. 90-11 Bldg. 201
   3251 Hanover St.
   Palo Alto, CA 94304
   Attention: Judy Conahan

9. Contributed

The Seasonal Variation in the Occurrence of Cyclotron Resonance Precipitation of Energetic Electrons by VLF Transmitters

D W DATLOWE and W L IMHOF (Lockheed Palo Alto Research Laboratory, Palo Alto, California 94304)

Precipitation of energetic $\sim$ 100 keV electrons from the inner radiation belt by cyclotron resonance with ground based transmitters has been observed by a number of satellites. A series of electron spectra recorded by a single satellite each show a narrow peak. The energy of the peak varies with L-value in a characteristic way, according to the condition for cyclotron resonance. Recent results from the S81-1/SEEP Satellite indicate that there may be a seasonal variation in the occurrence of these events. confirming an indication of the same effect in OV1-19 data previously reported by Vampola. The existence of a seasonal variation in the cyclotron resonance phenomenon would be important for understanding the coupling of the VLF transmitters to the magnetosphere. Unfortunately, none of the previous investigations had a data base covering as long as one year. We report here the detection of this variation using the EEM electron spectrometer data from the P78-1 satellite. The observations used in this study span the 4.5 year interval from January 1980 to mid 1984. With the P78-1 data we will show that the annual variation is a strong effect—night time events in the eastern hemisphere were rarely observed in the January-March time frame, but in the July-September time frame peaks were usually present.

1. 1989 Fall Meeting

2. 001380622

3. D. W. DATLOWE
   Dept. 91-20, Bldg. 255
   Lockheed Palo Alto Research
   Laboratory
   3251 Hanover St.
   Palo Alto, CA 94304

4. (SM) Magnetospheric Physics

5. No special session
   2716 (precipitating particles)

6. Oral

7. None

8. Invoice 50.00
   P.O. ZAP-217540X
   For more information
   contact: Judy Conahan
   Technical Information Center
   Lockheed Palo Alto Research
   Laboratory
   Dept. 90-11 Bldg. 201
   3251 Hanover St.
   Palo Alto, CA 94304

9. Contributed

10. No special instructions

11. Not a Student

Long Term Variations in the Equatorial Plasma Density near L=1.65 Measured by Resonant Precipitation of Energetic Electrons

D W DATLOWE and W L IMHOF (Lockheed Palo Alto Research Laboratory, Palo Alto, California 94304)

Powerful VLF transmitters are known to precipitate energetic electrons from the inner belt by cyclotron resonance interactions. The energy of the precipitated electrons is sharply peaked at a value determined by several factors, including the L-value of the observation, the transmitter frequency and the plasma density. In a series of observations made at the same L-value, the plasma density at the geomagnetic equator is the only time dependent factor which strongly influences the resonance energy. An extended set of measurements of the resonance precipitation peaks by the same transmitter at the same L-value, performed by the same electron detector, readily show time variations in the equatorial density. We describe here P78-1 Satellite observations of cyclotron resonance peaks to look for density changes over the period from 1979 to 1984. We find that during solar maximum (1979-1982) the density at L=1.65 was significantly higher than near solar minimum (1984). These findings are in accordance with the expectations of diffusive equilibrium models, where the equatorial density is driven by the solar ultraviolet flux.

1. 1990 Fall Meeting

2. 001380622

3. D. W. DATLOWE
   Dept. 91-20, Bldg. 255
   Lockheed Palo Alto Research
   Laboratory
   3251 Hanover St.
   Palo Alto, CA 94304

4. (SM) Magnetospheric Physics

5. No special session
   2716 (precipitating particles)

6. Oral

7. None

8. Invoice 60.00
   P.O. ZAP23198
   For more information
   contact: Jan Thomas
   Technical Information Center
   Dept. 90-11 Bldg. 201
   Lockheed Palo Alto Research
   Laboratory
   3251 Hanover St.
   Palo Alto, CA 94304
   (415) 424-2810

9. Contributed

10. No special instructions

11. Not a Student

APPENDIX C

COMPARISONS BETWEEN RELATIVISTIC ELECTRONS AT LOW AND HIGH ALTITUDES

RELATIVISTIC ELECTRON ENHANCEMENTS: SIMULTANEOUS MEASUREMENTS FROM SYNCHRONOUS AND LOW ALTITUDE SATELLITES

W. L. Imhof, H. D. Voss, J. Mobilia, D. W. Datlowe, J. P. McGlennon

Lockheed Palo Alto Research Laboratory, Palo Alto, California

and D. N. Baker

Goddard Space Flight Center, Greenbelt, Maryland

Abstract. We present here for the first time simultaneous measurements of trapped relativistic electron enhancements at synchronous altitude and precipitating electrons in the bounce loss cone at low altitudes. The measurements show that the daily variations in the precipitation flux for L>5 correlated well with the daily variations in the total flux at high altitude, both with respect to sudden enhancements as well as flux depletions. The daily averaged precipitating flux (E > 1 MeV) at L = 6.1 to 7.1 was about 0.3 percent of the daily averaged directional flux (E ≥ 1.5 MeV) observed at synchronous altitude, whereas within narrow spikes the precipitating directional fluxes were often within a factor of 10 of the daily averaged trapped fluxes. Strong depletions in the synchronous altitude ≥ 1.5 MeV electron intensities are shown to be associated with low altitude measurements of the equatorward movement of precipitating spikes to lower L shells.

Introduction

Relativistic electron enhancements have been studied extensively using measurements taken on synchronous-orbit satellites (e.g. Baker et al., 1986). Detailed information on the frequency of occurrence of these events and on the energy spectra was obtained. In the past, good correlations have been found between the relativistic electrons at synchronous altitude and the > 1 MeV electron fluxes at 840 km altitude (Baker et al., 1990), but the low altitude observations were not limited to directly precipitating electrons in the bounce loss cone. These measurements have not provided much knowledge of the extent in L-shell of the enhanced region or of the fluxes of relativistic electrons precipitating directly into the atmosphere. Vampola (1971) reported S3-3 measurements of precipitating relativistic electrons at altitudes from 362 to 4480 km. Some information on the L-shell extent and on the fluxes of relativistic electrons precipitating in the loss cone has currently become available for a few events (Imhof et al., 1991) from low altitude satellite measurements. However, many critical questions still remain unanswered. How well do electrons trapped at high altitude and those in the bounce loss cone track each other? In particular, when flux decreases are observed at synchronous altitude near the beginning of an event what are the corresponding changes at low altitude? How does the L-shell extent at low and high altitudes compare? Many of these questions can be answered with simultaneous relativistic electron measurements at high and low altitudes. Here such data are presented, and of particular interest are strong events with relatively steep onsets.

Description of Instrumentation

We present here a comparison of the data from electron detectors on the low altitude S81-1 satellite with the electron data from the synchronous altitude 1982-019 satellite. The instrumentation for the S81-1 payload is described in Voss et al. (1982) and in Imhof et al. (1991) and the instrumentation for the 1982-019 payload is described in Baker et al. (1986).

The Stimulated Emission of Energetic Particles (SEEP) experiment on the S81-1 spacecraft contained an array of cooled silicon solid state detectors to measure electrons and ions. The data were acquired over the period from May 28, 1982 until December 5, 1982. The S81-1 three-axis stabilized satellite was in a sun synchronous 1030 and 2230 local time polar orbit (inclination = 96.3°) at altitudes from 170 to 280 km. The electron spectrometer ME1 at a zenith angle of 0° (less than 30° pitch angle for much of the data presented and therefore in the bounce loss cone) and ME2 at a zenith angle of 180° had acceptance angles of ±30°. At these altitudes the field-of-view of the ME1 detector is entirely within the bounce loss cone. The silicon detectors in ME1 and ME2 were surrounded (except for the entrance aperture) by plastic scintillator anticoincidence shields. Counts were recorded in each corresponding anticoincidence counter, both singles and in coincidence with the silicon detector; only one threshold level was used and for electrons the threshold energy for detection was ~1 MeV. The geometric factor for the singles response was 3.09 cm^2 sr with an acceptance angle of ±30°.

Electron flux measurements at high altitude were taken with the Spectrometer for Energetic Electrons (SEE) flown at geostationary orbit on board spacecraft 1982-019. The spectrometer is a two element telescope consisting of two silicon detectors (operated in parallel) and a bismuth germanate scintillation crystal. The SEE sensor makes integral electron measurements at energies ≥ 1.5 MeV and four differential measurements at higher energies.

Presentation of Data

A survey for relativistic electron spikes well within the bounce loss cone was conducted with the SEEP data. To qualify as an event in this survey, it was required that the plastic scintillator singles counting rate in the ME1 spectrometer, which was viewing upward, increase above background by at least a factor of two and that the increase be significantly above that in the scintillator of the ME2 detector which was viewing downward.

Precipitating electrons above 1 MeV were measured with the anticoincidence detector in the ME1 spectrometer as noted above. When these fluxes were enhanced they were typically above background in the form of spikes near the trapping boundary with 10 second observation or less (equivalently a spatial width of less than 100 km (Imhof et al., 1991)). Precipitation spikes observed for less than one second were not included in the survey. For studying the time profiles one can use either the maximum flux or the time integrated flux (fluence) measured in each spike during a satellite pass. Both approaches have been used for comparisons of S81-1 data with measurements at synchronous altitude and give consistent results. Here we present analyses based on the maximum flux in each spike.

Averages of the peak fluxes have been obtained both for spikes at all L values and also restricting their inclusion only to spikes at L>5. In the latter case the enhancements were more pronounced; accordingly, all flux plots presented here are limited to L values above 5. Figure 1 shows these fluxes plotted as a function of time. The background rate which was typically about 60 counts per second has been subtracted from the peak counting rate in each spike. The spike fluxes vary considerably from one satellite pass to the next. Also shown are 24 hour averages of the average peak flux recorded on each pass: for these averages zero flux is assumed for a pass when no spikes were observed at L>5. On some days the averaged precipitating fluxes were below the threshold level for reporting a spike since no precipitation spikes were observed on many of the passes. Analyses of the low altitude data were performed for median flux values in addition to average values and gave nearly the same results.

For comparison, the two sets of data, S81-1 and S/C 1982-019, are plotted in Figure 2 as a function of day number in 1982. Daily averages of the precipitating electron flux above 1 MeV measured in the ME1 anticoincidence detector on the S81-1 spacecraft are shown. In converting from counting rate to flux we have used a geometric factor of 3.09 cm^2 sr which is rigorously applicable only to isotropic fluxes. Based on other measurements of electron precipitation near the trapping boundary (e.g. Imhof, 1988) we have assumed that many of the electron precipitation spikes considered here are isotropic. Also plotted are 24 hour averages (multiplied by a factor of 0.01) of the electron directional flux $\geq$ 1.5 MeV measured in the SEE detector on S/C 1982-019. It is clear that on a daily basis the > 1 MeV precipitating electrons in the bounce loss cone as observed at low altitudes track rather well the $\geq$ 1.5 MeV electrons trapped at synchronous altitude.

The daily averaged fluxes of electrons precipitating at L>5 were about an order of magnitude less than the fluxes of electrons trapped at high altitude on L = 6.6. The daily averaged fluxes of precipitating electrons at L = 6.1 to 7.1 were about 0.3 percent of the daily averaged fluxes observed at synchronous altitude. However, in the narrow spikes the precipitating fluxes were often within a factor of 10 of the daily averaged fluxes trapped at high altitude. Much of the reduction in the daily averaged precipitating fluxes relative to the trapped fluxes at high altitude can perhaps be attributed to irregular access of electrons to the bounce loss cone. Of course in many cases the precipitation may be only in the drift loss cone.
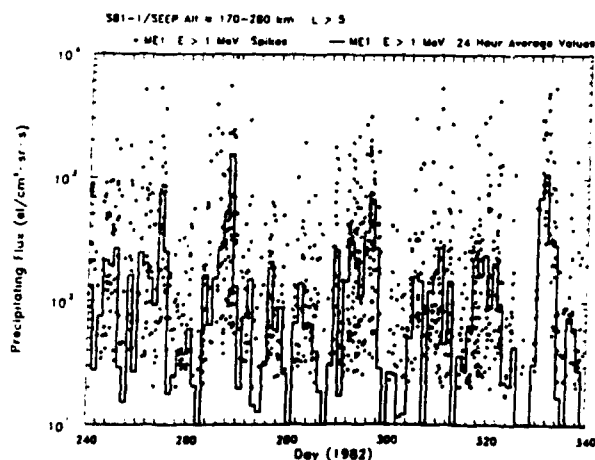

Fig. 2. Daily averaged fluxes of precipitating electrons >1 MeV measured at low altitudes on the S81-1 satellite and electrons recorded at synchronous altitude on S/C 1982-019. The latter electrons are at energies of $\geq$ 1.5 MeV and their corresponding fluxes are multiplied by 0.01 for clarity.

In prior studies of the high altitude data (e.g., Baker et al., 1986), there has been much attention paid to the 27-day recurrence tendency seen in the relativistic electron component. In the present study we have only 100 days of concurrent low-altitude and high-altitude data available and it is difficult to verify a true periodicity in such a limited interval. Moreover, the strong 27-day recurrences reported by Baker et al. for the SEE data become particularly prominent later (i.e., in 1984-85) than the present analysis interval. Nonetheless, Figure 2 does show some tendency for 27-day enhancements with, perhaps, an interleaving of two cycles to give evidence of 13-day recurrences.

In Figure 3 the daily averaged fluxes of precipitating electrons above 1 MeV as measured at L>5 in the anticoincidence scintillator of the ME1 spectrometer on the low altitude S81-1 satellite are plotted versus the daily averaged electron fluxes $\geq$ 1.5 MeV recorded at synchronous altitude in

Fig. 1. The maximum fluxes in each spike of precipitating electrons >1 MeV at low altitudes from the S81-1 satellite plotted as a function of time. Also shown are 24 hour averages of the maximum fluxes.
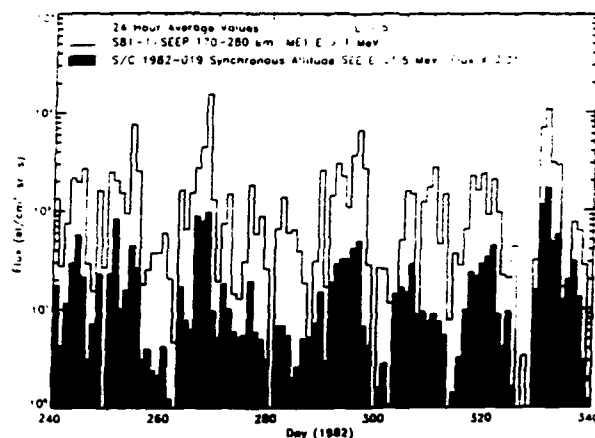

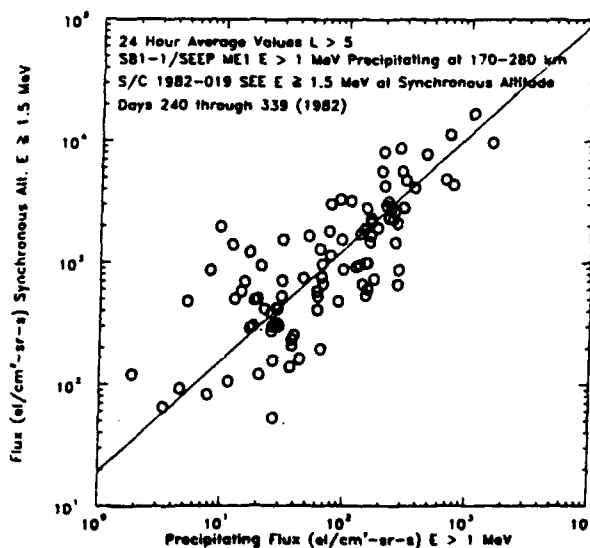Fig. 3. Daily averaged electron fluxes $\geq$ 1.5 MeV obtained at synchronous altitude on S/C 1982-019 versus the daily averaged fluxes of precipitating electrons >1 MeV as measured on the satellite S81-1.

the SEE instrument. By inspection. one can see that the precipitating flux > 1 MeV correlates well with the high altitude flux ≥ 1.5 MeV. The correlation coefficient is 0.77. significant at the 11.8 sigma level for 96 points. For spikes at L≤5 no significant correlations were found. The low altitude observations occurred at exactly the same L value (6.6) as the synchronous measurements for only a small fraction of the time. but the low altitude coverage of the precipitation spikes is sufficient to make a comparison of the two sets.

We have investigated the correlation between the precipitation fluxes at low altitudes and the rates of decrease of electrons at high altitudes. The latter quantities were obtained by considering the correlations between the precipitation flux at low altitudes and the trapped flux at high altitudes on the previous day and on the previous two days as well as on the following day and the following two days. These results are summarized in Table 1. The correlations are clearly best when both sets of measurements are simultaneous within one day.

At times of pronounced decreases in the high altitude flux there is often a significant equatorward movement in the L-value of the precipitation spikes. suggesting that the drop outs in the high altitude flux. which often occurred at times of increased geomagnetic activity. may be due to an inward movement of the trapped electrons. In Figure 4 the daily averaged high altitude fluxes of electrons ≥1.5 MeV are plotted

Table 1. Correlation Values Between the Precipitation Flux at Low Altitudes and the Trapped Flux at High Altitudes (for 96 Days)

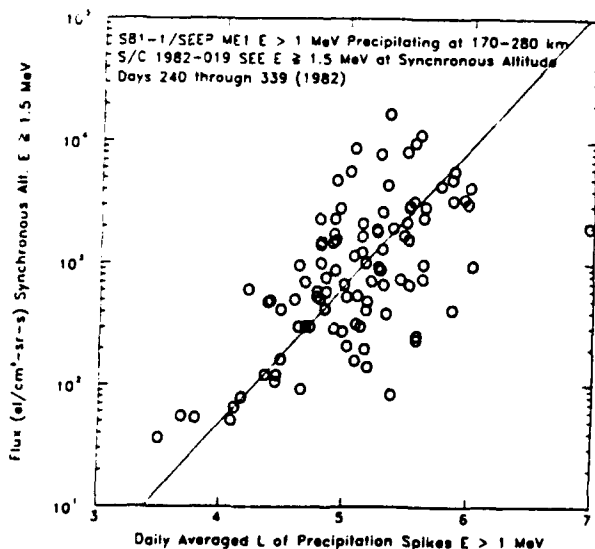| SEE Data	Correlation Coefficient	Statistical Significance (Sigma)
2 Days Before	+0.13	1.2
1 Day Before	+0.36	3.7
Same Day	+0.77	11.8
1 Day After	+0.50	5.5
2 Days After	+0.16	1.5

Fig. 4. Daily averaged fluxes of electrons ≥ 1.5 MeV at high altitude versus the daily averaged L values of electron > 1 MeV spikes measured in the bounce loss cone.

as a function of the daily averaged L values of the spikes of precipitating electrons above 1 MeV. The correlation coefficient is 0.62. significant at the 7.8 sigma level for 100 points. There is a reasonably clear relationship between the logarithm of the flux at 6.6 R_E and the averaged L value: thus the decrease at synchronous altitudes is associated with an inward motion.

Summary

We have found good correlations between the time dependence of the fluxes of relativistic electrons trapped at synchronous altitude and of relativistic electrons precipitating into the atmosphere. During narrow spikes well within the loss cone the precipitating directional intensities were often within a factor of 10 of the daily averaged trapped directional intensities at high altitudes. whereas the daily averaged precipitating fluxes were only about 0.3 percent of the trapped fluxes. A proper comparison of the high and low altitude electron populations would be to map adiabatically conserved quantities according to Liouville's theorem in a realistic magnetic field model. Such a comparison has not yet been performed in detail for each event. Additional precipitation may appear primarily only near the edge of the loss cone and not be within the field-of-view of the ME1 detector.

We have also investigated the L shell dependence of the precipitation of electrons above 1 MeV as a function of time. At the times of pronounced depletions in the high altitude fluxes the precipitation spikes observed at low altitudes appeared to move to lower L shells.

Ultimately. of course. it is likely that the transport of electrons into the equatorial loss cone is due to wave-particle interactions. The correlation between the fluxes of relativistic electrons measured at 6.6 R_E and the precipitating electron fluxes measured by the SEEP ME1 instrument was highest when data from the same day for the respective instruments were used (see Table 1). Thus. in this sense it is the current near-equatorial flux level that determines the precipitating fluxes rather than the time rate of change of the fluxes (at least on day-long time scales). From this behavior one might conclude that the precipitation of relativistic electrons observed in spikes in the bounce loss cone is not the principal or dominant loss mechanism. From this point of view. the data are consistent with the precipitation flux resulting from interaction of the flux trapped at high altitudes with a strength of waves that is constant on a long-term basis. Then the precipitation flux would be proportional to the flux trapped at high altitude and not the rate of change of flux trapped at high altitude.

On the other hand. Baker et al. (1987) suggested that relativistic electrons may be precipitated quite rapidly. They suggested that the electrons are strongly dumped into the atmosphere when fluxes are high in the outer zone. When such flux levels are lower (as is true much of the time). they evidently are not precipitated significantly. Thus. Baker et al. envisioned the electron fluxes and the wave levels going up and down together (on time scales < 1 day) primarily driven by variable source strength for the electrons. Hence the waves that ultimately precipitate the electrons could wax and wane along with the electron population rather than remaining constant over long periods. In this view. precipitation would be a much more significant loss process for the outer zone.

It is important to understand more globally what the outer zone electron flux variations are. It would be particularly valuable to measure relativistic electron flux variations at several different equatorial L values at the same time as we observe geosynchronous enhancements. This would more clearly delineate the global significance of this magnetospheric population and would shed light on its contribution to the global atmospheric ionization input (Baker et al.. 1987: Imhof et al.. 1991).

References

Baker, D.N., J.B. Blake, D.J. Gorney, P.R. Higbie, R.W. Klebesadel, and J.H. King, Highly relativistic magnetospheric electrons: a role in coupling to the middle atmosphere?, *Geophys. Res. Lett.*, 14, 1027, 1987.

Baker, D.N., J.B. Blake, R.W. Klebesadel, and P.R. Higbie, Highly relativistic electrons in the earth's outer magnetosphere. 1. Lifetimes and temporal history 1979-1984., *J. Geophys. Res.*, 91, 4265, 1986.

Baker, D.N., J.B. Blake, R.W. Klebesadel, D.D. Sentman, D.J. Gorney, P.R. Higbie, Highly relativistic magnetospheric electrons: lower ionospheric conductivity and long-term atmospheric variability, *Adv. Space Res.*, 10, 229-233, 1990.

Imhof, W.L., Fine resolution measurements of the L-dependent energy threshold for isotropy at the trapping boundary, *J. Geophys. Res.*, 93, 9743, 1988.

Imhof W.L., H.D. Voss, J. Mobilia, D.W. Datlowe, and E.E. Gaines, The precipitation of relativistic electrons near the trapping boundary, *J. Geophys. Res.*, in press, 1991.

Vampola, A. L., Electron pitch angle scattering in the outer zone during magnetically disturbed times, *J. Geophys. Res.*, 76, 4685, 1971.

Voss, H.D., J.B. Reagan, W.L. Imhof, D.O. Murray, D.A. Simpson, D.P. Cauffman, and J.C. Bakke, Low temperature characteristics of solid state detectors for energetic X-ray, ion and electron spectrometers, *IEEE Trans. Nucl. Sci.*, NS-29, 164, 1982.

D. W. Datlowe, W. L. Imhof, J. P. McGlennon, J. Mobilia, H. D. Voss, Lockheed Palo Alto Research Laboratory, Dept 91-20 Bldg. 255, 3251 Hanover Street, Palo Alto, CA 94304

D. N. Baker, NASA Goddard Space Flight Center, Code 690, Greenbelt, MD 20771

The Precipitation of Relativistic Electrons Near the Trapping Boundary

W. L. Imhof, H. D. Voss, J. Mobilia, D. W. Datlowe, and E. E. Gaines

Lockheed Palo Alto Research Laboratory, Palo Alto, California

Highly relativistic electrons are known to be present at synchronous satellite altitude in time-varying and sometimes large intensities; it is therefore important to consider the fluxes and locations of relativistic electrons precipitating into the atmosphere. Here we present measurements from the low-altitude three-axis-stabilized satellite S81-1 of trapped and precipitating electrons from 6 keV to above 1 MeV. Significant fluxes of precipitating relativistic electrons above 1 MeV within the bounce loss cone are much more often observed near midnight than noon and generally in narrow spikes <100 km in width typically at L values between 4 and 6 near the radiation belt boundary. The tendency for many of the relativistic spikes to be near the trapping boundary is consistent with the general pattern at lower energies confirmed by the measurements presented here of intensity and threshold energy for isotropy versus L shell. A trend was observed for the higher-energy precipitating electron fluxes to peak at somewhat lower L values. The precipitation of >1-MeV electrons has been measured to occur at intensities and in locations that are widely variable within a few minutes superposed on longer-term variations. On one of the days of strongest precipitation the total nighttime input to the atmosphere during 12 hours from >1-MeV electrons within the bounce loss cone near the trapping boundary was $\sim 10^{19}$ ergs, which was an order of magnitude less than the loss rates estimated by Baker et al. from high-altitude measurements, suggesting that precipitation in the drift loss cone may be significant.

INTRODUCTION

The population of relativistic electrons at high altitudes, such as those regions traversed by synchronous satellites, is known to experience major enhancements and depletions [e.g., *Baker et al.*, 1987]. The electron flux at synchronous altitude diminishes rapidly in association with an enhancement of geomagnetic activity and then increases [*Nagai*, 1988]. An important question subsequently arises: How many of these relativistic electrons are ultimately precipitated into the Earth's atmosphere, and where does such precipitation occur? This matter is important to consider from the standpoint of understanding both the electron transport processes and the associated effects in the atmosphere of relativistic electron precipitation. Here we investigate the precipitation of relativistic electrons.

Vampola [1971, 1977] investigated the precipitation of relativistic electrons using some examples from the S3-3 satellite data. High-energy ($E > 1.5$ MeV) electrons were found to be scattered more readily than lower-energy ($E \sim 300$ keV) electrons. *Thorne and Andreoli* [1980] made a study of relativistic electron precipitation (REP) events using S3-3 satellite data. The electron energies were in the range of a few hundred keV. It was found that many of the events occurred near the outer limit of electron trapping, but neither time profiles of the precipitation rates nor comparisons with synchronous altitude measurements were provided.

Over a wide range of energies the loss of electrons from the radiation belts is enhanced near the outer edge [e.g., *Fritz*, 1968, 1970]. For the first time the precipitation near the midnight trapping boundary was shown often to display an energy and L shell dependent flux enhancement and an energy selectivity which varies strongly with L value [*Imhof et al.*, 1977, 1979; *Imhof*, 1988]. The onset of isotropy (i.e., where the trapped and precipitating fluxes are equal) at low altitude typically occurs at a sharply defined energy threshold which decreases rapidly with increasing L value. Highly relativistic electrons might therefore be expected to experience enhancements in the low L shell portion of the trapping boundary.

The energy selective phenomenon observed by Imhof et al. has been interpreted in terms of the loss of adiabatic motion when the radius of field line curvature is less than an order of magnitude greater than the gyroradius of the electrons. The mechanism inherently has a threshold energy that is dependent upon the characteristics of the magnetic field line, and hence an L dependent threshold for isotropy is perhaps to be expected. For various magnetic field models, theoretical calculations have been made of the expectations [*Popielawska et al.*, 1985; *Büchner and Zelenyi*, 1989], and they are consistent with some of the observations. On the other hand, for wave-particle interactions a strongly L dependent threshold could result from changes with L in the frequency distribution of the waves or in the plasma density. So the L dependence of the threshold energy may by itself not provide a unique identification of the mechanism.

The energy selective outer boundary has been observed previously from two different satellites, but both of the earlier studies were performed from a spinning vehicle, and accordingly the precipitating fluxes were measured only within a limited duty cycle. With such a sampling, key portions of and even entire precipitation events could be missed. Several advantages are achieved when the measurements are performed from a three-axis-stabilized satellite. The advantages include the following: (1) All precipitation spikes of sufficient intensity are measured, with none being lost because of duty cycle effects. (2) Accurate measurements are obtained of the L shell width of the transition region for energy selectivity. (3) Any deviations from a monotonic pattern in the threshold energy for isotropy versus L value can be more readily observed.

Here we present relativistic electron precipitation data acquired with the SEEP (Stimulated Emission of Energetic Particles) experiment on the S81-1 spacecraft. Intensities

Fig. 1. Examples of flux enhancements observed on selected satellite passes. Backgrounds have not been subtracted.

and spatial distributions of precipitating electrons above 1 MeV are considered. For lower-energy electrons we investigate the threshold energy for isotropy and its dependence on L shell near the trapping boundary.

DESCRIPTION OF INSTRUMENTATION

The *Stimulated Emission of Energetic Particles* (SEEP) experiment on the three-axis-stabilized S81-1 spacecraft contained an array of cooled silicon solid-state detectors to measure electrons and ions [*Voss et al.*, 1982]. The data were acquired over the period from May 28. 1982. until December 5. 1982. The S81-1 satellite was in a Sun synchronous 1030 and 2230 local time polar orbit (inclination of 96.3°) at 170–280 km altitude. traveling southward during the daytime. The electron spectrometers were oriented at various angles to the local vertical. Here data are used from three of the spectrometers. The spectrometer TE2 at 90° zenith angle (approximately 90° pitch angle for the data presented) had an acceptance angle of ±20° and a geometric factor of 0.17 cm^2 sr. The pulse height analyzer for the data presented had a range of 6–930 keV with energy steps of 3.62 keV. The TE2 spectrometer had a very thin window on the Si detector so that >3-keV electrons and >30-keV protons could enter. The instruments ME1 and ME2 at zenith angles of 0° (approximately 30° pitch angle for most of the data presented and therefore in the bounce loss cone) and 180°, respectively, had acceptance angles of ±30°. geometric factors of 2.47 cm^2 sr. threshold energies of 45 keV. and energy resolutions of about 20 keV. The pulse height analyzer covered the range 45 keV to approximately 980 keV. The silicon detectors in ME1 and ME2 were surrounded except for the entrance aperture side by plastic scintillator anticoincidence shields with an internal energy threshold of about 100 keV. The ME1 and ME2 detectors had relatively thick windows: ~7 μm of Kapton double coated with ~0.1 μm of aluminum for a total thickness of ~1.1 mg/cm^2. The penetration threshold energy for electrons was ~22 keV and for protons was ~500 keV. Total integral counting rates above several thresholds in each of the spectrometers were recorded during successive 0.064-s intervals. and the pulse height address of the first count in each successive 0.004-s interval was recorded for TE2 and ME1.
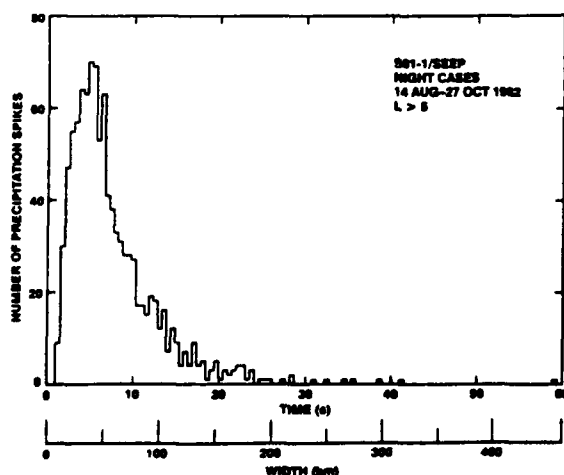

Fig. 2. Distribution in observed temporal/spatial width of the nighttime precipitation spikes.
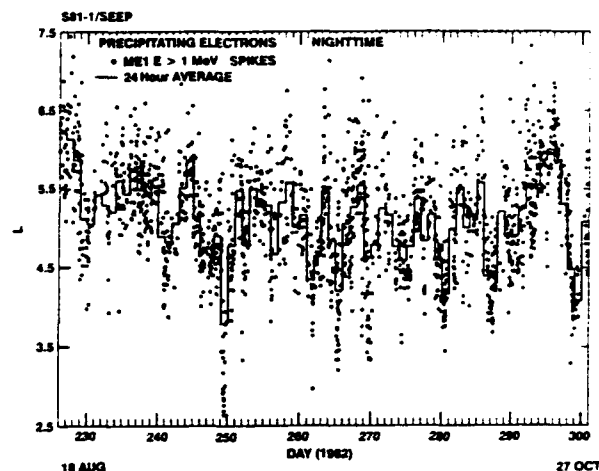

Fig. 3. L value for each nighttime spike of precipitating electrons >1 MeV versus day number for days 226–300. August 14. 1982. to October 27. 1982.

For ME2 the sampling interval is twice as long (0.008 s). During data analysis, energy spectra can be accumulated over any arbitrary time period. In the ME1 and ME2 spectrometers. counts were also recorded in each corresponding anticoincidence counter, both singles and in coincidence with the silicon detector: for electrons the threshold energy was ~1 MeV. The geometric factor for the singles response was 3.09 cm^2 sr with an acceptance angle of ±30°. Electrons above ~15 MeV could be detected with a nearly omnidirectional response. but based on the relative responses observed in ME1 and ME2 the latter contribution is ignored for the data studied here.

In the data analysis, L values were calculated using the Goddard Space Flight Center (GSFC 12/66) geomagnetic field model [*Cain et al.*, 1967] for the epoch 1980.

LOCATIONS OF PRECIPITATING ELECTRONS ABOVE 1 MeV

On midnight passes of the S81-1 satellite at high latitudes. narrow spikes of precipitating electrons above 1 MeV and well within the bounce loss cone were often observed. An example of a satellite pass with such flux enhancements is illustrated in Figure 1a. which shows the fluxes of mirroring (TE2) and precipitating (ME1) electrons above 300 keV. Due to the low altitude of the satellite. at certain locations locally mirroring electrons are precipitating because they are in the bounce loss cone (when the altitude of the conjugate point is below sea level), or in many places they are in the drift loss cone (when the minimum altitude upon longitude drift around the Earth. h_{min}, is <0 km). The case in Figure 1a is unusual in that within the same satellite pass. significant fluxes of electrons above 1 MeV are precipitating in narrow spikes both near the trapping boundary and at somewhat lower latitudes. If present. the precipitation observed with the ME1 detector is generally at only one location. although the widths and shapes may differ considerably, as illustrated in Figures 1b and 1c. In the latter figures are shown the fluxes of precipitating electrons above 45 keV. 300 keV. and 1 MeV. Throughout this paper the fluxes above 1 MeV are based on the total counting rate in the anticoincidence shield. The rate of coincidences between the silicon sensor
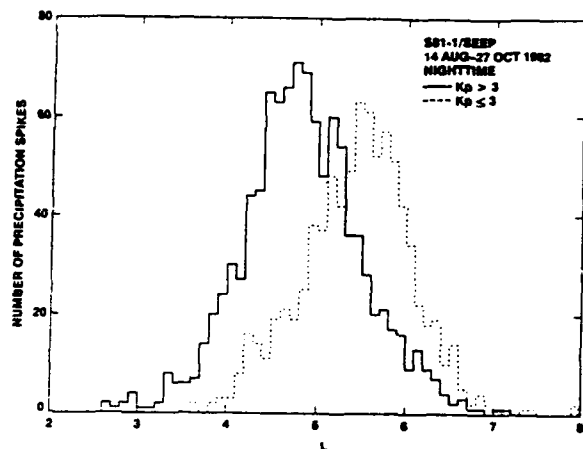
Fig. 4. Distribution in L value for each nighttime spike of >1-MeV precipitating electrons. separately for $Kp \leq 3$ and for $Kp > 3$ for days 226–300. August 14, 1982, to October 27, 1982.

and the antiscintillator shield was typically about 80% of the antisingles rate for the data presented here. Backgrounds due to cosmic rays have not been subtracted.

A survey for relativistic electron spikes well within the bounce loss cone was conducted. To be qualified as a point in this survey, it was required that the anticoincidence counting rate in the ME1 spectrometer, which was viewing upward, increase above background by at leas' a factor of 2 and that the increase be significantly above that in the antichannel of the ME2 detector, which had an acceptance angle in the downward direction. A variety of narrow spikes occurred, but most commonly the enhanced fluxes above 1 MeV were observed for less than 10 s (77 km) and were generally between L of 4 and 6. The distribution in transit time (or equivalent spatial width) of the nighttime spikes is shown in Figure 2. Here the full widths are taken to be at one-fifth maximum. The equivalent spatial widths in kilometers are shown for a satellite velocity of 7.7 km/s. The transit time intervals shown in the figure should not have been influenced by the selection criteria used in the original survey except that
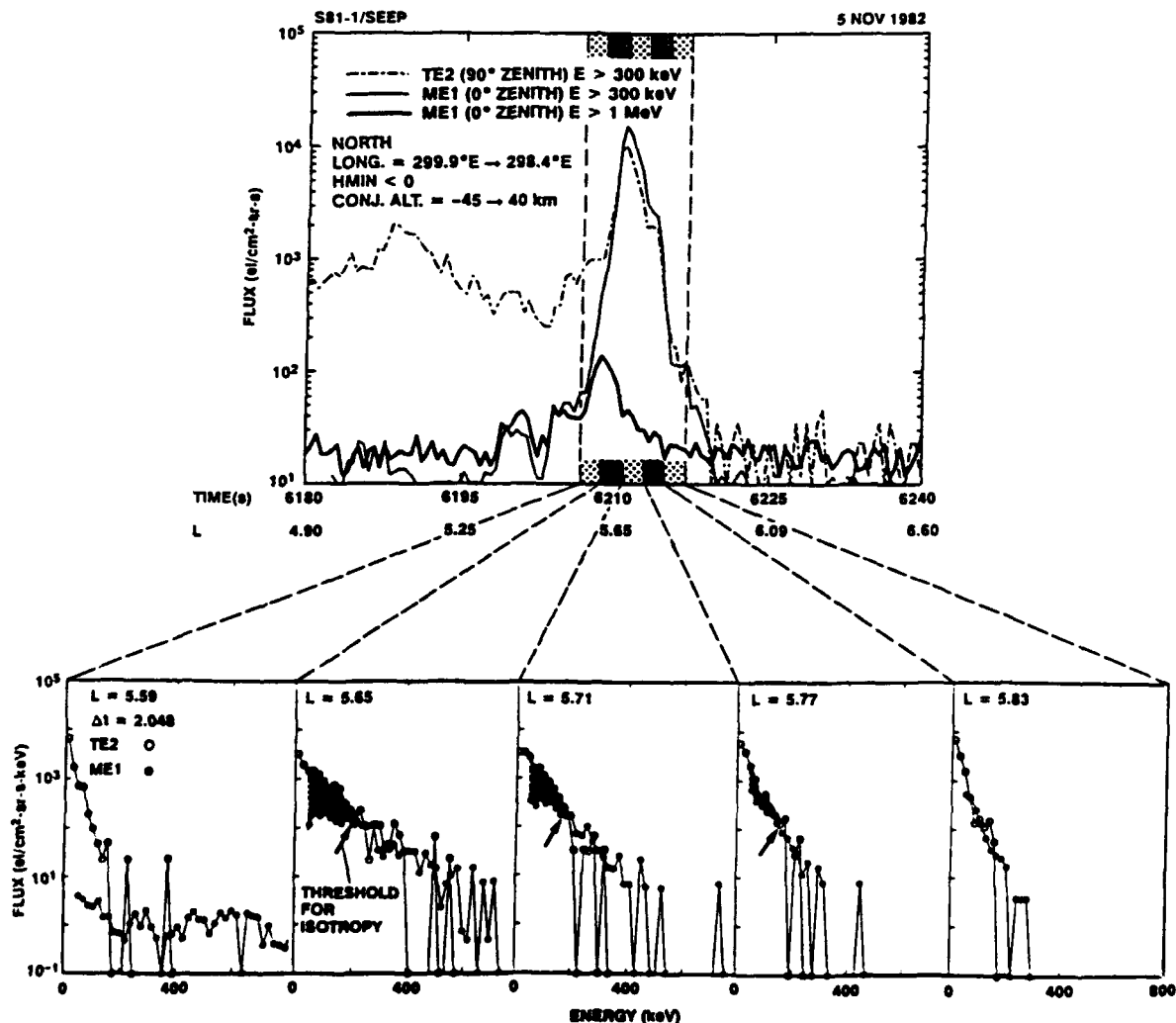

Fig. 5. Integral fluxes above various threshold energies at 0° and 90° zenith angle versus time (upper section). At selected times are shown differential energy spectra for accumulation time periods of 2.048 s each for detectors ME1 (0°) with a vertical field of view and TE2 (90°) with a horizontal field of view (lower section).
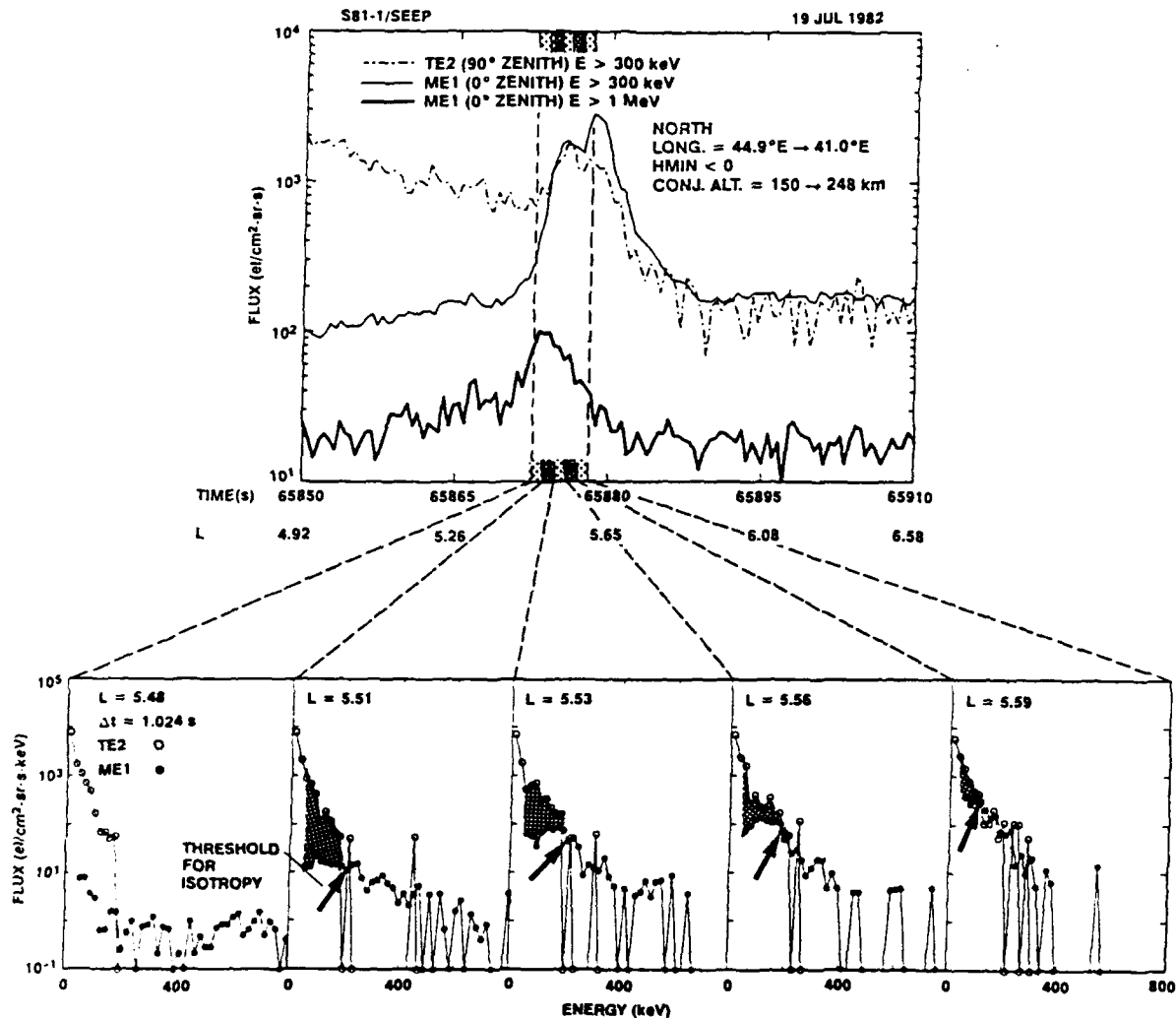
Fig. 6. Integral fluxes above various threshold energies at 0° and 90° zenith angle versus time (upper section). At selected times are shown differential energy spectra for accumulation time periods of 1.024 s each for detectors ME1 (0°) and TE2 (90°) (lower section).

spikes narrower than ~1 s were not included in the survey. The data indicate that relativistic electron precipitation in the bounce loss cone tends to occur over very localized regions. Seldom does the enhanced precipitation extend over a broad latitude interval on any given satellite pass. The average width is about 40 km, and 90% of the spikes have a width <100 km. This finding has important implications both for total energy input into the atmosphere and for efforts to understand the responsible precipitation mechanisms. Of course, some or many of the spikes may have been arclike in extent perpendicular to the satellite path.

Some of the questions which naturally arise are, What is the L value at which the relativistic precipitation spikes occur, and how does the L shell of this location change with geomagnetic activity? To study the problem in greater detail, a representative period, from August 14, 1982, to October 27, 1982, was selected. For this time period the location of the observed precipitation is plotted in Figure 3 for each spike. Twenty-four-hour averages are also shown in the figure. Very low latitude spikes were found on day 249

(September 6, 1982), with several precipitating flux enhancements occurring at calculated L values between 2.5 and 3.0. The overall distributions in L value are shown in Figure 4, separately for $Kp \leq 3$ and $Kp > 3$. It is clear from the figure that at times of higher Kp the relativistic electron precipitation spikes tend to occur at lower L values. Nearly all of the spikes below an L value of 4.5 occur during geomagnetically active times.

ISOTROPY NEAR THE TRAPPING BOUNDARY

Since the spikes of precipitating electrons above 1 MeV generally occur in the outer portions of the radiation belt, it seems appropriate to investigate the consistency of these patterns with those of lower-energy electrons at such positions. Near the midnight trapping boundary the occurrence of L dependent peaks in the flux of precipitating electrons that vary with energy and energy selective thresholds for isotropy has previously been reported [Imhof et al., 1977, 1979; Imhof, 1988], but the measurements were all from
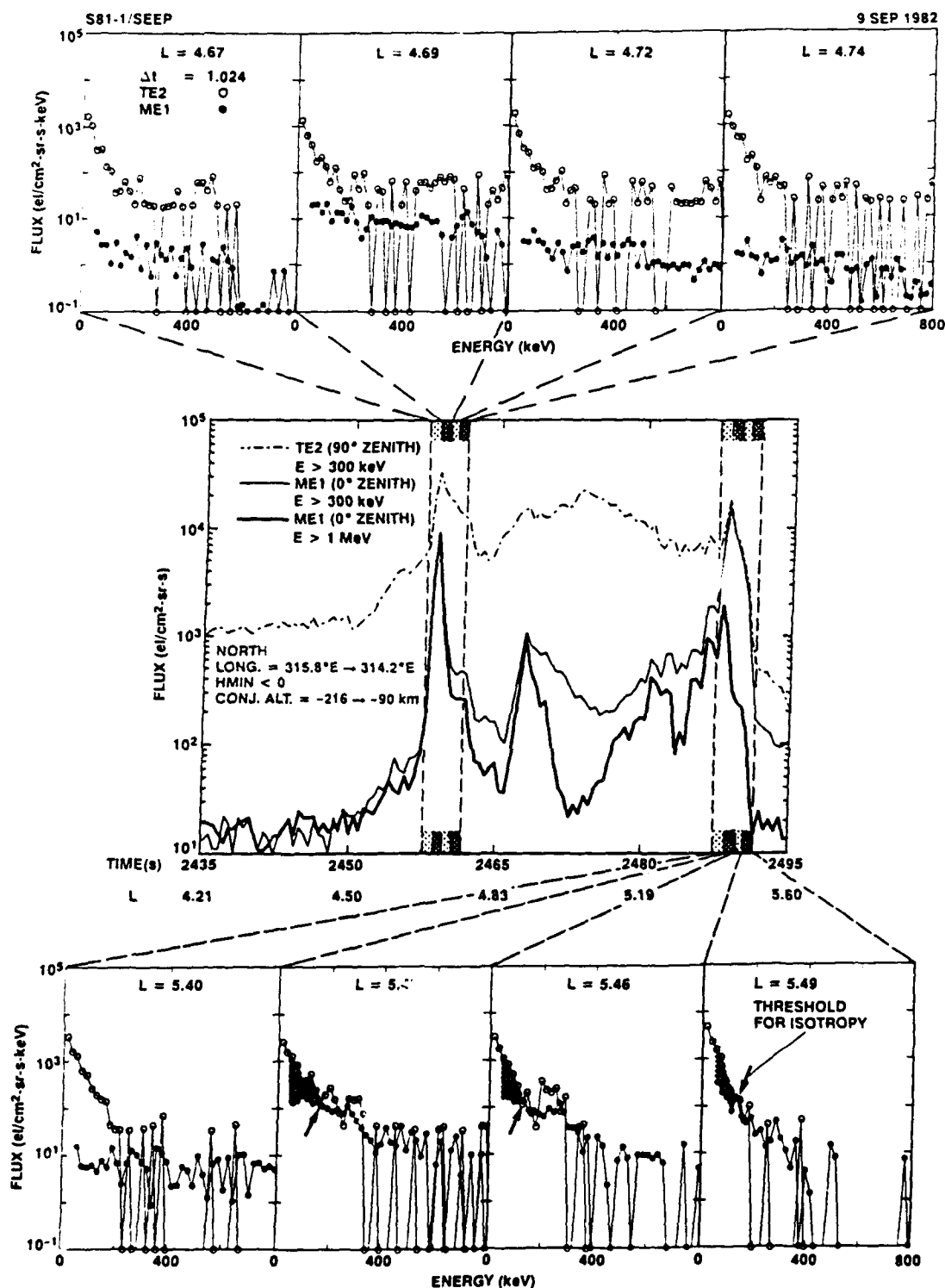
Fig. 7. Integral fluxes above various threshold energies at 0° and 90° zenith angle versus time (middle section). At selected times are shown differential energy spectra for accumulation time periods of 1.024 s each for detectors ME1 (0°) and TE2 (90°) (top and bottom section).

spinning satellites, and accordingly the precipitating electrons were recorded during only a small fraction of the observing time. Now we consider nighttime data from the S81-1 satellite in which the precipitating and trapped electrons were each observed continuously with 0.064-s time resolution. Integral fluxes above 300 keV threshold energy at 0° (ME1) and at 90° (TE2) zenith angle are plotted as a function of time in the upper section of Figure 5. Also plotted
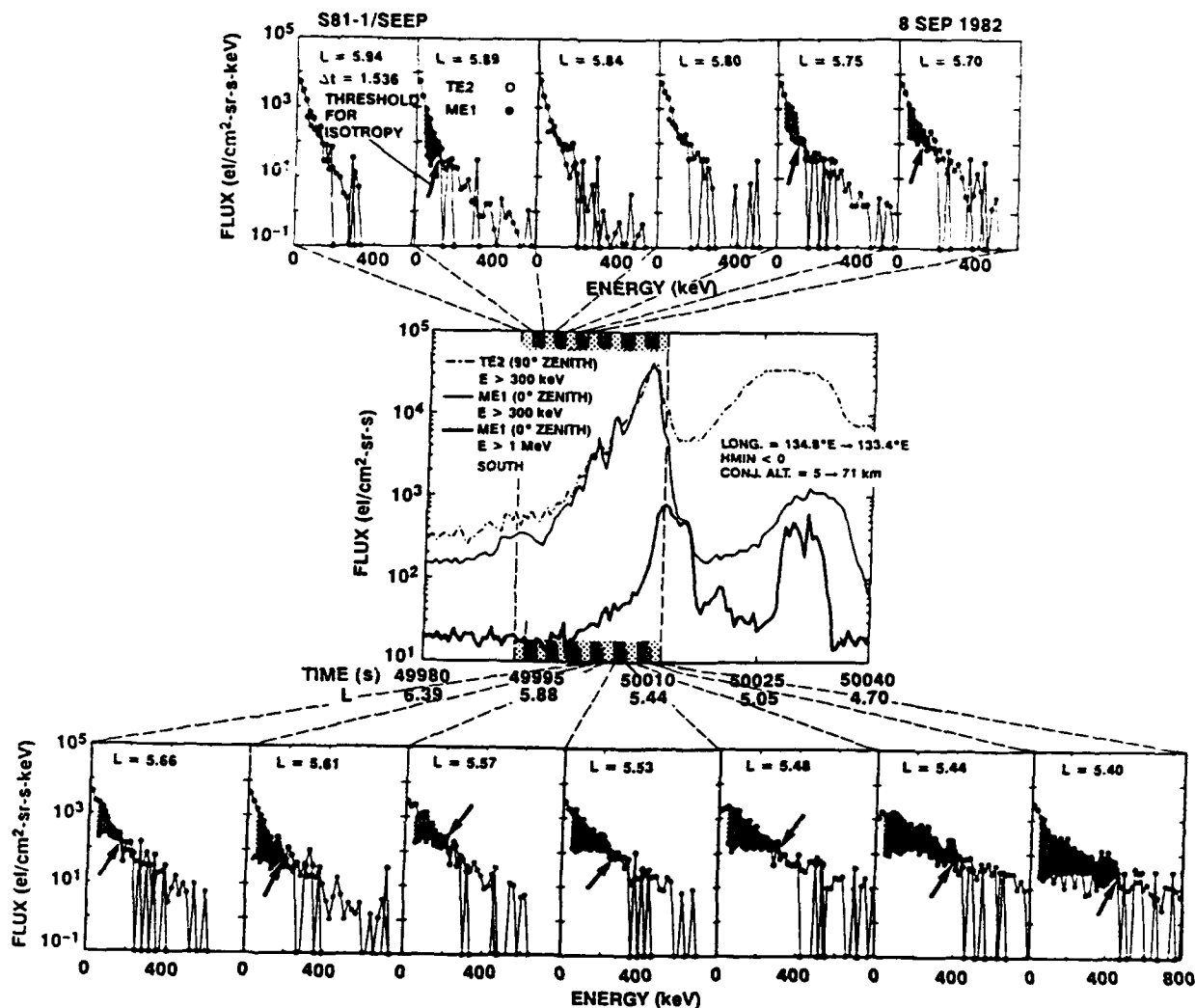
Fig. 8. Integral fluxes above various threshold energies at 0° and 90° zenith angle versus time (middle section). At selected times are shown differential energy spectra for accumulation time periods of 1.536 s each for detectors ME1 (0°) and TE2 (90°).

are the integral fluxes above 1 MeV of precipitating electrons as measured with the ME1 anticoincidence detector. Backgrounds, which are small compared to the counting rates in many of the spikes, have not been subtracted. The typical flux enhancement at the trapping boundary is evident. The figure illustrates the trend for the higher-energy electrons to precipitate over a more confined region at somewhat lower L shells.

Differential spectra with fine energy resolution were obtained by recording individual addresses at a maximum rate of 250 per second. Differential energy spectra for detectors ME1 and TE2 are shown in the lower sections of Figure 5 at selected times during the crossing of the trapping boundary for accumulation time periods of 2.048 s each. At certain locations the appearance of a threshold energy for isotropy is evident. At energies below this threshold a crosshatch pattern is placed between the trapped and precipitating fluxes. Consistent with previous publications the threshold energy tends to decrease with increasing L value. A similar pattern for another nighttime crossing of the satellite is shown in Figure 6 for spectral accumulation time periods of 1.024 s each.

Figure 7 shows an example of a nighttime satellite pass when several pronounced precipitation spikes occurred within the outer radiation belt in addition to a spike at the trapping boundary. Selected energy spectra are shown for accumulation time periods of 1.024 s each. A threshold energy for isotropy appeared in the spectra near the trapping boundary, and the energy tended to decrease with increasing L value, but no such spectra appeared in the spike near 2460 s at lower L values. The spectra at the lower L shells were harder than those near the trapping boundary.

More complex cases than the data just shown were observed. Figure 8 contains a nighttime example in which energy selective isotropy did not display a monotonic behavior at all L values. The spectral accumulation time periods were 1.536 s each. Pronounced threshold energies for isotropy occurred poleward of the trapping boundary. One might speculate that at such positions the magnetic field line geometry may be similar to that at the trapping boundary.

The changes in spectral shape of the trapped and precipitating electrons during narrow and pronounced variations in
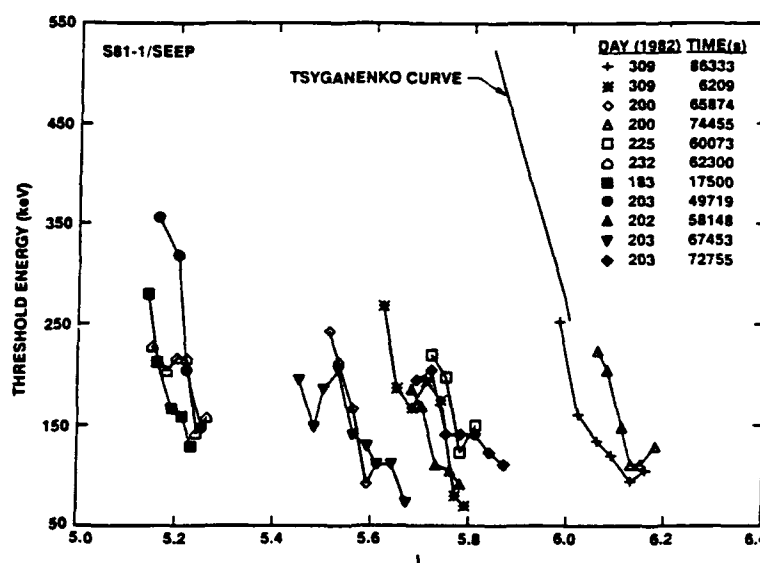
Fig. 9.   Observed threshold energy for isotropy versus L for 1.024-s intervals on passes near the midnight trapping boundary.

flux can be obtained with much finer time resolution by using the observed counting rates above 45, 100, and 300 keV rather than the differential spectra which have limited statistical accuracy due to the low sampling rate. From such analyses it can be shown that changes in spectral shape for the ME1 detector sometimes occur in close coincidence with the strong decreases in precipitating flux.

In Figure 9 the observed threshold energy for isotropy is plotted as a function of L at positions near the midnight trapping boundary for 11 passes. The figure shows the highest energy at which the flux in the loss cone is less than the flux of locally mirroring electrons, as a function of L value for each pass. Whereas the energy spectra just shown were for accumulation time periods of 1.024–2.048 s, all of the threshold energies plotted in Figure 9 were taken from spectral accumulations of 1.024 s each. Also shown are theoretical calculations using the Tsyganenko strong storm model as published in the work by *Popielawska et al.* [1985]. The slopes of the measurements are consistent with the theory. However, the data were acquired during geomagnetically quiet periods, whereas the calculations of Tsyganenko were for storm time conditions. On these passes the observed values of the threshold energy for isotropy versus L are in good agreement with the calculations, assuming loss of adiabatic motion for small radii of field line curvature. However, the observed L shell patterns of threshold energy for isotropy at nighttime are sometimes quite different. Such examples might indicate the importance of other mechanisms or the occurrence of variations in the magnetic field geometry.

ELECTRONS ABOVE 1 MeV

We have surveyed the nighttime data on many satellite passes across the trapping boundary and searched for times when the counting rate in the ME1 anticoincidence detector was enhanced and significantly greater than in the ME2 anticoincidence counter. The peak fluxes were tabulated, as were the fluxes integrated over the time duration of each spike. The peak precipitation fluxes at $L > 5$ from August 14 through October 27, 1982, are plotted in the top section of

Figure 10 as a function of time. A background of 60 counts/s was subtracted from the peak counting rate in each spike. In converting from counting rate to flux we have used a geometric factor of 3.09 cm^2 sr which is rigorously applicable only to isotropic fluxes. Based on other measurements of electron precipitation near the trapping boundary [e.g., *Imhof*, 1988] we have concluded that many of the electron spikes considered here are isotropic. Also shown are 24-hour averages of the average peak flux recorded on each pass, including zero flux for passes when no spikes were observed. On some days the average precipitating fluxes were below the threshold level of about 20 electrons (>1 MeV)/cm^2 sr s for reporting a spike since few or no precipitation spikes were observed on certain passes.

Although there is considerable variation from one pass to the next in the fluxes of precipitating electrons above 1 MeV, some overall trends are apparent. The longer-term increases of the order of days shown in Figure 10 tended to occur at the times of relativistic enhancements observed at synchronous altitude [*Baker et al.*, 1986]. Bars near the top of the figure show the time periods of these events. For comparison the Kp and Dst values are plotted in the lower two sections of Figure 10. Large variations appear in the observed flux from one satellite pass to the next.

We have investigated how much of the scatter in data points may be associated with variations in geomagnetic field geometry. The dependence of the flux upon the longitude of observation is plotted in Figure 11, separately for the northern and southern hemispheres. Figure 12 shows the variation of flux with the conjugate point altitude and with the minimum drift altitude, h_{min}. The precipitating fluxes show no obvious dependence upon the altitude of the conjugate point, and upon h_{min}. From the low-altitude S81-1 satellite, positive values of h_{min} were encountered primarily in the southern hemisphere, but the range of positive h_{min} values corresponds to only a small portion of the southern hemisphere longitudes plotted in Figure 11.

To see how the flux varies with geomagnetic activity, the distributions in peak flux at nighttime of the spikes of

precipitating electrons above 1 MeV are presented in Figure 13 separately for $Kp \leq 3$ and for $Kp > 3$ for the period of August 14 through October 27. This display illustrates the large variations in flux that occur and the lack of a strong dependence on Kp.

We can also check the day/night dependence of these events. All of the observations presented so far were acquired during satellite nighttime. A comparison with daytime observations is shown in Figure 14, which gives the frequency of occurrence versus the flux. The data come from a representative sample of the S81-1 data, using all of the precipitation events which were observed between September 6, 1982, and October 2, 1982. Satellite data coverage was nearly complete, both day and night, during this time interval. It is clear from the figure that ~80% of the cases occurred on the nightside of the Earth.

SUMMARY AND DISCUSSION

In the vicinity of the midnight trapping boundary of the radiation belt, highly relativistic electrons frequently precipitate in the bounce loss cone in narrow spikes, often at high intensity. From a low-altitude satellite the spikes typically have an observing time duration shorter than 10 s or a width of less than 100 km. At nighttime the precipitation of electrons above 1 MeV in energy has been measured to occur at widely variable intensities and locations. Most of the nighttime precipitation spikes of such electrons occur at

Fig. 11. Fluxes of nighttime precipitating electrons above 1 MeV plotted as a function of longitude, separately in the northern and southern hemispheres.

L values between 4 and 6. Precipitating electrons of this energy in the bounce loss cone were also observed in the daytime, but significant precipitation occurred less often. The preferred nighttime occurrence within a narrow latitude band is consistent with the findings of *Vampola* [1971] and of *Thorne and Andreoli* [1980]. Many of the highly relativistic electron spikes presented here are near the trapping boundary, usually at the low L shell portion of the boundary consistent with the general pattern at lower energies of intensity and threshold energy versus L shell. Stimulated by the need to understand in detail the positions of precipitation of relativistic electrons as well as the mechanism(s) responsible for an energy threshold for isotropy we have used the SEEP data to study electron precipitation near the trapping boundary.

We have found that near the outer edge of the nighttime radiation belt the L shell dependence of the energy threshold for isotropy is often consistent with loss of adiabatic motion when the radius of field line curvature is less than an order of magnitude greater than the gyroradius of the electrons. The mechanism was found by *Büchner and Zelenyi* [1989] to be more effective for very small equatorial pitch angles. It would then affect primarily electrons mirroring at low altitudes and not necessarily require that at the trapping boundary there be a collapse of the magnetic field line at high altitudes. Near the trapping boundary the observed L shell patterns of threshold energy for isotropy are sometimes quite different, indicating the importance of other mechanisms or the occurrence of variations in the magnetic field geometry. These results confirm earlier studies using spinning satellites.
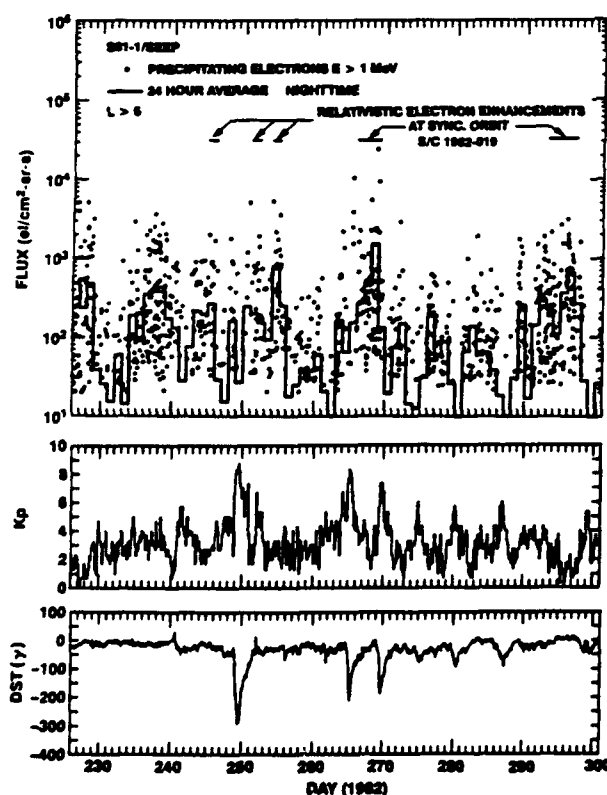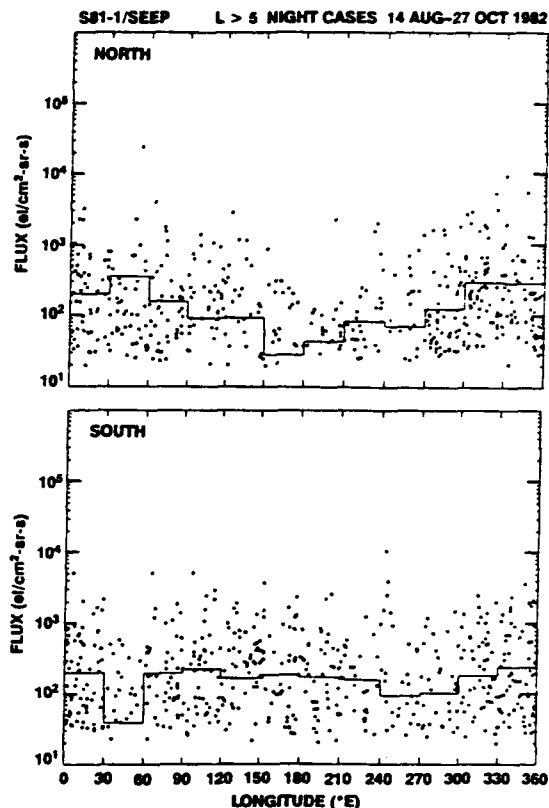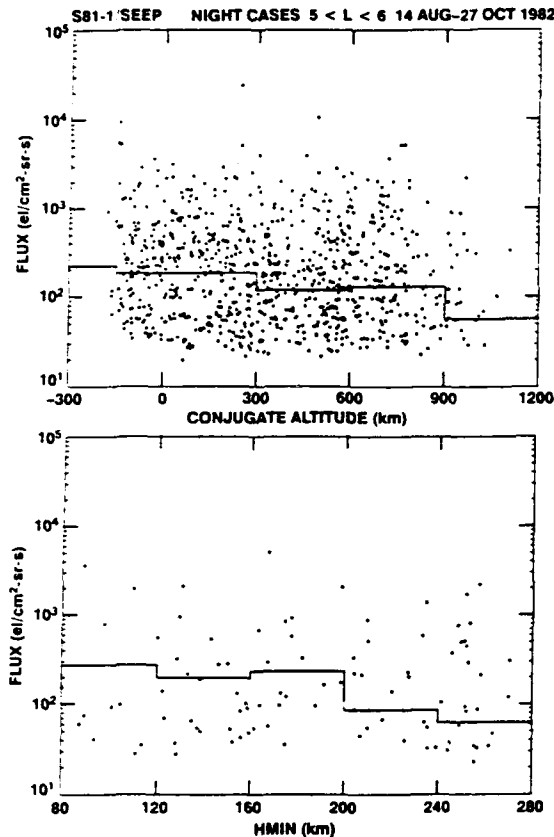

Fig. 10. Fluxes of nighttime precipitating electrons above 1 MeV plotted as a function of time (top section). The bars represent time periods of relativistic electron enhancements at synchronous altitude. The 3-hour Kp index and the Dst index are plotted versus time in the lower sections.

S81-1/SEEP   NIGHT CASES 5 < L < 6 14 AUG–27 OCT 1982

S81-1/SEEP
14 AUG–27 OCT 1982
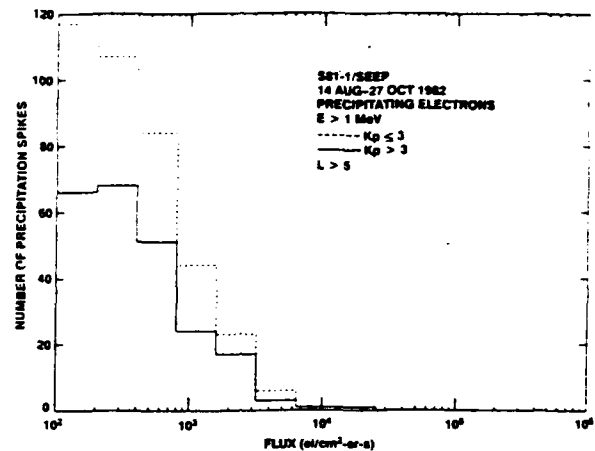PRECIPITATING ELECTRONS
E > 1 MeV
------ Kp ≤ 3
——— Kp > 3
L > 5

Fig. 13. Distribution in the peak flux of the spikes of precipitating electrons above 1 MeV separately for $Kp \le 3$ and for $Kp > 3$ where $L > 5$. For the lower geomagnetic activity range there were a total of 382 spikes whereas 231 spikes occurred when Kp was above 3.

Fig. 12. Fluxes of nighttime precipitating electrons above 1 MeV plotted as a function of the conjugate altitude (upper section) and the minimum drift altitude, h_{min} (lower section).

between low-altitude data and available measurements at synchronous altitude.

The satellite S81-1 typically passed through the interval $L = 4$ to $L = 6$ in about 100 s. In the first 12-hour period on day 252 (September 9) the average total counts acquired at nighttime in the spikes of directly precipitating electrons above 1 MeV during a pass through all L values was 10^5, compared to $\sim 5 \times 10^3$ when there were no spikes. Most of the latter counts were background in nature and not associated with precipitating electrons. This average counting rate of ~ 1000 counts/s yields an average flux of 324 el/cm^2 sr s in the interval $4 < L < 6$ (invariant latitudes 60°–65.9°). This region is where most of the precipitation of electrons above 1 MeV occurs. The area of this interval over 12 hours of local time is approximately 6×10^{16} cm^2 in each of the northern and southern hemispheres. If the relativistic electron precipitation at all nighttime hours was the same as at ~ 2230 and

Consideration should be given to the possible importance of wave-particle interactions. Vampola [1977] and Koons et al. [1972] demonstrated that a number of outer zone electron boundary phenomena can be explained on the basis of a rapid pitch angle scattering by electrostatic wave interaction. Although wave-particle interactions are clearly very important, a threshold energy for isotropy is present on most satellite passes across the boundary, and to attribute this always to waves would require the nearly continuous presence of waves at this position with a characteristic pattern for the L dependence of a cutoff in frequency.

From a superposed epoch analysis of the fluxes at synchronous altitude, Nagai [1988] found there is a rapid decrease in the flux of electrons above 2 MeV in association with an enhancement of geomagnetic activity followed by an increase in the flux which peaks approximately 4–5 days after the enhancement of geomagnetic activity. The 24-hour averages presented in Figure 10 of this paper show time profiles for precipitating electrons above 1 MeV that are not inconsistent with those reported by Nagai [1988]. However, at the peak of geomagnetic activity the fluxes of >1-MeV precipitating electrons were generally located at lower L values than that of a synchronous satellite and were often below $L = 5$. In a future survey, comparisons will be made

S81-1/SEEP
6 SEP–2 OCT 1982
PRECIPITATING ELECTRONS
E > 1 MeV
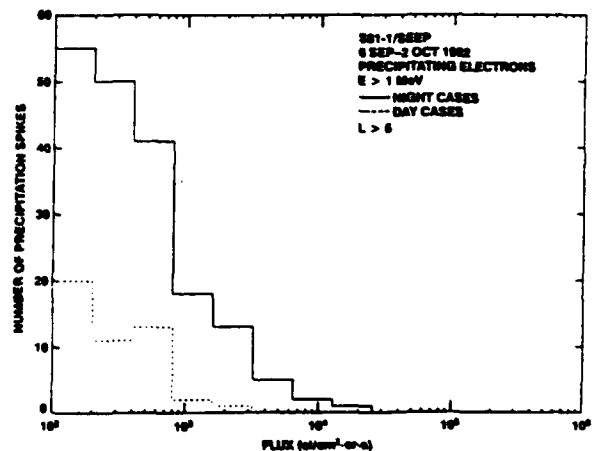——— NIGHT CASES
------ DAY CASES
L > 5

Fig. 14. Distribution in the peak flux of the spikes of precipitating electrons above 1 MeV, separately for day and night data. The time period covered is from September 6, 1982, through October 2, 1982. For $L > 5$ at nighttime there were 185 spikes, whereas in the daytime over this same time period there were 48 spikes.

was the same in both hemispheres, then the total rate of precipitation of electrons above 1 MeV was -1.2×10^{20} el/s or -5×10^{24} electrons in 12 hours. With an average energy per precipitated electron of 2 MeV [Baker et al., 1987], the total nighttime energy input from electrons in the bounce loss cone during this 12-hour period on September 9, 1982, was -10^{19} ergs. We have shown that the frequency of occurrence of spikes of precipitating relativistic electrons is much smaller in the daytime than at night. We have also shown (Figure 11) that the precipitating flux is not strongly dependent upon longitude and therefore these same precipitating fluxes should apply on a global scale. After normalization for time duration differences this value is an order of magnitude less than the rough estimate of the total energy input for a 2.5-day period from >1-MeV electrons of 7×10^{20} ergs reported by Baker et al. [1987] for a different electron event in June 1980. This finding may indicate that much of the precipitation is in the drift loss cone, a phenomenon not covered in the measurements reported here. A major cause of the difference between these two sets of values appears to be the large difference in invariant latitude width taken for the precipitation: 17° for Baker et al., compared to about 5.9° found in the present study.

The total loss rate into the atmosphere of electrons in the bounce loss cone above 1 MeV as measured at low satellite altitudes seems to be inconsistent with the loss rates inferred from synchronous high-altitude measurements. The difference between low-altitude and synchronous measurements is even greater when the low-altitude measurements are limited to L shells near those at synchronous satellites, about 6.7. Precipitation spikes of electrons above 1 MeV were not often evident in the low-altitude satellite data acquired near $L = 6.7$. Suitable high-altitude measurements at other L shells are not available in the published literature. Precipitating fluxes as high as 1400 el/cm^2 s were inferred from synchronous data by Baker et al. [1987], and such fluxes were observed in the bounce loss cone low-altitude measurements presented here only at very localized positions. It would appear that many of the relativistic electrons lost from the synchronous positions were not precipitated in the bounce loss cone directly into the atmosphere but were perhaps in the drift loss cone or were transported radially inward or outward.

A possible mechanism for the acceleration of electrons to relativistic energies has been postulated by Baker et al. [1989]. The mechanism involved inward radial diffusion of the electrons in which a large energy gain was followed by an energy-preserving outward transport, thus returning the accelerated population to the outer magnetosphere. Baker et al. suggested that in the inner magnetosphere the electrons are scattered in pitch angle with many not being scattered completely into the loss cone. In the present observations, significant fluxes of precipitating electrons were observed on September 6 prior to the time of an event, at $L \approx 2.5-3.5$, as shown in Figure 3. This finding is not presented as a validation of any mechanism, but it may be important to realize that enhanced fluxes of relativistic electrons were precipitating in the inner magnetosphere near the time of maximum flux of relativistic electrons at geostationary orbit.

REFERENCES

Baker, D. N., J. B. Blake, R. W. Klebesadel, and P. R. Higbie, Highly relativistic electrons in the Earth's outer magnetosphere, 1. Lifetimes and temporal history 1979–1984, J. Geophys. Res., 91, 4265, 1986.

Baker, D. N., J. B. Blake, D. J. Gorney, P. R. Higbie, R. W. Klebesadel, and J. H. King, Highly relativistic magnetospheric electrons: A role in coupling to the middle atmosphere?, Geophys. Res. Lett., 14, 1027, 1987.

Baker, D. N., J. B. Blake, L. B. Callis, R. D. Belian, and T. E. Cayton, Relativistic electrons near geostationary orbit: Evidence for internal magnetospheric acceleration, Geophys. Res. Lett., 16, 559, 1989.

Büchner, J., and L. M. Zelenyi, Regular and chaotic charged particle motion in magnetotaillike field reversals, 1. Basic theory of trapped motion, J. Geophys. Res., 94, 11,821, 1989.

Cain, J. C., S. J. Hendricks, R. A. Langel, and W. V. Hudson, A proposed model for the International Geomagnetic Reference Field, J. Geomagn. Geoelectr., 19, 335, 1967.

Fritz, T. A., High-latitude outer-zone boundary region for ≥40-keV electrons during geomagnetically quiet periods, J. Geophys. Res., 73, 7245, 1968.

Fritz, T. A., Study of the high-latitude, outer-zone boundary region for ≥40-keV electrons with satellite Injun 3, J. Geophys. Res., 75, 5387, 1970.

Imhof, W. L., Fine resolution measurements of the L-dependent energy threshold for isotropy at the trapping boundary, J. Geophys. Res., 93, 9743, 1988.

Imhof, W. L., J. B. Reagan, and E. E. Gaines, Fine-scale spatial structure in the pitch angle distributions of energetic particles near the midnight trapping boundary, J. Geophys. Res., 82, 5215, 1977.

Imhof, W. L., J. B. Reagan, and E. E. Gaines, Studies of the sharply defined L dependent energy threshold for isotropy at the midnight trapping boundary, J. Geophys. Res., 84, 6371, 1979.

Koons, H. C., A. L. Vampola, and D. A. McPherson, Strong pitch angle scattering of energetic electrons in the presence of electrostatic waves above the ionospheric trough region, J. Geophys. Res., 77, 1771, 1972.

Nagai, T., "Space weather forecast": Prediction of relativistic electron intensity at synchronous orbit, Geophys. Res. Lett., 15, 425, 1988.

Popielawska, B., E. Szalinska-Piechota, and N. A. Tsyganenko, On the nonadiabatic particle scattering in the Earth's magnetotail current sheet, Planet. Space Sci., 33, 1433, 1985.

Thorne, R. M., and L. J. Andreoli, Mechanisms for intense relativistic electron precipitation, in Exploration of the Polar Upper Atmosphere, edited by C. S. Deehr and J. A. Holtet, p. 381, D. Reidel, Hingham, Mass., 1980.

Vampola, A. L., Electron pitch angle scattering in the outer zone during magnetically disturbed times, J. Geophys. Res., 76, 4685, 1971.

Vampola, A. L., The effect of strong pitch angle scattering on the location of the outer-zone electron boundary as observed by low-altitude satellites, J. Geophys. Res., 82, 2289, 1977.

Voss, H. D., J. B. Reagan, W. L. Imhof, D. O. Murray, D. A. Simpson, D. P. Cauffman, and J. C. Bakke, Low temperature characteristics of solid state detectors for energetic X-ray, ion and electron spectrometers, IEEE Trans. Nucl. Sci., NS-29, 164, 1982.

D. W. Datlowe, E. E. Gaines, W. L. Imhof, J. Mobilia, and H. D. Voss, Lockheed Palo Alto Research Laboratory, 3251 Hanover Street, Palo Alto, CA 94304.

Energy Selective Precipitation of Electrons Near the Trapping Boundary

W L Imhof H D Voss J Mobilia E E Gaines and D W Datlowe
(Lockheed Palo Alto Research Laboratory, 3251 Hanover St.,
Palo Alto, CA 94304)

The energy selective precipitation of electrons with an L shell
dependence near the midnight trapping boundary of the outer
radiation belt has previously been reported, but the measure-
ments were all from spinning satellites and therefore the pre-
cipitating electrons were observed during only a small fraction
of the time. Here we report measurements of the phenomenon
with fine resolution silicon electron spectrometers on an oriented
satellite SEEP/S81-1 such that the precipitating electrons were
observed continuously with 0.064 sec. time resolution. The L-
dependent energy thresholds were measured in detail and often
found to span the energy range 45 to ~500 keV in less than
10 seconds travel time of the low altitude polar-orbiting satel-
lite. The precipitation regions were also simultaneously mapped
in bremsstrahlung x-rays with ~40 km resolution using a spec-
trometer in the SEEP payload and were typically found to follow
constant L shell contours.

The Precipitation of Relativistic Electrons Near the Trapping Boundary

W L Imhof, H D Voss, J Mobilia, D W Datlowe and E E Gaines, Lockheed Palo Alto Research Laboratory, 3251 Hanover St., Palo Alto, CA 94304

Highly relativistic electrons are known to be present at synchronous satellite altitudes in time varying and sometimes large intensities; it is therefore important to consider the fluxes and locations of relativistic electrons precipitating into the atmosphere. Here we present measurements from the low altitude three-axis stabilized satellite S81-1 of trapped and precipitating electrons from 6 keV to above 1 MeV. Significant fluxes of precipitating relativistic electrons above 1 MeV are much more often observed near midnight than noon and generally in narrow spikes, < 100 km in width, typically at L values between 4 and 6 near the radiation belt boundary. These electrons occur at intensities and in locations that are widely variable. The total nighttime input to the atmosphere in 12 hours on one of the days of strongest precipitation from electrons above 1 MeV was ~ 10^{19} ergs. These low altitude observations have ꞏn compared with simultaneous measurements of the total x of relativistic electrons at synchronous altitude; the variations in the precipitating flux correlate well with the variations in the total flux at high altitude.

1. 1990 Fall Meeting

2. 001429913

3. Dr. W.L. Imhof
    Dept. 91-20, Bldg. 255
    Lockheed
    3251 Hanover St.
    Palo Alto, CA 94304
    (415) 424-3252

4. Magnetospheric
    Physics
    (SM)

5. (a) No special session
    (b) 2716 (Energetic
    Particles,
    Precipitating)

6. Oral

7. 0%

8. Invoice $60.00
    P.O. ZAP23195
    Inquiries to:
    Technical
    Information
    Dept. 90-11, Bldg. 201
    Lockheed
    3251 Hanover St.
    Palo Alto, CA 94304
    Attn: Jan Thomas
    (415) 424-2810

9. Contributed

10. No special request

11. Not student paper

Detection of Kilometer Scale Structures at the Polar Cap Boundary by Combining Satellite X-ray Images with in situ Energetic Electron Flux Profiles

D W DATLOWE, W L IMHOF and H D VOSS (Lockheed Palo Alto Research Laboratory, Palo Alto, California 94304)

X-ray images of the Earth's auroral zone give a large scale view of the precipitation patterns of energetic electrons through the bremmstrahlung produced by the electron stopping in the atmosphere. Many of the features detected by the XRIS imager on the polar orbiting S81-1 satellite were near the low latitude boundary of the polar cap and poleward of the trapping boundary. In these arcs precipitation patterns on spatial scales much smaller than an X-ray imager's pixel size have been brought out by comparison with direct particle measurements. The FWHM spatial resolution of XRIS was 40 km, but high time resolution measurements of electrons above 64 keV detected 2 km spatial variations in one dimension along the track of the satellite. The technique was used to study 30 auroral arcs observed in 4-24 keV X-rays by the XRIS. Several of the X-ray arcs were resolved into multiple features by the electron measurements. In cases where the X-ray emission is uniform along the arc segment in the field of view, we can extrapolate the locally measured electron flux profile to distances hundreds of km from the path of the satellite. Extrapolation is the best that has been done so far. In cases where the X-ray arcs are more complex, the comparison with electron data leads to the conclusion that kilometer scale features are often present in the energetic electron precipitation patterns.

1. 1991 Fall Meeting

2. 001380622

3. D. W. DATLOWE
   Dept. 91-20, Bldg. 255
   Lockheed Palo Alto Research Laboratory
   3251 Hanover St.
   Palo Alto, CA 94304
   tel: 415-424-3274
   fax: 415-424-3333

4. (SM) Magnetospheric Physics

5. No special session
   2704 (Auroral Phenomena)

6. Oral

7. None

8. Invoice 60.00
   P.O. ZAP24251
   For more information contact: Jan Thomas
   Technical Information Center
   Dept. 90-11 Bldg. 201
   Lockheed Palo Alto Research Laboratory
   3251 Hanover St.
   Palo Alto, CA 94304
   (415) 424-2810

9. Contributed

10. No special instructions

11. Not a Student

APENDIX D

MICROBURSTS OF PRECIPITATING RELATIVISTIC ELECTRONS

Relativistic Electron Microbursts

W. L. Imhof, H. D. Voss, J. Mobilia, D. W. Datlowe, E. E. Gaines,
J. P. McGlennon

Lockheed Palo Alto Research Laboratory, Palo Alto, California

U. S. Inan

STAR Laboratory, Stanford University, Stanford, California

Abstract

We report the first satellite observations of relativistic (> 1 MeV) electron precipitation in microbursts with durations of less than one second. The locations of many of the relativistic microbursts are concentrated at the outer edge of the trapped radiation belt, where the gyroradii of the electrons are comparable to the curvature of the magnetic field lines and stable trapping may therefore not occur. Microbursts of lower energy electrons (10-100 keV) have been studied previously and found to be closely associated with VLF chorus emissions. To investigate whether wave-particle interactions with ELF/VLF waves are responsible for the triggering of the relativistic microbursts, we have searched VLF wave data recorded at Siple Station, Antarctica (L= 4.2) and at Roberval, Quebec at times when the satellite was near Siple or its conjugate point (Roberval). Neither VLF chorus events nor other magnetospheric ELF/VLF wave activity was observed on the ground at the times when relativistic microbursts were detected during nearby passes of the low altitude polar orbiting S81-1 spacecraft. Also, the relativistic electron microbursts occurred more frequently near 2230 LT than 1030 LT in contrast with the predominantly morning sector occurrence of discrete ELF/VLF emissions and lower energy microbursts. The available data on these relativistic microbursts thus appear to indicate that many of the bursts may not be due to wave-particle interactions. Rather, the preferred location of the microbursts implies the possible importance of irregularities in the magnetic field lines near the trapping boundary as a loss mechanism.

Introduction

Relativistic electrons are known to be present in the radiation belts with pronounced spatial and temporal enhancements and depletions (e.g. Baker et al., 1986), but the source and loss mechanisms are not well understood. Bursts of relativistic electrons precipitating into the atmosphere have been observed for durations typically of one to ten seconds (Imhof et al., 1991). In order to understand the precipitation mechanisms it is important to study these bursts in more detail since they display a variety of time durations. The different time-width bursts may or may not be produced by the same class of mechanism(s). As with lower energy electron precipitation the short time bursts may provide unique information, particularly with respect to the importance of wave-particle interactions as a possible cause for their precipitation.

Microbursts of precipitating electrons were first described by Anderson and Milton (1964). The electrons were detected from balloons by measuring the x-rays produced when they encountered the atmosphere and the electron energies were mostly in the tens to hundreds of keV range. The microbursts were characterized by durations of ~ 0.2 second and interburst spacings of ~ 0.6 second. Most observations of microbursts have been conducted from balloons or rocket-borne parachute deployments and have involved measurements of the bremsstrahlung x-rays produced by the electrons as they encounter the atmosphere (e.g. Parks, 1978; Rosenberg et al., 1981; Bering et al., 1988). Microburst events have been found to be closely associated with VLF chorus waves observed on the ground (Rosenberg et al., 1990).

One set of early observations of microbursts was made from the Injun 3 satellite and involved the direct measurement of precipitating electrons > 40 keV (Oliven et al., 1968). The microbursts were found to occur preferentially in the early daylight hours and seldom near midnight. Oliven et al. reported that the microbursts occur predominantly at L= 6 to 8.5 and MLT = 0430 to 1230. They found that the microbursts were always accompanied by VLF chorus, but one-to-one associations between the microbursts and chorus emissions were not observed. The latter can be attributed to the fact that the electron precipitation induced by chorus in whistler-mode gyroresonance interactions observed at one hemisphere would first be deposited at the conjugate hemisphere.

Short bursts of electrons with energies above 45 keV were studied with data from the S81-1 low-altitude polar orbiting satellite (Imhof et al., 1989). The bursts met all of the criteria for microbursts, and had soft spectra with negligible flux above 1 MeV. The study included 87 satellite passes. Bursts occurred in 44

2

(72%) out of 61 daytime passes and in 14 (54%) out of 26 nighttime passes, thus indicating a higher occurrence rate during daytime. In all 33 cases when the satellite was near Siple Station and microbursts were detected, chorus activity was also observed at ground stations within nearby times.

Measurements on the S81-1 satellite of electrons at energies above 1 MeV in bursts longer than one second were recently published (Imhof et al., 1991). That study was limited to bursts ranging from 1 to 10 seconds in duration which were found primarily at L-values between 4 and 6. These relativistic electron precipitation bursts of > 1 sec duration were found much more often near midnight than noon.

In this paper, we present for the first time observations of relativistic electron microbursts of durations typically < 1 sec. These microbursts are believed to be of a different nature than the previously reported bursts of longer durations. Previously reported studies of microbursts have involved primarily electrons of energy below a few hundred keV. Since earlier microburst studies showed an association with ELF/VLF waves, we report here also an extensive analysis of associated ELF/VLF wave activity.

Description of Instrumentation

The Stimulated Emission of Energetic Particles (SEEP) experiment on the S81-1 spacecraft contained an array of cooled silicon solid state detectors to measure electrons and ions (Voss et al., 1982). The data were acquired over the period from May 28, 1982 until December 5, 1982. The S81-1 three-axis stabilized satellite was in a sun synchronous 1030 and 2230 local time polar orbit (inclination = 96.3°) at altitudes from 170 to 280 km. The data used in this study were obtained primarily from two electron spectrometers, one at a zenith angle of 0° (ME1) and the other at a zenith angle of 180° (ME2). Both detectors had acceptance angles of ± 30° and at these altitudes the fields-of-view were entirely within the bounce loss cone. The ME1 detector responded to electrons about to precipitate into the atmosphere whereas the ME2 sensor responded to the backscattered electrons. Except for the entrance aperture the silicon detectors in both spectrometers were surrounded by plastic scintillator anticoincidence shields for background reduction. For electrons the threshold energy for detection by the anticoincidence counters was ~ 1 MeV due to a combination of the shielding from the silicon detector and the signal threshold. The geometric factor was 3.09 cm^2 sr with an acceptance angle of ± 30°. The bulk of the data presented here was acquired by the ME1 anticoincidence detector with the ME2 anticoincidence counter providing a measure of background response. Some lower energy electron data presented make use of the silicon detector in the ME1 spectrometer. Fluxes of electrons above 45, 100, and 300 keV were obtained from the outputs

of scalars which, as with the anticoincidence counters, recorded counts during successive 0.064 second intervals. The silicon detectors were 1000 microns thick and had geometric factors of 2.47 cm^2 sr.

The wave data used in this study were acquired with the Stanford University broadband VLF receivers located at Siple and Palmer Stations, Antarctica and Roberval, Quebec (geomagnetic conjugate to Siple Station). These receivers were operated nearly continuously during 1982 in a synoptic mode (recording 1 out of every 5-minutes) and also (in addition) during overpasses of the SEEP satellite within ± 30° longitude of the stations and/or their conjugate region. The recordings were generally made in analog form on reel-to-reel 1/4 inch audio tapes. The data were high-pass filtered with a lower cut-off frequency of 300 Hz. The linear dynamic range of the preamplifier and line receiver systems were ~ 120 dB.

Presentation of the Measurements

In Figures 1 through 3 the precipitating electron fluxes above 1 MeV, 300 keV, 100 keV, and 45 keV are plotted as a function of time for three nighttime passes of the S81-1 satellite in which bursts were observed for short time durations. To be qualified as a burst it was required that the counting rate in the ME1 spectrometer, which was viewing upward, increase above background by at least a factor of 2 and that the increase be statistically significant above that in the ME2 detector which had an identical acceptance angle in the downward direction. Microbursts are taken to be those bursts in which the full width at one-fifth maximum is < 1 second and relativistic microbursts are taken to be those that display these features in the integral counting rates above 1 MeV. Examples of relativistic microbursts that are the subject of this paper are indicated by arrows in Figures 1 through 3. The arrows are located at the times of maximum counting rate in each microburst. An example of data from a daytime pass with microbursts is provided in Figure 4. The data in all four figures were acquired with the ME1 electron spectrometer at 0° zenith angle and the fluxes given are based on raw counting rates with no background subtraction. Many of the bursts of less than 1 second duration observed with this spectrometer are isolated, but some occur in trains of several narrow bursts. More than one train is observed on certain satellite passes. Both the temporal structure and occurrence features of these bursts are identical to those of previously reported microbursts. Accordingly, we refer to these short pulses as microbursts in the rest of the paper. The microbursts of electrons > 1 MeV are generally less prevalent than the previously studied wider (> 1 sec) bursts in terms of energy loss rates and in most past analyses only bursts longer than one second were included. As in the examples shown, the relativistic microbursts display a variety of electron energy

4

spectra with the fluxes sometimes being predominantly above 1 MeV. For example, on 26 September 1982 at 8720 to 8725 seconds (Figure 1) the fluxes >1 MeV were nearly the same as those > 45 keV. At other times, such as the case of 28 September 1982 around 6280 sec (Figure 2), the > 45 keV flux is much greater than that for > 1 MeV.

The distributions in L-shell of the peak flux of each microburst of precipitating relativistic electrons observed from the S81-1 satellite are plotted in Figure 5. Most of the microbursts occurred in the interval L= 4 to 6 with a median value near L= 5, similar to those of the previously reported 1 to 10 second duration bursts (Imhof et al., 1991). From an examination of the data for relativistic electron passes it is apparent that both the bursts and microbursts often occurred at positions that are considered to be near the trapping boundary (e.g. Imhof, 1988).

In 90 nighttime passes of the satellite microbursts were observed on 42 of them (47%) whereas in the daytime microbursts were observed only on 9 out of 64 passes (14%). Thus, the relativistic electron microbursts occurred much more often near 2230 LT than near 1030 LT. This local time preference of relativistic microbursts is opposite to the published local time occurrence of chorus bursts (Burtis and Helliwell, 1976) and of the lower energy electron microbursts (Oliven et al., 1968; Imhof et al., 1989). We note that microbursts with much softer energy spectra were observed from the same satellite. An example of such soft microbursts observed in the daytime is shown in Figure 6.

The possible role of wave-particle interactions in precipitating > 1 MeV electrons was investigated by examining simultaneous ELF/VLF wave data taken at times of satellite passes close to Siple Station, Antarctica or its conjugate point at Roberval, Quebec. There were 26 nighttime passes with relativistic microbursts in the longitude range 250° E to 310° E in which simultaneous wave data were recorded at Siple or Roberval. Chorus was observed on only 5 of these cases (19%). Figure 7 shows an example of the simultaneous wave and particle data. In view of the relativistic energies of the electrons and the possibilities of cyclotron resonance interactions with waves at entirely low frequencies, wave data in both 0-10 kHz and 0-500 Hz ranges are shown. In the satellite pass shown relativistic electron microbursts were observed and chorus features were evident in the waves recorded on the ground, but one to one correlations were not observed. Daytime data were recorded at 250° E to 310° E on 8 passes when wave data were recorded at Siple. ELF/VLF chorus events were observed on one of these cases whereas neither chorus nor any other discrete ELF/VLF waves were observed for the remaining 7 passes. From this portion of the investigation one concludes that chorus events are generally not associated with relativistic electron microbursts. We note here that typical chorus frequencies are indeed

much higher than that required for gyroresonant interactions with > 1 MeV electrons near the geomagnetic equator. However, in principle interactions can occur off from the equator where the resonant energies for typical chorus waves would be higher. The frequency of occurrence of electron microbursts at two local times and with and without the presence of chorus bursts or other wave activity is summarized in Table 1 and Figure 8.

Comparison of the satellite observations of relativistic electron microbursts and the wave data recorded at Siple Station has indicated that the microbursts were generally not accompanied by ELF/VLF chorus or other magnetospheric wave activity. The validity of this conclusion depends upon the location of the microbursts relative to the positions of observation of the waves. One must consider whether associated wave activity may be observed only when the microburst measurements are very close to the ground stations. To investigate this matter the locations of the relativistic microbursts with or without the presence of magnetospheric wave activity are plotted in Figure 9. Clearly, there is no obvious longitudinal correlation between the presence of microbursts alone and those which were accompanied by ELF/VLF chorus activity, indicating that the lack of correlation between relativistic electron microbursts and wave activity is not likely to be due to the geometry of the measurements.

Table 1

Electron and Wave Data Summary
For Electrons > 1 MeV

Item	LT=1030	LT=2230
Number of passes (250° E to 310° E)	64	90
Number of passes with microbursts	9	42
Fraction of passes with microbursts	0.14	0.47
Average number of microbursts per pass	0.67	1.73
Number of passes with microbursts and with waves recorded at Siple	8	26
Number of passes having microbursts in which chorus was recorded	1	5
Fraction of passes having microbursts in which chorus was recorded	0.125	0.192
Fraction of all passes having both microbursts and chorus	0.018	0.090

Discussion

For relativistic electron precipitation similar locations were found for the occurrences of both the wide bursts and the narrow microbursts, leading to speculation as to whether they might originate from the same precipitation mechanism. When considering the responsible loss mechanism(s) it is important to recognize that sometimes several microbursts occur within a single wide burst. Such bursts might be considered as trains of microbursts.

Many of the relativistic electron precipitation spikes have been found to occur very close to the outer boundary of the radiation belt. Enhanced precipitation is known to occur often near the "last closed field line." From a low-altitude polar-orbiting satellite the precipitation at this location often displays L-dependent energy selectivity on a time scale of a few seconds or a distance of a few kilometers (e.g. Imhof et al., 1988, 1991). The precipitation mechanism may be due to the loss of adiabatic motion when the radius of field line curvature is less than an order of magnitude greater than the gyroradius of the electrons. For various magnetic field models theoretical calculations have been made of the expectations (Popielawska et al., 1985; Buchner and Zelenyi, 1989; Popielawska and Zwolakowska, 1991). The occurrence of multiple bursts on the same satellite pass might be accounted for in such a model in terms of temporal variations in the magnetic field configuration.

Comparisons of microburst occurence with wave activity have led to considerably different findings for soft electron microbursts than for the hard relativistic microbursts. Soft microbursts are usually associated with chorus wave activity (Oliven et al., 1968; Imhof et al., 1989; Rosenberg et al., 1990) whereas the relativistic microbursts presented here were generally not accompanied by any wave activity observable on the ground. Although waves were not observed on the ground in conjunction with many of the relativistic electron microbursts one cannot necessarily conclude that the precipitation was not associated with waves. It is possible that the responsible waves may not have been observed on the ground because of poor transmission through the ionosphere. In terms of association with VLF chorus we also note that for typical wave frequencies, equatorial gyroresonance is not expected to occur with > 1 MeV electrons on the L-shells of 4 < L < 6.

From the data presented here the following conclusions can be made in regard to the mechanisms responsible for the precipitation of microbursts of relativistic electrons:

8

- Relativistic electron microbursts were observed more often at local times near 2230 than near 1030, a pattern distinctly different from the more favored occurrence of softer energy microbursts near the daytime hours.

- ELF/VLF chorus or other magnetospheric wave activity was generally not observed at ground stations during the times that microbursts were observed on the satellite during passes overhead or near the conjugate point.

- The relativistic electron microbursts at nighttime often occurred near the trapping boundary, consistent with geomagnetic field line irregularities as their cause.

We conclude that microbursts of relativistic electrons have a different origin from low energy microbursts and that the underlying precipitation mechanisms may not involve wave-particle interactions.

Acknowledgements

References

Anderson, K. A., and D. W. Milton, Balloon observations of X rays in the auroral zone, 3, High time resolution studies, J. Geophys. Res., 69, 4457, 1964.

Baker, D. N., J. B. Blake, R. W. Klebesabel, and P. R. Higbie, Highly relativistic electrons in the earth's outer magnetosphere, 1. Lifetimes and temporal history 1979-1987, J. Geophys. Res., 91, 4265, 1986.

Bering, E. A., J. R. Benbrook, H. Leverenz, J. L. Roeder, E. G. Stansbery, and W. R. Sheldon, Longitudinal differences in electron precipitation near L=4, J. Geophys. Res., 93, 11385, 1988.

Buchner, J., and L. M. Zelenyi, Regular and chaotic charged particle motion in magnetic taillike field reversals, 1. Basic theory of trapped motion, J. Geophys. Res.. 94, 11821, 1989.

Burtis, W. J., and R. A. Helliwell, Magnetospheric chorus: occurrence patterns and normalized frequency, Planet. Sp. Sci., 24, 1007, 1976.

Imhof, W. L., Fine resolution measurements of the L-dependent energy threshold for isotropy at the trapping boundary, J. Geophys. Res., 93, 9743, 1988.

Imhof, W. L., H. D. Voss, J. Mobilia, M. Walt, U. S. Inan, and D. L. Carpenter, Characteristic of short-duration electron precipitation bursts and their relationship with VLF wave activity, J. Geophys. Res., 94, 10079, 1989.

Imhof, W. L., H. D. Voss, J. Mobilia, D. W. Datlowe, and E. E. Gaines, The precipitation of relativistic electrons near the trapping boundary, J. Geophys. Res., 96, 5619, 1991.

Oliven, M. N., D. Venkatesan, and K. G. McCracken, Microburst phenomena 2. Auroral-zone electrons, J. Geophys. Res., 73, 2345, 1968.

Parks, G. K., Microburst precipitation phenomena, J. Geomagn. Geoelect., 30, 327, 1978.

Popielowska, B., E. Szalinska - Piechota, and N. A. Tsynanenko, On the nonadiabatic particle scattering in the earth's magnetotail current sheet, Planet. Sp. Sci., 33, 1433, 1985.

Popielowska, B., and D. Zwolakowska, An assessment of a magnetospheric model by tracing the energetic particle trapping boundary, Geophys. Res. Lett., 18, 1489, 1991.

Rosenberg, T. J., J. C. Siren, D. L. Matthews, K. Marthinsen, J. A. Holtet, A. Egeland, D. L. Carpenter, and R. A. Helliwell, Conjugacy of electron microbursts and VLF chorus, J. Geophys. Res., 86, 5819, 1981.

Rosenberg, T. J., R. Wei, D. L. Detrick, and U. S. Inan, Observations and modeling of wave-induced microburst electron precipitation, J. Geophys. Res., 95, 6467, 1990.

Voss, H. D., J. B. Reagan, W. L. Imhof, D. O. Murray, D. A. Simpson, D. P. Cauffman, and J. C. Bakke, Low temperature characteristics of solid state

detectors for energetic X-ray, ion and electron spectrometers, IEEE Trans. Nucl. Sci., NS-29, 164, 1982.

Figure Captions

Figure 1   The fluxes of precipitating electrons above various energies versus time for a pass of the S81-1 satellite in the nighttime.

Figure 2   The fluxes of precipitating electrons above various energies versus time for a pass of the S81-1 satellite in the nighttime.

Figure 3   The fluxes of precipitating electrons above various energies versus time for a pass of the S81-1 satellite in the nighttime.

Figure 4   The fluxes of precipitating electrons above various energies versus time for a pass of the S81-1 satellite in the daytime.

Figure 5   The number of microbursts of precipitating relativistic electrons at nighttime versus L-shell.

Figure 6   The fluxes of precipitating electrons above various energies versus time for a pass of the S81-1 satellite in the daytime.

Figure 7   Simultaneous wave intensities and electron fluxes versus time for a pass of the S81-1 satellite in the nighttime.

Figure 8   The frequency of occurrence of the electron microbursts.

Figure 9   The locations of microbursts observed in the 250^0 E to 310^0 E longitude interval.
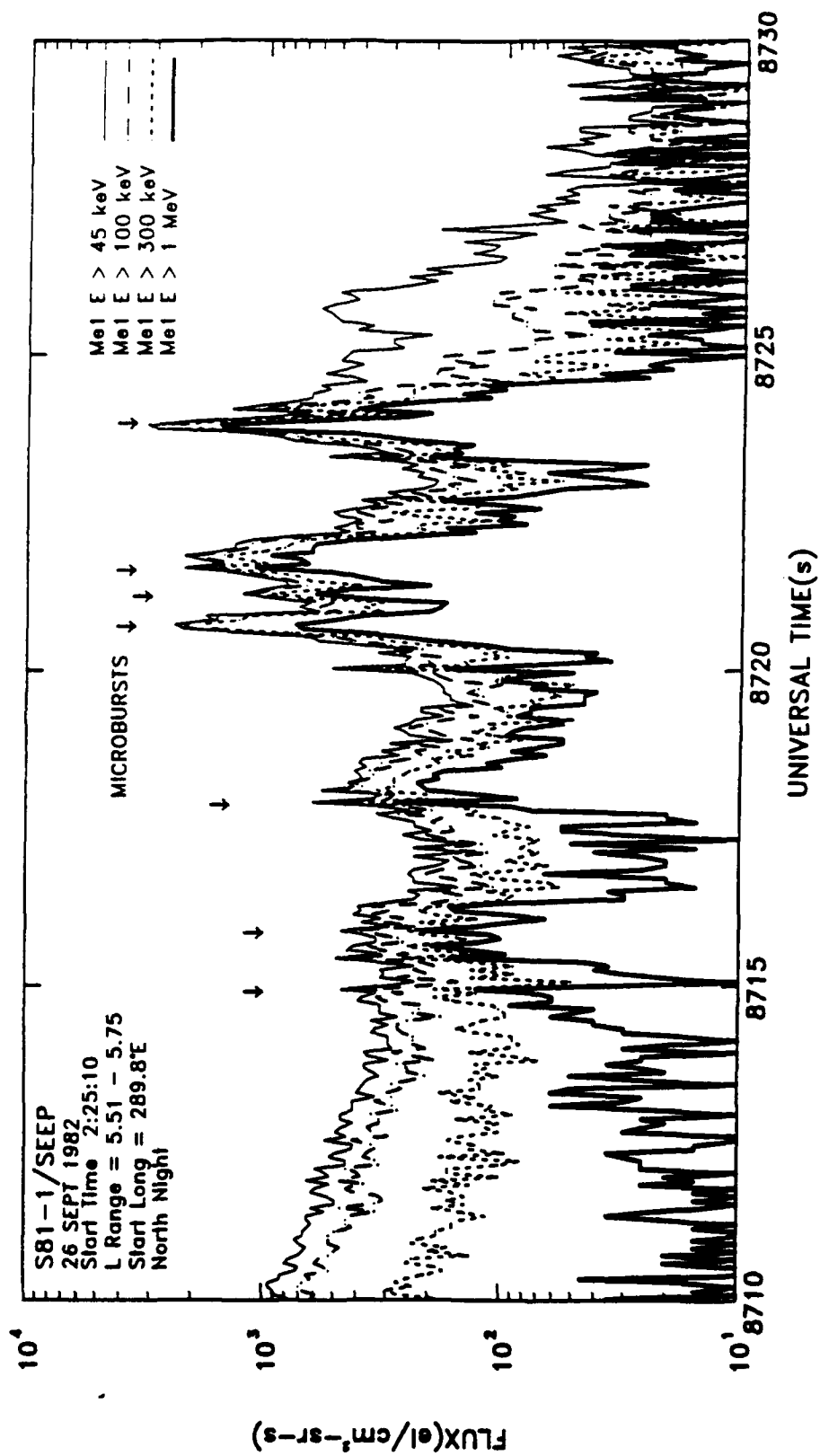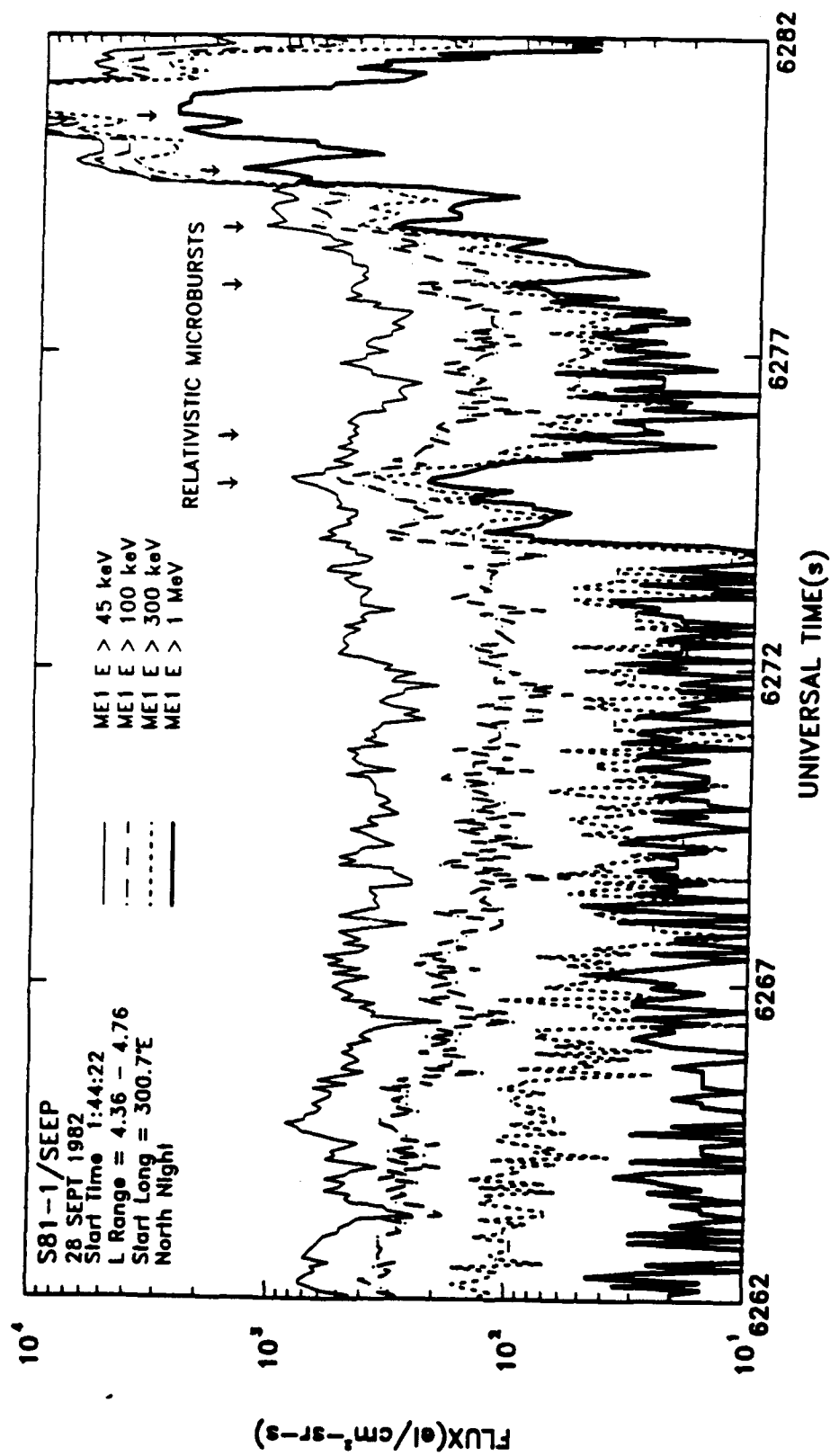
FIGURE 1

FIGURE 2

S81-1/SEEP
28 SEPT 1982
Start Time 1:44:22
L Range = 4.36 - 4.76
Start Long = 300.7°E
North Night

ME1 E > 45 keV
ME1 E > 100 keV
ME1 E > 300 keV
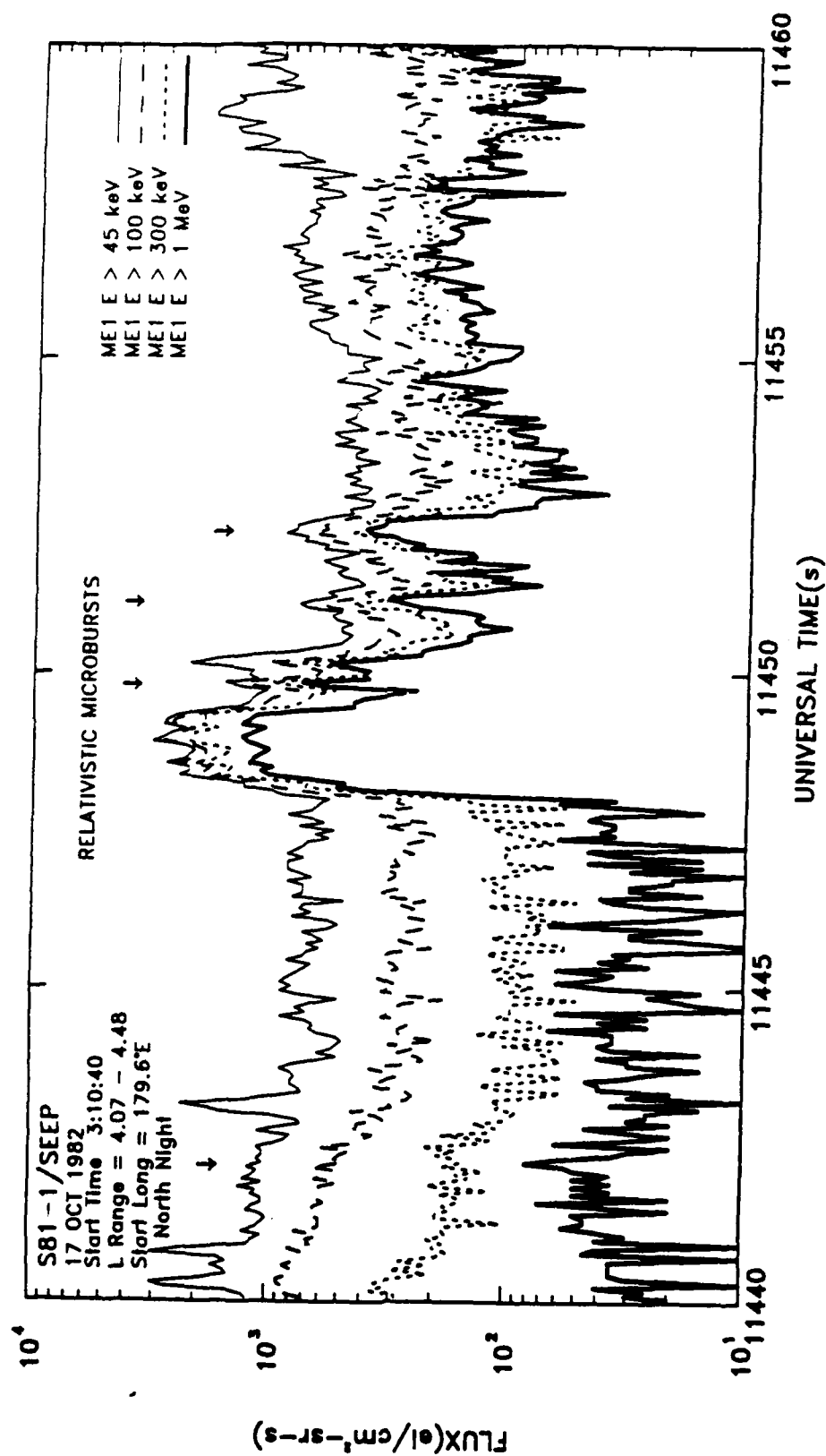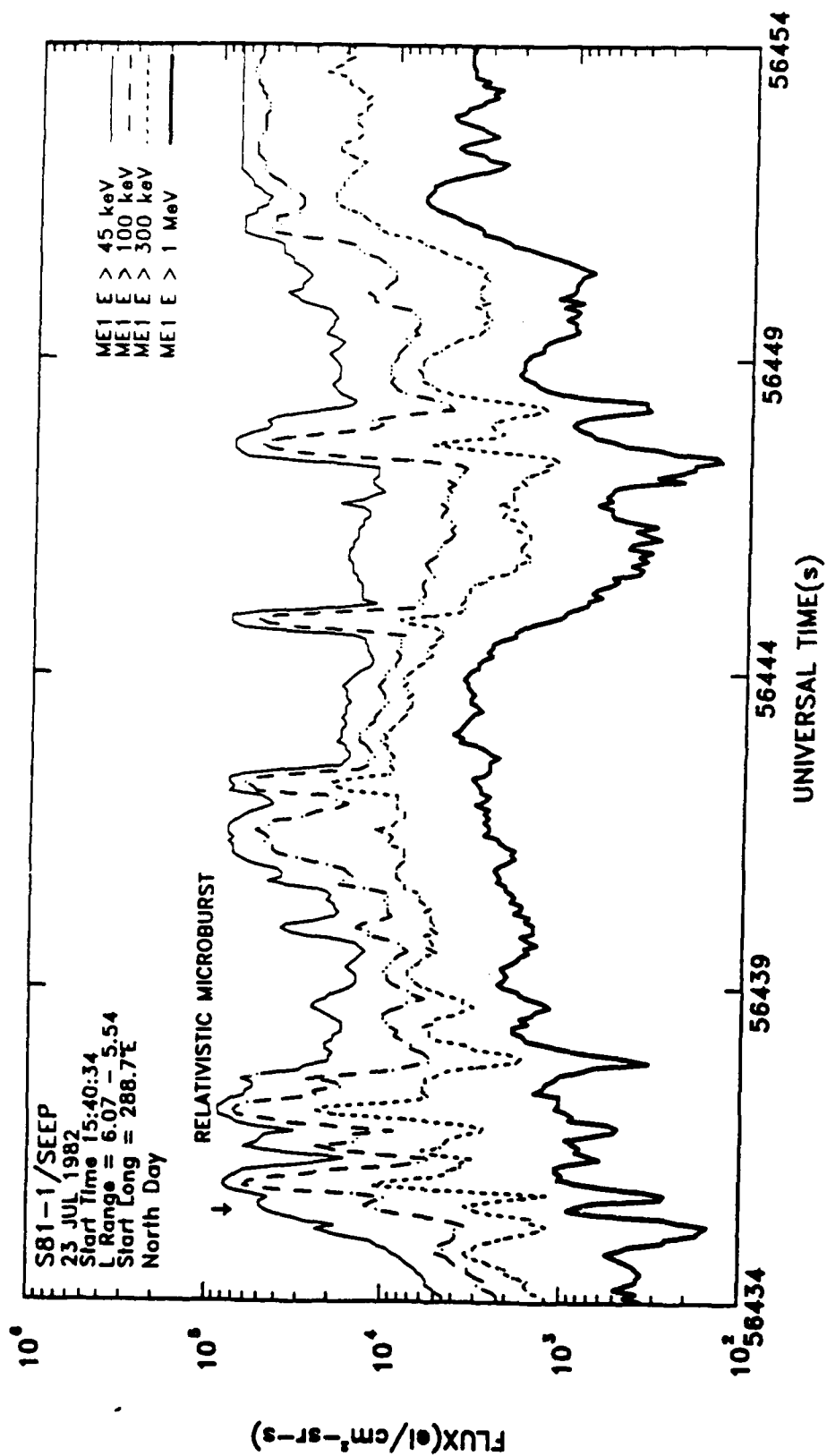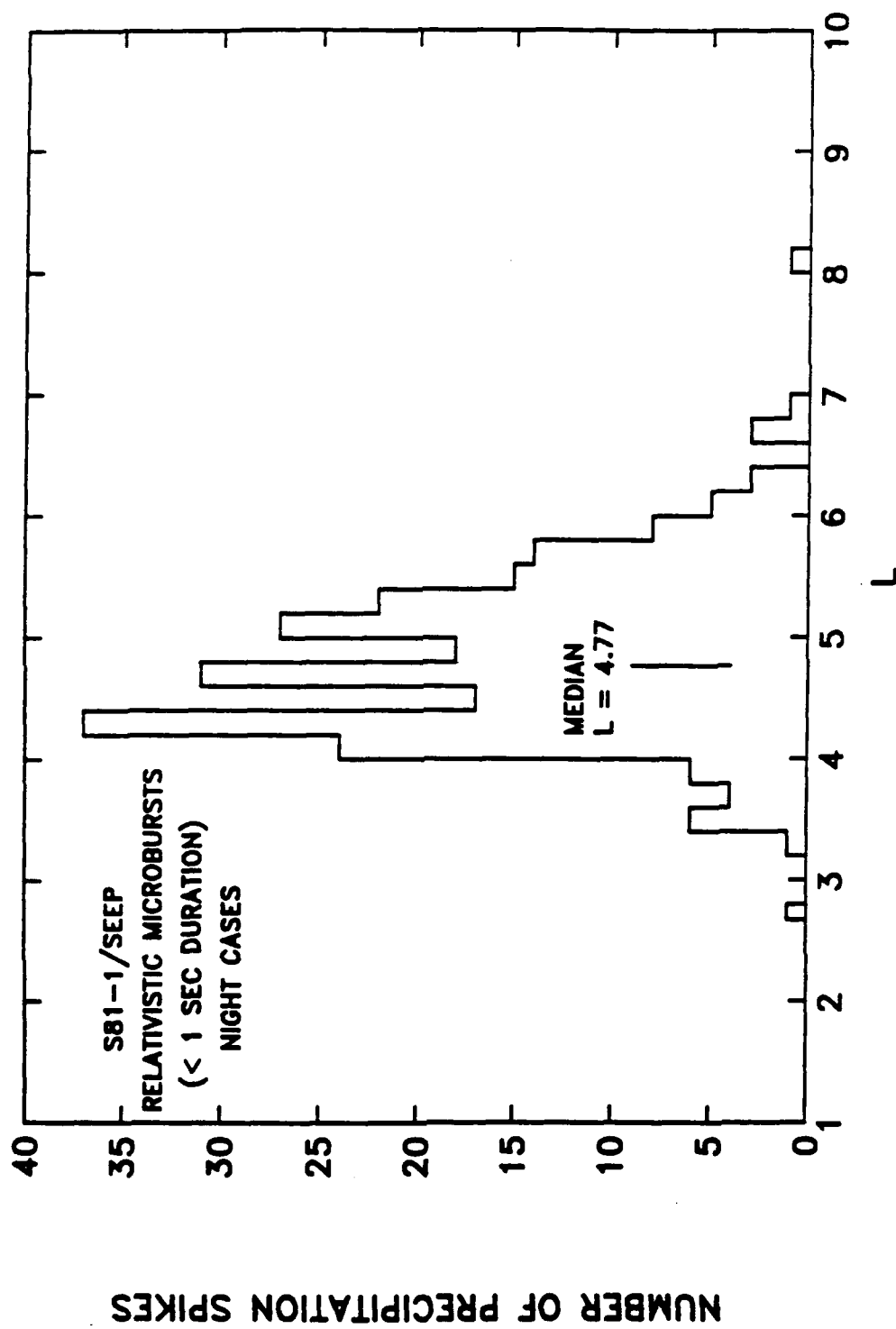ME1 E > 1 MeV

RELATIVISTIC MICROBURSTS

FLUX(el/cm²-sr-s)

UNIVERSAL TIME(s)

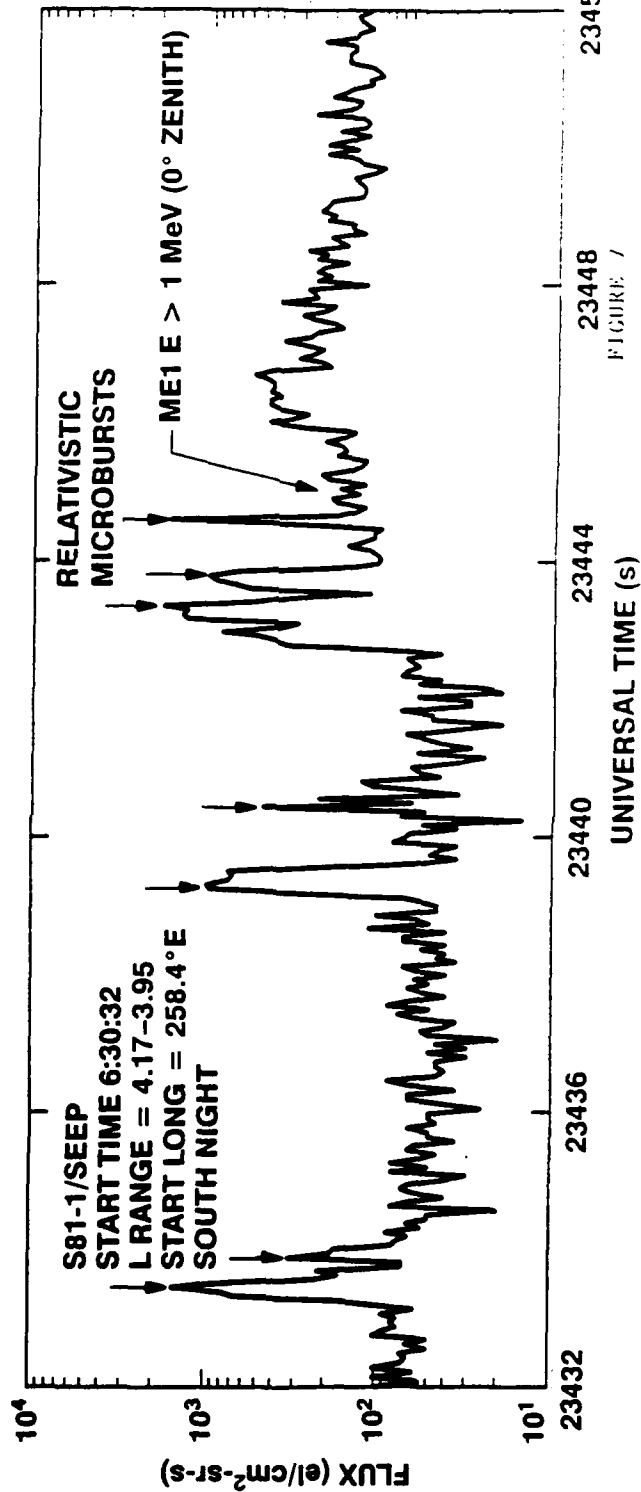FIGURE 3
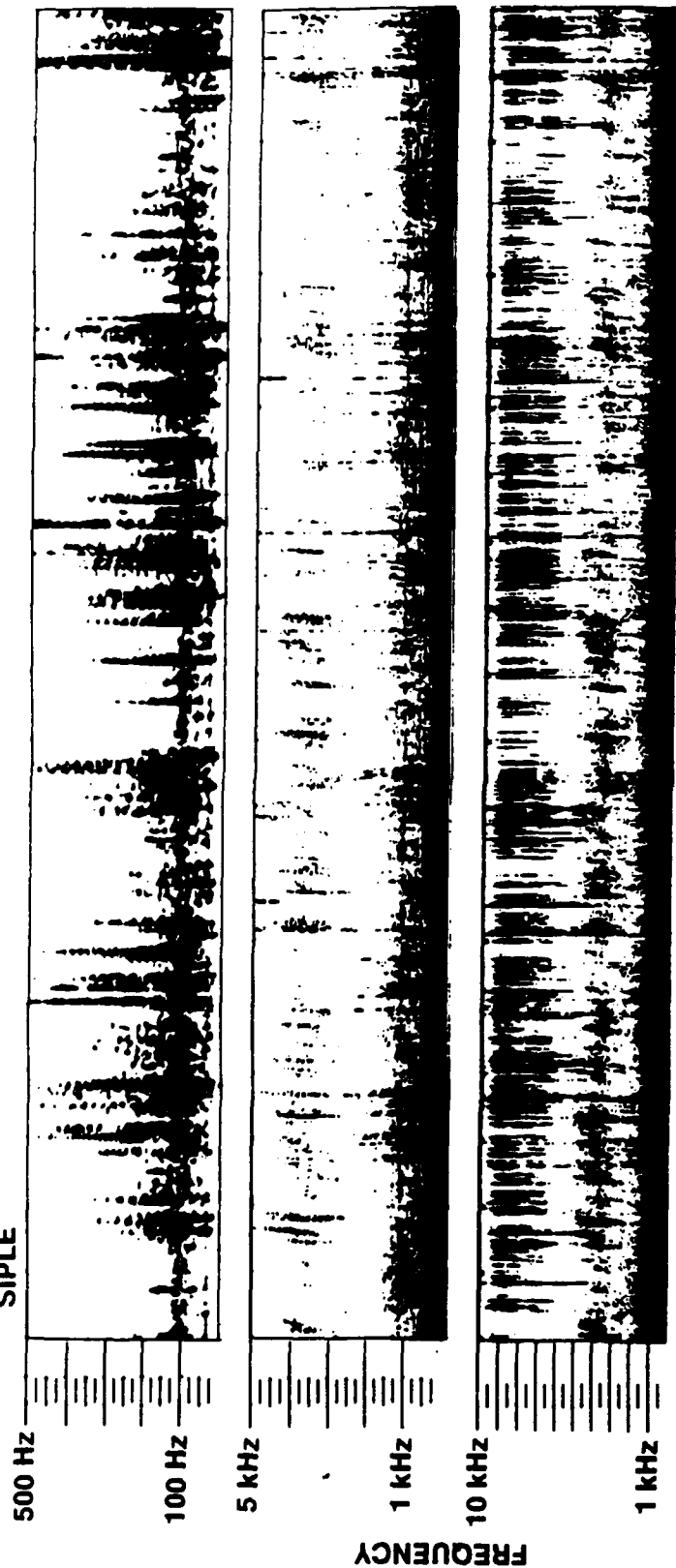
FIGURE 4

FIGURE 5
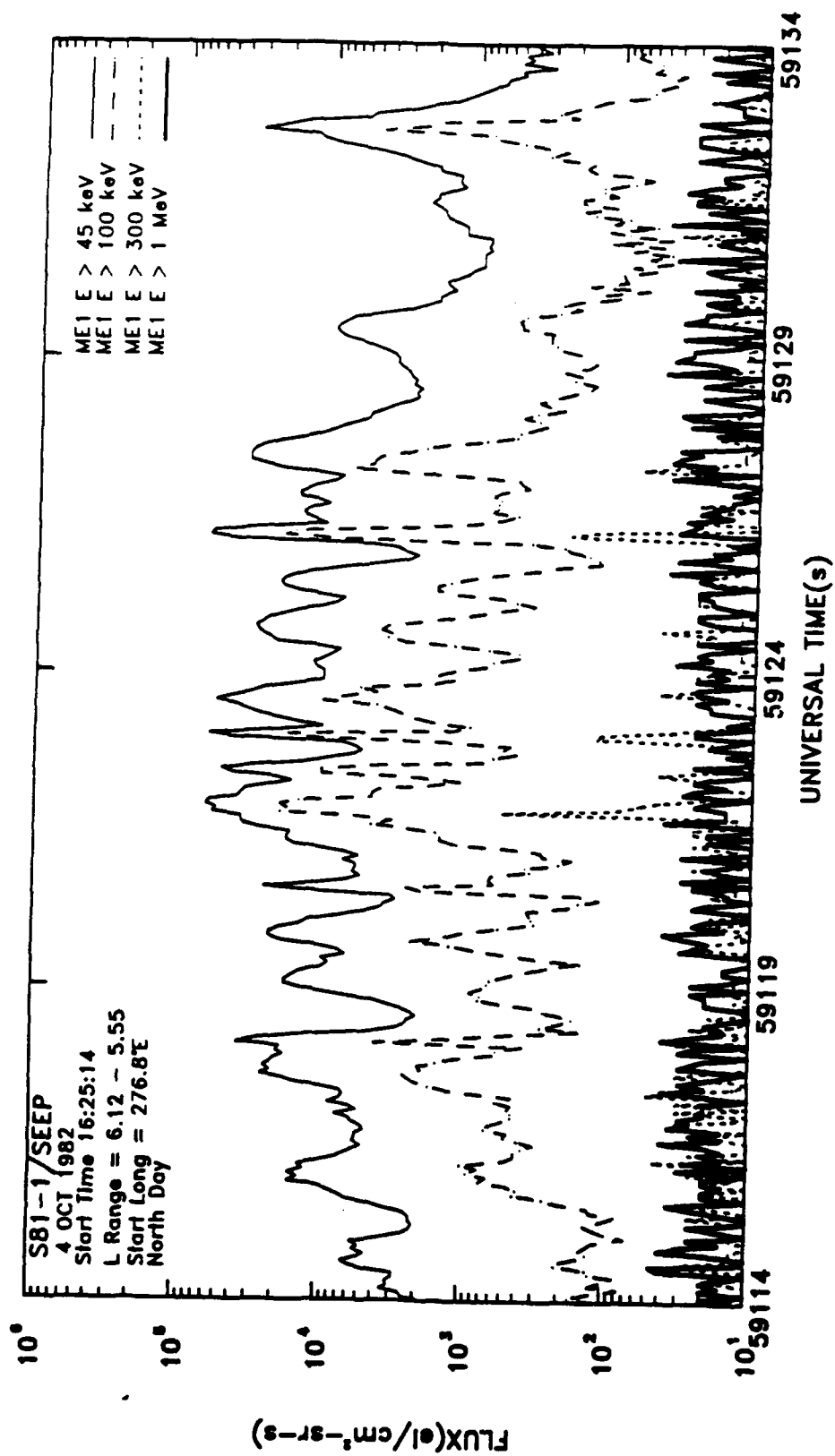
FIGURE 6

21 SEP 1982
SIPLE

FREQUENCY

500 Hz
100 Hz
5 kHz
1 kHz
10 kHz
1 kHz

RELATIVISTIC
MICROBURSTS

ME1 E > 1 MeV (0° ZENITH)

S81-1/SEEP
START TIME 6:30:32
L RANGE = 4.17–3.95
START LONG = 258.4°E
SOUTH NIGHT

FLUX (el/cm²-sr-s)

10^4
10^3
10^2
10^1

23432   23436   23440   23444   23448   23452

UNIVERSAL TIME (s)

FIGURE /

ELECTRON (E > 1 MeV) and WAVE DATA

FRACTION OF PASSES WITH MICROBURSTS

FRACTION OF PASSES WITH MICROBURSTS AND CHORUS

LT = 2230

LT = 1030

LT = 2230

LT = 1030

FRACTION OF PASSES

10^0

10^{-1}

10^{-2}

FIGURE 8

SB1-1/SEEP

Relativistic Microbursts (< 1 sec duration) with simultaneous wave data

106 Microbursts on 26 Satellite passes   ✳ chorus at Siple

29 Satellite passes with no microbursts   ○ no chorus at Siple

NORTH

SOUTH

▲SIPLE

LATITUDE (DEG)

LONGITUDE (°E)

FIGURE 9